THE ROLE OF CSF AND SAS TRABECULAE IN HEAD/BRAIN INJURIES: A NEW LOCAL/GLOBAL AND SOLID /FLUID MODELING

by

Mohamad Zoghi Moghadam Kodehi

A dissertation submitted to the Graduate Faculty in Engineering in partial fulfillment of the requirements for the degree of Doctor of Philosophy, The City University of New York

2006

UMI Number: 3213133

ProQuest Information and Learning Company
300 North Zeeb Road
P.O. Box 1346
Ann Arbor, MI 48106-1346

This manuscript has been read and accepted for the Graduate Faculty in Engineering in satisfaction of the dissertation requirement for the degree of Doctor of Philosophy.

Ali M Sadegh, PhD (Mentor)

Professor of Mechanical Engineering, CCNY

Date — Chair of Examining Committee

Mumtaz K Kassir, PhD

Date — Executive Officer

Charusheel N Bapat, PhD

Professor of Mechanical Engineering, CCNY

Susannah P Fritton, PhD

Professor of Biomedical Engineering, CCNY

Peter A Torzilli, PhD

Senior Scientist and Director, Laboratory for Soft Tissue Research, Hospital for Special Surgery, NY

Charles B Watkins, PhD

Professor of Mechanical Engineering, CCNY

Supervision Committee

THE CITY UNIVERSITY OF NEW YORK

Abstract

THE ROLE OF CSF AND SAS TRABECULAE IN HEAD/BRAIN INJURIES:

A NEW LOCAL/GLOBAL AND SOLID /FLUID MODELING

by

Mohamad Zoghi-Moghadam

Adviser: Professor Ali Sadegh

Blunt and rotational head impacts due to vehicular collisions, falls and contact sports cause relative motion between the brain and skull. This increases the normal and shear stresses in the interface region consisting of cerebrospinal fluid (CSF) and subarachnoid space (SAS) trabeculae. The relative motion between the brain and skull can explain many types of traumatic brain injuries (TBI) including acute subdural hematomas (ASDH). ASDH is caused by the rupture of bridging veins that transverse from the deep brain tissue to the superficial meningeal coverings.

The complicated geometry of the SAS trabeculae makes it impossible to model all the details of the region. Investigators have simplified this layer with solid elements, which may lead to inaccurate results. The goal of this research was to investigate the role of the CSF and SAS trabeculae in the failure of the cerebral blood vessels, ASDH, during blunt and rotational head impacts.

Two global models, namely global solid model (GSM) and global fluid model (GFM), were constructed. The relative displacement between the brain

and skull was determined from GSM. To determine the CSF pressure and considering the fluid-solid interaction, CSF was replaced by an equivalent fluid. The viscosity of the equivalent fluid was found to mimic the head/brain system. That is, through a damping analysis on an experimental study performed on human cadavers, the damping ratio of the system was evaluated. The damping ratio was used to calculate the equivalent viscosity of the system. The two global models were subjected to two types of load known to create injuries, a blunt impact and a rotational impact. To study the mechanism of the injury, the relative displacement between the brain and skull along with the equivalent fluid pressure were implemented into a new local solid model (LSM). The strains of the cerebral blood vessels were determined from LSM. These values were compared with their relevant experimental ultimate strain values. The results showed an agreement with the experimental values indicating that the applied loads are strong enough to create ASDH.

It has been shown that this research provides a reliable tool to relate the head impacts to ASDH. This contributes to the knowledge of the head/brain biomechanics underlying the understanding of ASDH.

ACKNOWLEDGEMENTS

I am deeply indebted to my advisor, Dr. Ali Sadegh, for all his support, education and patience, for giving me the opportunity to work in the field of Biomechanics

I am thankful to Dr. Charles Watkins for his support and guidance throughout this research

I would like to thank Dr. Peter Torzilli for giving me the opportunity to work in his lab

I am thankful to Dr. John Ehteshami for all his unconditional support

I would like to thank my committee members for their time and advice.

I am grateful to Departments of Mechanical and Biomedical Engineering of CCNY, my instructors, Professors Andreopoulos, Bapat, Benenson, Cowin, Delale, Fritton, Ganatos, Khanbilvardi, Price, Raj, Rouson, Subramaniam, Wiener, and my colleagues, Ericka Calton, Cesare Ciani, Kelly Emerton, Amir Eshraghi-Azar, Carlos Llinas, Ozlen Ozkurt, Alexis Pierdes, Abraham Tchako, Hupai Wang, Qianhong Wu, Savvas Xanthos, Young June Yoon, Xiaobing Zhang and also my friends in PSA group.

I would like to thank my family; my sister, Bahar Zoghi-Moghadam for all her non-stop support and patience, my brother-in-law, Bahman Azmoudeh, for all his help, my niece, Yaas Azmoudeh, for cheering me up after hard working days, my step father Bijan Azmoudeh and my brothers Khashayar and Mahyar Zoghi-Moghadam

I am very much grateful to my wife, Jennifer Madeo, for all her support and guidance, without which I would not have come this far.

In memory of my father, Rahim Zoghi-Moghadam, despite the absence of this hero since 1982, his influence carries on

Lastly, it is beyond words to express how grateful I am to my mother, Behesht Ahari; her first name means “paradise” in Persian, and I am in paradise whenever I am thinking of her (always).

This is dedicated to my mother

Behesht Ahari

TABLE OF CONTENTS

LIST OF TABLES

LIST OF FIGURES

1- INTRODUCTION

Blunt head impacts or non-impact rotational assaults due to motor vehicle collisions, falls, or sports such as football, diving etc., cause relative motion between the brain and skull. This increases the shear stresses in the meningeal region and the brain tissue. These blunt impacts can lead to Traumatic Brain Injuries (TBI) that can have devastating consequences. The average US incidence rate of fatal and nonfatal hospitalizations due to brain injury is approximately 175 to 200 per 100,000 population (Kraus and McArthur 1996). According to the last annual estimation of the Center for Disease Control and Prevention (Center for Disease Control and Prevention, www.cdc.gov), 1.4 million people sustained TBI with 22% rate of death and hospitalization. This type of injury is more frequent among children of ages 0 to 14 years (about 30%). The leading causes of TBI are falls (28%), motor vehicle accidents (20%), struck by/against (19%) and assaults (11%).

Brain injuries generally cause physical and psychological distress, which creates enormous burdens, economically and emotionally, on the social and personal levels. According to Thurman (2000) the direct and indirect cost of TBI in the year 1995 has been approximated to be $56.3 billion. Acute subdural hematoma (ASDH) accounts for 30% of the incidences of TBI (Kraus and Mc Arthur 1996). In this pathology veins that transverse from the deep tissue of the brain to its more superficial connective tissue coverings (the meningeal layers discussed in more detail in the anatomy section) rupture due to shearing forces. Despite the fact that medical procedures can drain the excess blood that

accumulates due to these injuries, thus relieving the pressure, the mortality rate of ASDH is 74% (Kraus and Mc Arthur 1996). This high rate shows that ASDH continues to be a major problem. Intervention strategies aimed at prevention or the minimization of these injuries is the best way to lower this mortality rate. A good understanding of the physical mechanisms underlying TBI is necessary for the development of prevention strategies.

Animal studies, cadaver studies, analytical and numerical models of brain and head have been shown to be useful tools for understanding the mechanism of injuries. These efforts can be categorized in four branches:

1. Experimental studies, where researchers conduct experiments on human cadaver heads or animals. Hardy et al. (2001) and Al-Bsharat et al. (1999) performed a series of experiments on human cadavers to find the relative displacement of the brain with respect to the skull. Trosseille et al. (1992) and Nahum et al. (1977) used human cadavers to find the intracranial pressure in long-term and short-term impacts, respectively. The latter is the most frequently referenced study in this field. There are a limited number of cadaver studies and more such studies are needed. Many other researchers have carried out experimental studies on animal surrogates. Gurdjian and Lissner (1944) and Gurdjian et al. (1955) used dogs for their studies. However, most of the animal studies have been conducted on different species of monkeys. This includes the studies of Ommaya and Hirsch (1971), Ommaya et al. (1971), Gennarellie et al.

(1972), Abel et al. (1978), Hodgson and Thomas (1979), Ono et al. (1980), Gennarelli et al. (1982), Gennarelli and Thibault (1982) and Hodgson et al. (1983). It seems that due to the tight regulation of the animals rights agencies such research have been discontinued.

2. Analytical studies, where researchers use a mathematical model to analytically solve the kinetics and kinematics of the head injury. The following are a few of such studies. Anzelius (1943) studied the impact on a spherical liquid mass. Engin (1969) studied a fluid-filled spherical model under a local radial impulse. Newman (1980) analytically examined the validity of head injury criteria (HIC). Kleinberger et al. (1998) worked on developing a new injury criterion for the assessment of advanced automotive restrained systems. Newman et al. (2000) introduced a new head injury criterion that accounts for impacts in all 6 degrees of freedom. Young (2003) applied a blunt head impact to his fluid-filled shell analytical model to determine the response of the model.
3. Physical models, where researchers create physical models to simulate head injury scenarios. This includes that by Holbourn (1943), Gurdjian and Lissner (1961), Aldman (1981), Margulies (1987), Margulies et al. (1990), Viano et al. (1997), Ivarsson et al. (2000) and Bradshaw et al. (2001). Such studies can partially compensate for the lack of experimental studies.

4. Numerical studies using finite element (FE) modeling. Many researchers have used this method to study head/brain injuries. All the aforementioned types of studies can be combined into numerical studies. For example, these studies are usually validated by comparing them to human cadaver studies, primarily the one performed by Nahum et al. (1977). These studies include the 2 dimension (2D) work of Lee et al. (1987), Ruan et al. (1991), Ueno and Melvin (1995), and Zhang et al. (2002). There are more extensive studies performed using 3 dimensional (3D) models: Ward and Chan (1980), Trosseille et al. (1992), Ruan et al. (1994), Eppinger et al. (1995), Willinger et al. (1995), Zhou et al. (1995), Turquier et al. (1996), Claessens (1997), Al-Bsharat et al. (1999), Huang et al. (1999), Nishimoto and Murakami (1999), Willinger et al. (1999), Zhang et al. (2001), Kleiven and Hardy (2002), Kleiven and Von Holst (2002a), Kleiven and Von Holst (2002b), Kleiven (2003) and Sarkar et al. (2004) are only a few of them.

The biomechanical response of the brain to external impact is difficult to measure experimentally. Previous studies have been performed with Rhesus monkeys and human cadavers (Gennarelli et. al. 1982 and Nahum et. al 1977). These results provided some insights and guidelines into important mechanical considerations for the study of brain injury but a detailed biomechanical analysis is beyond the scope of experiments. Instead, finite element (FE) analysis has proven to be a powerful tool. The finite element method can include the complex

geometry and non-linear material properties of the head and hence provide a more detailed and accurate model for head injuries.

In a blunt or rotational (non contact) head impact the brain moves relative to the skull, which may rupture the bridging veins causing contusions, intracerebral hematomas, coup and countercoup lesions and cerebral contusions. In some severe cases the rupture of bridging veins may lead to acute subdural hematomas (ASDH), which could be fatal (Blumenfeld, 2002). Dynamic simulations of these injuries using Finite Element (FE) models can calculate the internal stress, relative displacement and pressure gradient at all locations and at any instant during an impact. Models that describe the complex geometry and the multiple material compositions of the skull, meninges and the brain have been useful. In their recent 3D model, the Wayne State University (WSU) group, (Zhang et al. 2001), simulated a 50^{th} percentile male head. They simplified the CSF properties by using a solid layer with bulk modulus of water and very low shear modulus. Many finite element head models, as well as physical and animal head models, have been developed by several research groups to investigate TBI. A more detailed description is presented in the Reviewed Literature Section.

The material properties of the brain tissue have been studied by many investigators. These include the insightful studies of Miller (1999), Miller and Chinzei (1997, 2002), and Shuck and Advani (1972). Many researchers have investigated the properties of the cerebral vessels (see Lowenhielm (1974), Lee and Haut (1989) and Monson et al. (2000, 2003)). Zhang et al. 2002 has recently studied the effect of vasculature on the mechanical properties of the human

brain. Still, more experimental research is needed to determine the mechanical properties of the meningeal layers and blood vessels.

While global models of the brain and skull have been used to study brain injuries, local models for the effect of individual components of the brain tissue do not appear to have been addressed in the literature. In particular, the brain injury related to the subarachnoid space, Acute Subdural Hematoma (ASDH), has not sufficiently been investigated.

ASDH is commonly caused by the tearing of veins that cross the subdural space from the cerebral surface on their way to the venous sinuses above (Gennarelli and Thibault, 1982). The strain rate sensitivity of these veins appears to be the most significant factor governing the incidence of ASDH. The relative motion between the cerebral cortex and skull causes the laceration of bridging veins. Due to the forward orientation of bridging veins ASDH is more commonly caused by occipital impacts where the brain moves forward relative to the skull. In particular, those bridging veins that drain into the superior sagittal sinus have the highest incidence of tearing (Blumenfeld, 2002). The relative motion between the brain and skull can cause the tearing of these veins by stretching them to the point of mechanical failure. Venous blood then spills over into the potential space between the dural and arachnoid junction. This will cause the intracranial pressure to rise, which will lead to decrease in cerebral perfusion pressure. This ceases the arterial blood flow to the brain and the person dies quickly from the lack of oxygen to the brain (ischemia).

The purpose of this study was to investigate the mechanical role of the cerebrospinal fluid (CSF) and collagenous trabeculae in subarachnoid space (SAS) during blunt head impacts or when the head is subjected to a high angular acceleration. CSF is a water-like fluid covering the central nervous system (CNS). It behaves like a Newtonian fluid as reported by Bloomfield et al. (1998), Brydon and Hayward (1995) and Ommaya (1968). The complexity in the geometry of the SAS trabeculae is due to the fact that there is an abundance of connective tissue bridges extending from the arachnoid mater to the pia mater, called trabeculae. These fluid and solid phases work together to mechanically support the brain.

Due to the irregular shape of the brain, the subarachnoid space also has an irregular shape. This makes the distribution of CSF around the brain non-uniform. For example, the subarachnoid space is very thin (volume) over the surface of cerebral gyri (places where the brain tissue protrudes outward), larger over cerebral sulci (places where the brain tissue sinks inward) and has the highest volume over other regions of the brain that have surface irregularities.

The complicated geometry of the SAS and trabeculae makes it impossible to accurately model all the details of the region. Therefore, to model this region investigators have used solid elements having the bulk modulus of water and very low shear modulus (Kleiven (2003), Zhang et al. (2001, 2002), Kleiven and Hardy (2002), Al-Bsharat et al. (1999), Willinger et al. (1999), Nishimoto and Murakami (1998), Turquier et al. (1996), Willinger et al. (1995), and Trosseille et

al. (1992)). Looking at the entire head model (global view) the simplified assumption could be sufficient to mimic the behavior of the entire head/brain model. The shortcoming of this assumption arises when a local study of the SAS region is desired for the study of bridging veins that are the main cause of brain injuries. It has been confirmed that using solid elements to represent CSF and SAS region is not the best solution (Kleiven (2003), Zhang et al. (2001), Willinger et al. (1999), Bandak and Eppinger (1994)).

One hypothesis that was investigated is that the CSF and its surrounding subarachnoid space, coupled with the anchoring trabeculae, have an important dampening effect. This dampening effect reduces the impact force on the brain thereby reducing relative motion between the brain and skull. A three-dimensional solid finite element model of the human head, a three-dimensional fluid model of the CSF and a three-dimensional local model of the meningeal layers that includes the subarachnoid space are all used to investigate this hypothesis.

In the following sections the significance and the objectives of the research are presented. In chapter 2, the anatomy of the head is described, followed by the literature review in chapter 3. Different types of head/brain injuries are described in chapter 4. Dynamics of head injuries and the head models are presented in chapters 5 and 6, respectively. The three 3D FE models will be discussed in detail in chapters 7, 8 and 9. Finally, discussions and proposed future studies are presented in chapter 10.

1-1 Significance

Brain injuries are among the most likely types of injuries to cause death or permanent disability. CDC reported 1.5 million people suffering TBI annually, which is 8 times the number of people diagnosed with breast cancer and 34 times the number of new cases of HIV/AIDS (Figure 1).

The major causes of TBI are crashes involving motor vehicles, bicycles, pedestrians, firearm use, contact sports and falls. In the US, in 1995, direct and indirect costs of TBI totaled an estimated $56.3 billion (Thurman 2000).

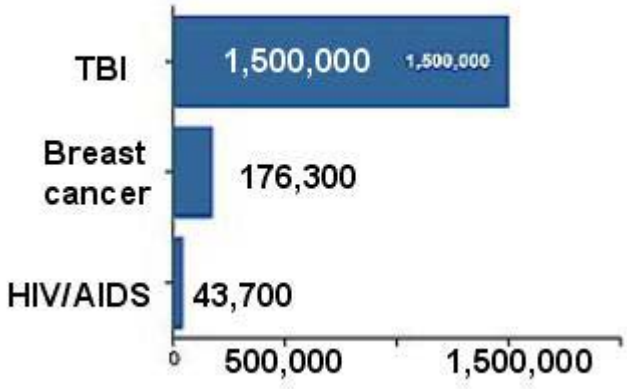

Figure 1. Comparison of the yearly incidences of three selected health problem in the US (CDC 2003, www.cdc.gov)

A significant clinical TBI occurs in subarachnoid space (SAS) and manifests itself as an acute subdural hematoma (ASDH). ASDH occurs in nearly 30% of head impact injuries. ASDH has the highest mortality rate of 74% from all the intracranial lesions (Kraus and McArthur 1996).

As indicated before, ASDH is commonly caused by the tearing of bridging veins. This will cause the intracranial pressure to rise. This leads to reduction of arterial blood flow to the brain and causes lack of oxygen to the brain.

The main causation of ASDH is the relative motion of brain with respect to skull. Many research groups have investigated ASDH through experimental, physical and numerical models. To the best of our knowledge, to date, no analysis has been performed where the CSF fluid and the solid models were interacting as a coupled model. That is, in all numerical modeling, CSF has been assumed as a solid layer with low shear modulus and high Poison ratio. The significance of the current study is to couple fluid and solid mechanic analyses. A new injury criterion may be proposed for ASDH using the outcomes of the solid and fluid models.

1-2 Objectives

The goal of this research is to investigate the biomechanics of the head injury related to the subarachnoid space. Specific objectives are:

1. To quantify the magnitude of forces, accelerations and velocities during a blunt head impact in a real life accident involving a fork lift truck using rigid body dynamic analysis.

2. To create a two dimensional global solid model of the head including the skull, meningeal layer and the brain, and to validate the model with the

experiment. This model will provide the magnitude of the relative motion of the brain with respect to the skull.

3. To create two 2D global fluid models of the head including the skull, CSF and the brain, with and without trabeculae. This model provides the pressure distribution of the CSF in subarachnoid space.

4. To create the local model of the head representing the skull, dura mater, arachnoid, trabeculae, pia mater and the brain. With this model the effect of the CSF and the SAS trabeculae on the absorption of the impact will be studied.

5. To create a set of three-dimensional detailed models, which includes 2 global models and 1 local model, similar to the 2D global solid and fluid, and local models mentioned in items 2 to 4, including the skull, dura mater, arachnoid, trabeculae, pia mater and the brain.

6. To include the bridging veins in the 3D local model (item 5), in order to investigate the mechanism of acute subdural hematoma.

7. To investigate the effect of the CSF and SAS trabeculae in damping an impact load or a sharp angular acceleration to the head, and to determine the causation of hematomas or other head injuries.

8. To develop an injury criterion for subdural hematomas based on the loading condition.

It is hypothesized that the existence of the CSF coupled with the SAS collagenous trabeculae play a major role in reducing relative motion between the brain and the skull, thereby damping blunt impact forces.

2- ANATOMY

To appreciate its significance and complexity, the anatomy of the head is described below. The head may be described as consisting of four components (Moore, 1999):

1) Scalp: the most superficial layer of the head that includes skin and other soft tissues;

2) Skull; the bony structure of the head including cranial and facial bones;

3) Meninges; three connected tissue layers between the brain and skull; and

4) Brain; the tissue capsulated in the skull.

Figure 2 depicts the frontal cross- section of the head describing the four components and different layers. Each component is described in detail below.

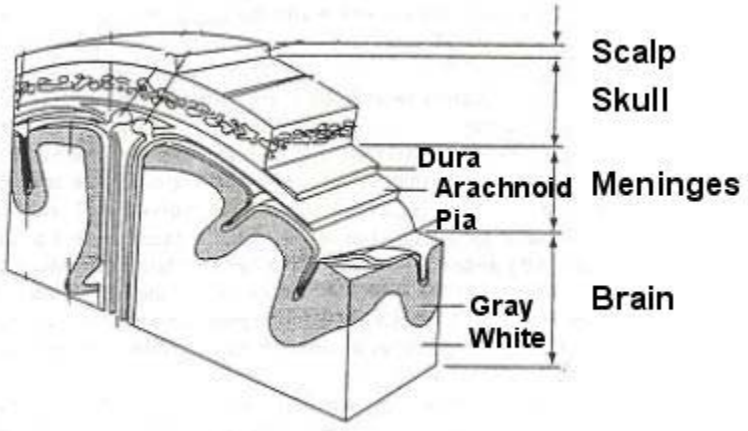

Figure 2. A schematic frontal cross-section of the head including: the Scalp, Skull, Meninges and Brain.

2-1 The Scalp

The head, like the rest of the body, has an outer covering of skin, which is part of the scalp. Below the skin there are four tissue layers included in the scalp. Listed from superficial to deep, these layers are: 1) connective tissue (subcutaneous), 2) aponeuromuscular (also called “galea”), 3) loose connective tissue and 4) pericranium. Figure 3 shows the five layers of the scalp in a schematic way. The average thickness of the scalp is 6 mm.

The three most superficial layers of scalp frequently are regarded as a single layer because they tend to remain together, even if the scalp is torn away from the skull (Moore, 1999). They form the region of so called Scalp Proper, as shown in Figure 3. Underneath the scalp proper is the fourth layer, which is composed of a relatively loose connective tissue. Beneath this is the pericranium, which contacts the skull bones directly (similar to the periosteum of long bones). Nerves and blood vessels are also found in the scalp. These structures are found between the skin and subcutaneous connective tissue and within aponeurosis (Moore, 1999).

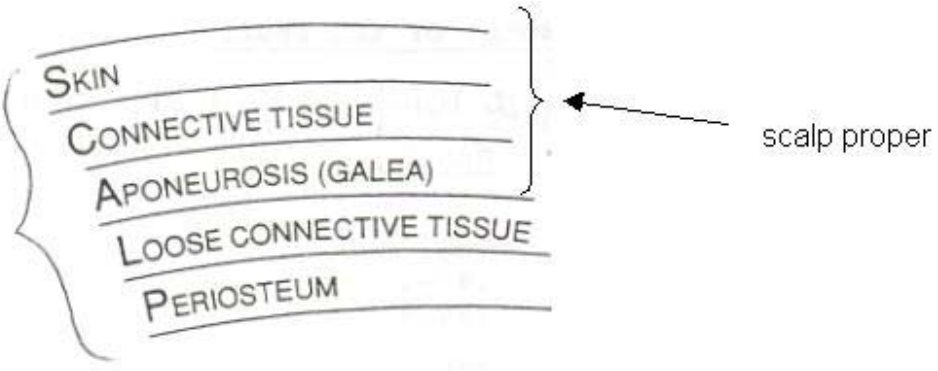

Figure 3. The five layers of the scalp.

2-2 The Skull

The skull contains all the bones in the head. It consists of two parts: 1) cranium, which includes the top, side, back and bottom of the head and 2) the face, which forms the front of the head. Of facial bones, only the back of the nose (the cribiform plate), the posterior walls of the frontal sinuses and the back of the sphenoid sinus, are in contact with the brain (Moore, 1999). Almost 5 percent of the brain surface is in contact with any portion of the face.

The skull contains 22 bones, 8 of which are cranial bones and 14 of which are facial bones (Moore, 1999). The 8 cranial bones are joined together by immovable highly convoluted joints of minimal connective tissue, called sutures. There are 4 big sutures and several small ones. Sutures are shown in Figure 4. These include the sutures of the frontal, side and rear views of the cranium and the face. A sagittal cross section of the skull is shown in Figure 5, which depicts the major bones of the cranium (frontal, parietal, temporal and occipital).

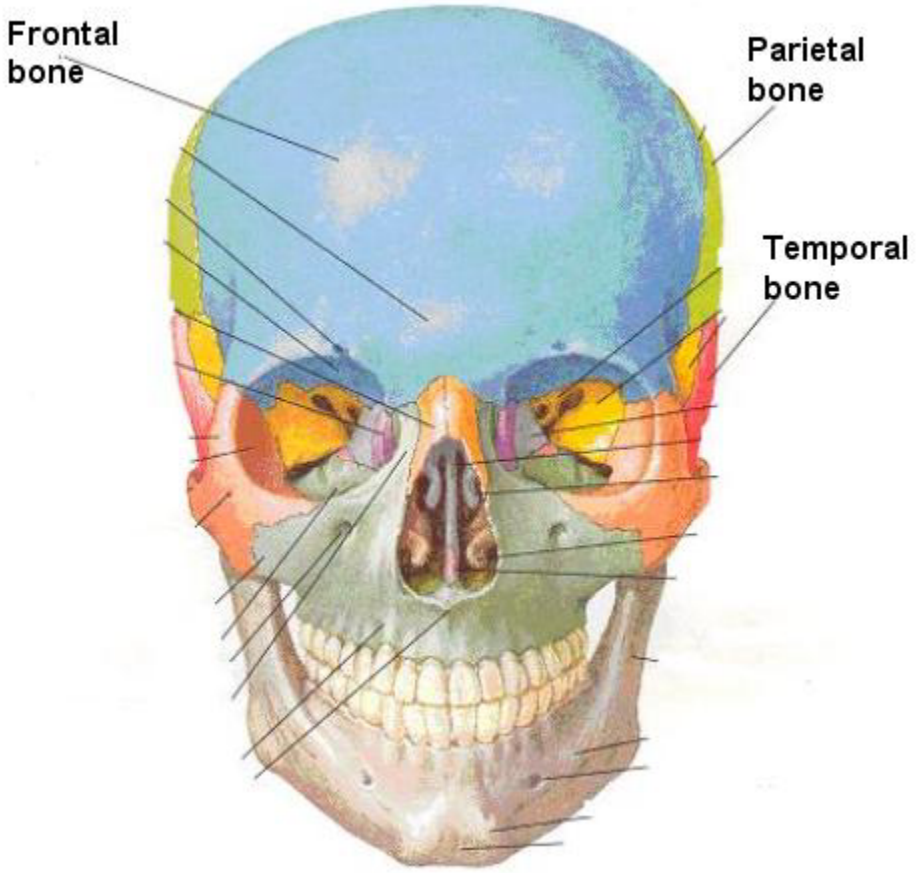

Figure 4. Anterior view of skull (Netter 1997).

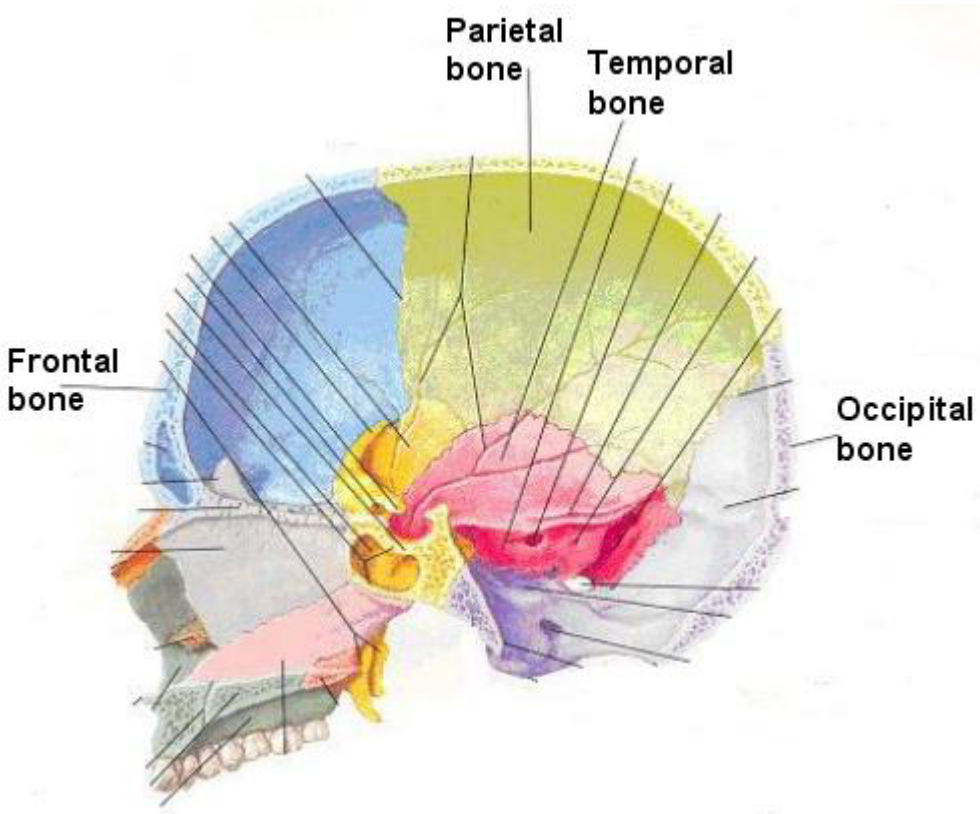

Figure 5. Mid-sagittal section of skull (Netter 1997).

2-3 Meninges

Anatomically, human brain is made of soft and highly deformable tissue. To protect the brain from external forces and to maintain its proper shape and function, the brain is encased in the skull. In addition, the brain is suspended and supported by a series of three fibrous tissue layers. Moving from skull to brain these layers are called, dura mater, arachnoid and pia mater. Collectively, these three layers are known as the meninges and they stabilize the shape of the brain and its position during head movements. One way that the meninges accomplish their function is by physically anchoring the brain to the skull so that it moves with the head. A second way is through a special fluid called cerebrospinal fluid (CSF)

located in the space between the arachnoid and pia mater or the subarachnoid space (SAS). The buoyant effect of this fluid environment greatly decreases the tendency for external forces to distort the brain (Nolte, 1999). It has been shown that isolated fresh brain, unsupported by its usual surroundings, becomes seriously distorted under the influence of gravity. A brain weighing 1500 grams in air, effectively weighs less than 50 grams in its normal CSF environment (Nolte, 1999). Therefore the CSF plays a very important mechanical role in maintaining normal brain shape and function.

Figure 6 is a cartoon representation of the meninges. The dura mater is the outermost meningeal layer. It is mechanically strong because it is thick and has a high content of collagen fibers (Nolte, 1999). Under normal circumstances it adheres directly to the inner surface of the skull, although in certain regions it folds inward to generate dural sinuses for the venous drainage of the brain. This internal layer of dura is continuous with the dura mater of the spinal cord. The potential space between the skull and the dura, called the epidural space, is only visible under pathological conditions such as hemorrhage (Blumenfeld, 2002). The dura is directly connected to the middle meningeal layer called the arachnoid. The potential space between the dura and the arachnoid, called the subdural space, is only visible under pathological conditions (Blumenfeld, 2002).

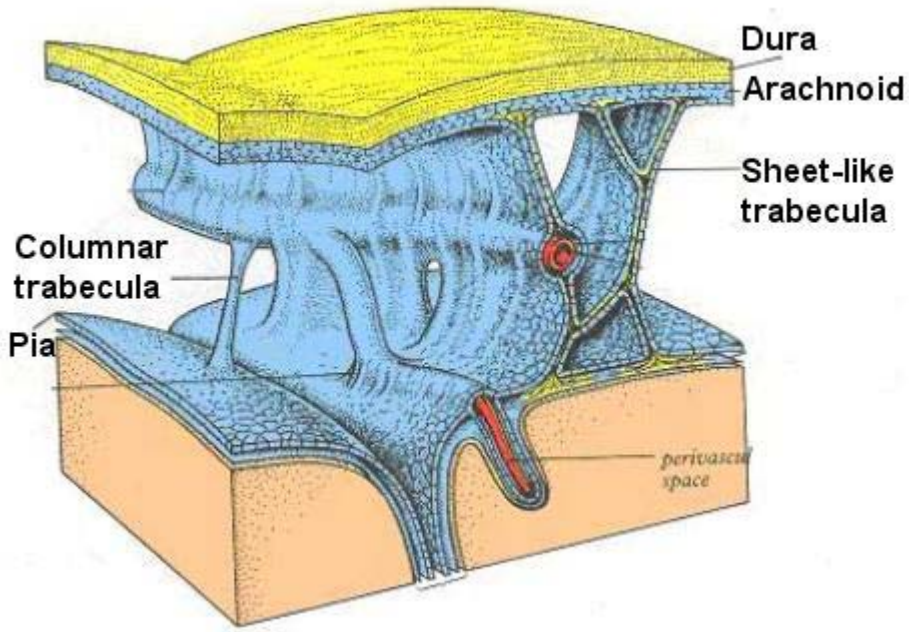

Figure 6. Schematic picture of the meninges (Gray 1995).

Aside from its protective mechanical role, the dura mater is important for structural support of the brain. The dura itself has two distinct layers; the external periosteal layer and internal meningeal layer (Nolte, 1999). The external layer is the lining of the skull. At specific places, the internal layer folds away from the external, into the cranial cavity to form compartments that separate different regions of the brain from one another. These separations are referred to as dural infoldings or dural reflections. Dural infoldings conform to the general shape of the brain without following the most intricate contours of brain surface. In general, these infoldings separate the cerebrum, the cerebellum and the pituitary gland. These infoldings structurally support their regions and hence are important for global support of overall brain structure (Nolte, 1999). Figure 7 shows a cadaver section of the meninges in which the dura mater is clearly shown.

In addition to its mechanical functions, the dura mater plays an important role in the venous drainage of the brain (Nolte, 1999). Dural venous sinuses are endothelium-lined channels formed within the dural infoldings. Large veins from the surface of the brain empty into these sinuses. Arteries and nerves can also be found in these sinuses (Nolte, 1999). Ultimately all of the blood from the brain drains through them into the internal jugular veins of the neck (Moore, 1999). From there the blood can return back to the heart. The venous drainage is explained in detail in section 2-7.

The middle meningeal layer is called the arachnoid. The arachnoid is a thin avascular layer composed of layers of fibroblast cells interspersed with bundles of collagen (Nolte, 1999). Flattened cells are pushed up against the innermost surface of the dura forming a 100μ thick cellular layer. These cells adhere to one another very strongly through intercellular structures known as tight junctions. These tight junctions occlude the extracellular space in this layer. This is an important part of the protective barrier between the blood (from venous sinuses above) and the brain.

Extending from this layer are strands of collagenous tissue called arachnoid trabeculae. The trabeculae are composed of irregularly shaped fibroblast cells within an extracellular collagen matrix. These trabeculae extent to and merge with the deeper pia mater (Nolte, 1999). Arachnoid trabeculae are important structures for keeping the brain suspended within the meninges. Figure 8 is an electron microscopic view of a trabecula.

Arachnoid trabeculae are located in the space between the arachnoid and pia mater called the subarachnoid space. This is a closed volume filled with CSF. This is the only substantial fluid-filled space normally found surrounding the brain. The pia mater below is a very thin layer that adheres to the surface of the brain and follows all its contours including the folds of the cerebral and cerebellar cortices. This gives the subarachnoid space a highly irregular shape and makes the distribution of CSF around the brain non-uniform (Nolte, 1999). For example, the subarachnoid space is very thin over the surface of gyri, larger over cerebral sulci and has the highest volume over other regions of the brain that have surface irregularities (Nolte, 1999). Places where the subarachnoid space is large, due to the shape of the brain surface in that region, are called subarachnoid cisterns. The volume of CSF is highest within these cisterns. Arachnoid trabeculae are more concentrated in the subarachnoid cisterns, sometimes even coalescing into membranes that partially occlude the subarachnoid space. This correlation between the CSF and the trabeculae suggests that their functions are not independent. These fluid and solid phases work together to mechanically support the brain.

An important physiological role of the arachnoid layer is maintenance of the CSF. The CSF is generally separated from the venous blood in the dural sinuses by a tight layer of arachnoid, a layer dura and the endothelium lining. This strong barrier is important for keeping blood and CSF in their particular compartments (Nolte, 1999). However, at some locations, small protrusions of the arachnoid, called arachnoid villi, penetrate into the dural venous sinuses.

Collections of arachnoid villi are called arachnoid granulations. At these places the dura is weak and the arachnoid lacks tight junctions hence the CSF can exchange with venous blood. Functionally, these villi act as one-way valves allowing flow only from subarachnoid to venous blood and not the reverse (Nolte, 1999). Under normal circumstances CSF pressure is greater than venous pressure hence the flow is passive. It has been shown that even when the pressure gradient is reversed, the flow is not (Nolte, 1999). The reason for this is still not clear but it apparently involves physiological input. Figure 9 is another cadaver section showing the arachnoid trabeculae in their anatomical orientation.

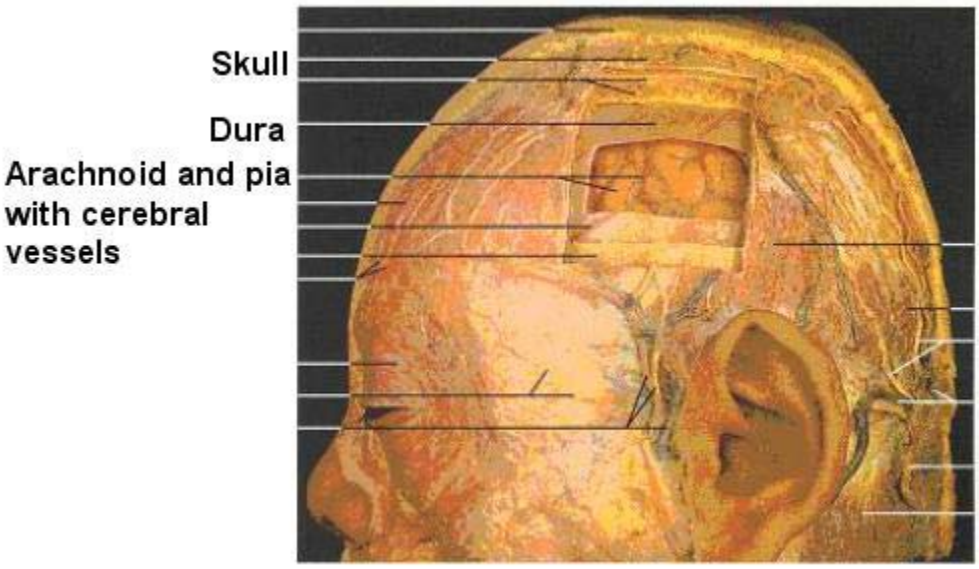

Figure 7. A cadaver section (Rohen et al. 1998).

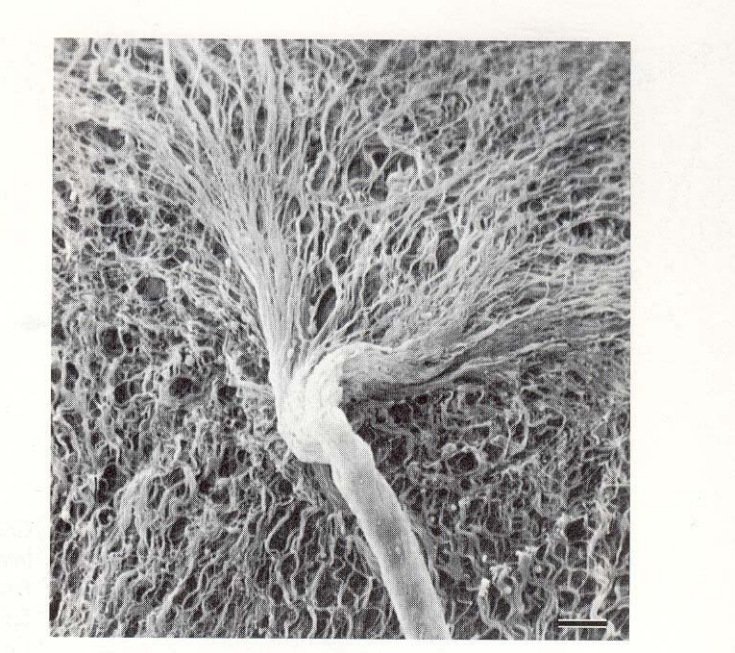

Figure 8. Scanning electron microscope (× 240) of an arachnoid trabeculae (Alcolado et al. 1988).

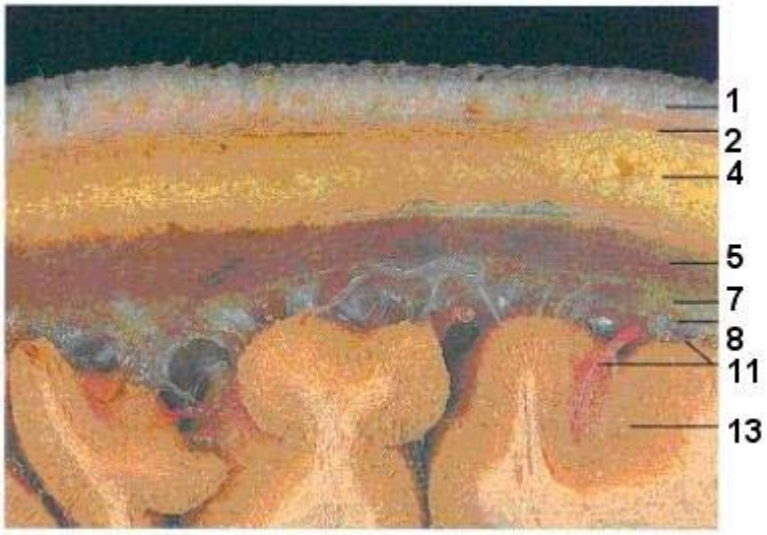

Figure 9. A cadaver photograph showing the meninges and arachnoid trabeculae:

1, Skin; 2, aponeurosis; 4, loose connective tissue layer of scalp; 5, dura mater; 7, arachnoid mater; 8, subarachniod space with trabeculae; 11, pia mater; 13, cerebral cortex (Rohen et al. 1998).

2-4 The Brain

The brain is anatomically divided into three major parts, namely: the cerebrum, the brainstem and the cerebellum. The cerebrum, which forms the largest region of the brain, is divided into left and right hemispheres (Nolte, 1999). The cerebral surface is composed of gyri (folds) and sulci (grooves). The hemispheres are further divided into regions known as lobes. For each cerebral hemisphere there is a frontal, parietal, occipital and temporal lobe (Figure 10). The diencephalon forms the central core of the brain and consists of the epithalamus and the thalamus.

The brainstem, which is continuous with the spinal cord, consists of the midbrain, the medulla oblongata and the pons. The cerebellum lies dorsal (behind) the pons and medulla oblongata. The cerebellum is also divided into two lateral hemispheres. The hemispheres are united by a narrow middle structure called the vermis.

In addition to the solid structures described above, the brain consists of a system of fluid-filled cavities called ventricles (Nolte, 1999). The fluid is CSF and it is continuously circulating throughout the system. This ventricular system is located in the central portion of the brain. This system consists of two lateral ventricles (located in the left and right cerebral hemispheres), the third ventricle (located in the diencephalon) and the fourth ventricle (located between the pons and cerebellum) (Nolte, 1999). The lateral ventricles are the largest. All of the ventricles are inter-connected by ducts and form a closed system with the subarachnoid space. The walls of the ventricles contain epithelial cells that are

responsible for the production and secretion of CSF. A total of 400-500 ml of CSF are secreted daily by these cells (Nolte, 1999). The walls of the lateral ventricles are the largest and most important for this function.

At the tissue level, the brain is divided into gray matter and white matter. The division is visible on whole human brain. Gray area refers to places that are predominately cell bodies and dendrites. Dendrites are long, thin extensions of the main cell body that receive information from other neurons. White matter refers to areas that are predominately axons. Axons are long, cylindrical processes that conduct information away from the main cell body. The white appearance is due to the fatty layer of myelin that covers the axon. Myelin acts as an electrical insulator that greatly increases the speed of signal propagation along the axon.

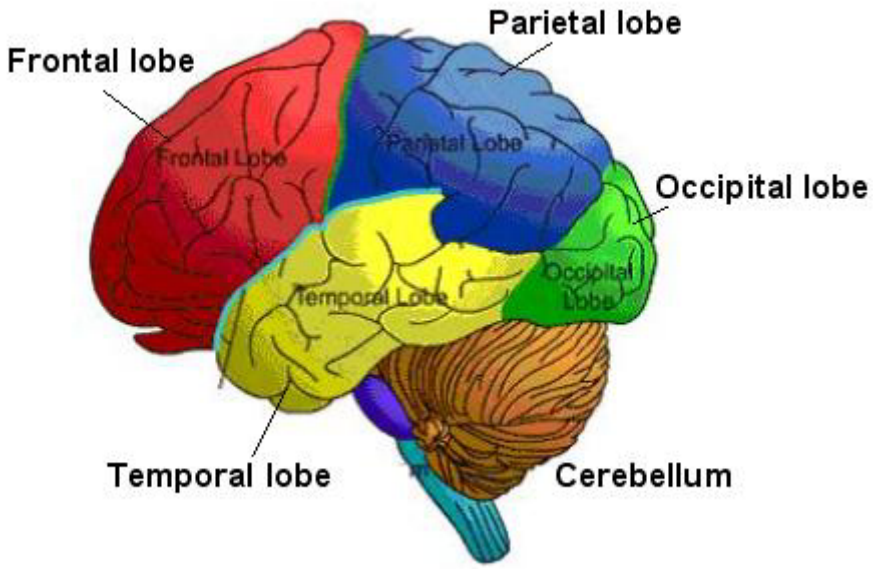

Figure 10. Lobes of the brain (http://www.stanford.edu/group/hopes/basics/braintut/).

2-5 CSF Circulation and Function

CSF leaves the lateral ventricles and then flows into the third and fourth ventricles, respectively. There are three openings in the fourth ventricle that lead into the subarachnoid space (Nolte, 1999). Most of the CSF that flows into the SAS goes into the cisterns (dilatations of the SAS). The CSF is generally separated from the venous blood in the dural sinuses by a layer of arachnoid (containing cells with tight junctions as mentioned above), a layer dura and the endothelium lining. However, as mentioned in section 2-3, at some locations, small protrusions of the arachnoid, called arachnoid villi, penetrate into the sinus. At these places the dura is weak and the arachnoid lacks tight junctions hence the CSF can exchange with venous blood. Most of the CSF absorption is into the superior sagittal sinus, which is the most superior dural sinus. Functionally, these villi act as one-way valves allowing flow only from subarachnoid to venous blood and not the reverse. Approximately 330-380 mL of CSF enters the venous circulation each day (Nolte, 1999). As mentioned before, under normal circumstances CSF pressure is greater than venous pressure hence the flow is passive.

It is believed that the CSF protects the brain by providing a cushion against head impacts. The CSF also provides buoyancy so that the weight of the brain does not compress nerves and blood vessels (Nolte, 1999). The cranial cavity is like a closed box, there are no spaces and all the volume is accounted for by either solid or fluid elements. This means that any changes in intracranial volume will be reflected in pressure changes. Overproduction or obstruction of

flow of CSF results in brain damage due to the intolerable increase in intracranial pressure (Blumenfeld, 2002). The CSF is, therefore, very important for maintaining intracranial pressure. Another important function is to help the brain adapt if injury does occur and a hematoma starts to form (see section 4-3). Figure 11 represents the CSF circulation in the head. CSF also plays an important biochemical role in sensing blood pH and carbon dioxide levels (Guyton, 2006). CSF is very sensitive to changes in pH, which is related to the levels of carbon dioxide and oxygen in the blood. In this way the brain is informed of these gas levels and can trigger physiological compensations if necessary.

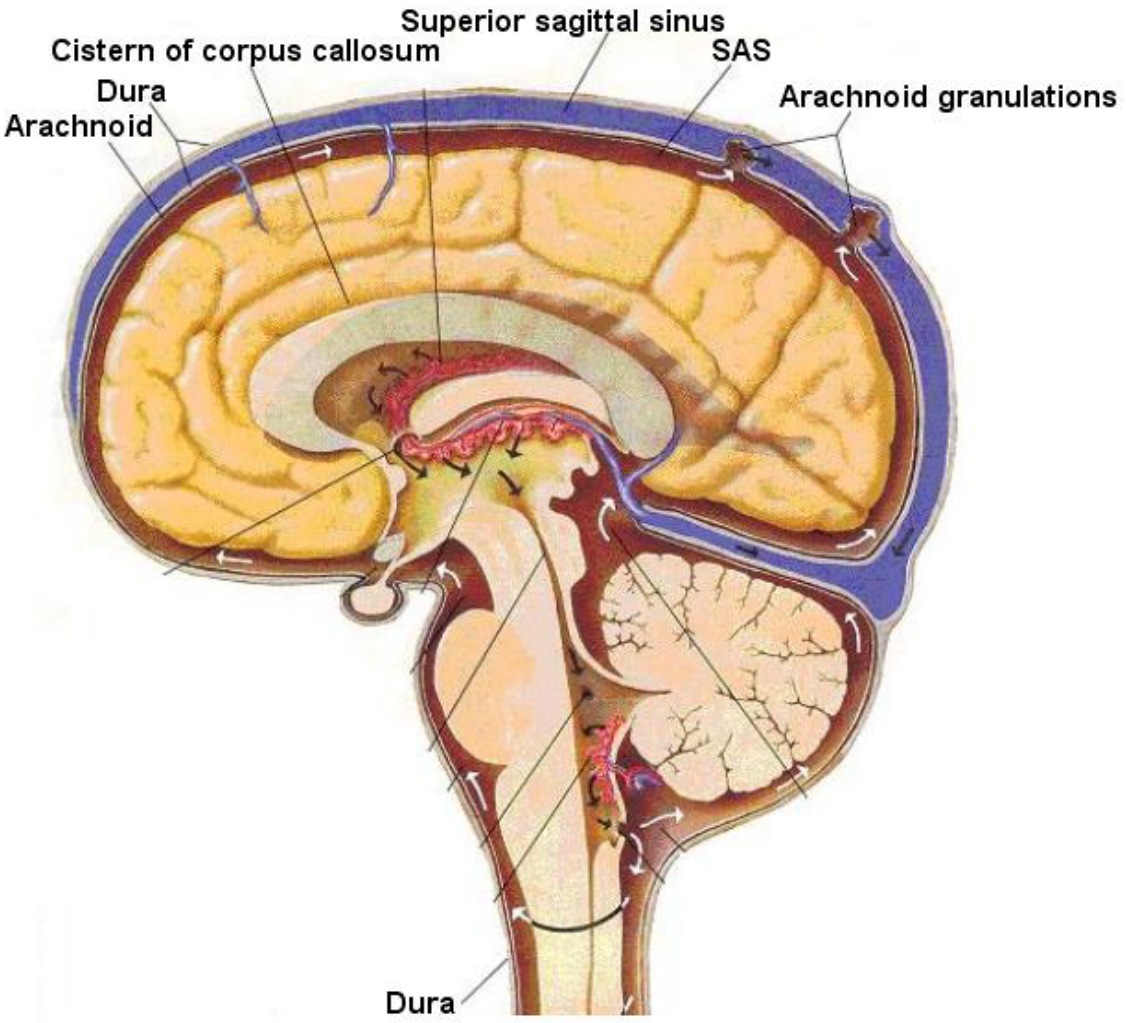

Figure 11. CSF is formed in ventricles and absorbed into the sinuses through arachnoid villi (Netter 1997). CSF is formed in ventricles by the choroid plexus. This clear fluid circulates through the ventricles from the lateral ventricles (left and right) to the third and then through the cerebral aqueduct into the fourth ventricle. Canals in the fourth ventricle (such as the foramen of Luschka shown here) allow CSF to communicate with the subarachnoid space. Eventually the CSF is absorbed into the venous sinuses through arachnoid granulations. Notice the bridging veins crossing the subarachnoid space (Netter 1997).

2-6 Blood Flow in the Brain

The brain is a highly blood consuming organ. The weight of the brain is only 2% of the total human body, yet it receives 20% of the resting cardiac output (Guyton, 2006). After just a few minutes without oxygen, irreversible brain damage occurs. To meet such high metabolic demands, blood vessels form a very dense meshwork in the brain. No neuron is more than about 100μm from a capillary (Nolte, 1999). The two main blood supplies to the brain is derived the internal carotid arteries (left and right) and the vertebral arteries (left and right). These arteries ascend vertically in the neck to their cranial cavity entrances and then divide into narrower branches called arterioles. The entrances for the internal carotid arteries are called the carotid canals and are located in the temporal bones (Moore, 1999). Upon entering the cavity the two carotid arteries make 180° turns and eventually join together in a circle of inter-connected arteries, located at the base of the brain, called the cerebral arterial circle (circle of Willis). The branches from this system supply most of the cerebrum. The two vertebral arteries fuse together and form the basilar artery at junction between the pons and medulla (Nolte, 1999). The basilar artery joins the cerebral arterial circle as well. Branches from this system supply the brainstem, cerebellum and the rest of the cerebrum. All primary branches, from both systems, are located in the SAS.

2-7 Venous Drainage

As mentioned above, the dural sinuses are responsible for venous drainage of the brain. These valveless sinuses are formed between two layers of dura mater at specific dural infoldings. They drain the deoxygenated blood out of the brain, into the internal jugular vein which courses down the neck and eventually back to the heart (Guyton, 2006). The superior cortical veins, from the brain tissue, transverse the SAS and then the inner dura mater membrane to become continuous with these sinuses (Nolte, 1999). These veins, which transverse the SAS, are called bridging veins. Bridging veins can be seen transversing the subarachnoid space in Figure 11. Bridging veins are thin-walled, due to the absence of muscular tissue, and hence tear easily when subjected to dynamic forces (Blumenfeld, 2002). The parasagittal bridging veins are those emptying into the superior sagittal sinus, the most superior of all the venous sinuses (see Figures 12 and 13). There is usually a free segment of vein, 10 to 20 mm in length, in the subdural space between the vein's exit from its bed in the SAS and its entrance into the sinus (Blumenfeld, 2002). Shear forces that tear the wall of these bridging veins causes ASDH (acute subdural hematoma), a pathological condition in which blood fills the potential space between the dura and arachnoid mater. In this potentially lethal condition the excess fluid pressure can compress nerves and blood vessels giving a variety of clinical symptoms (Blumenfeld, 2006).

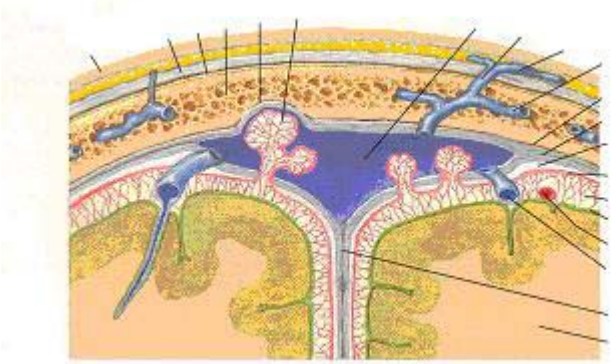

(a)

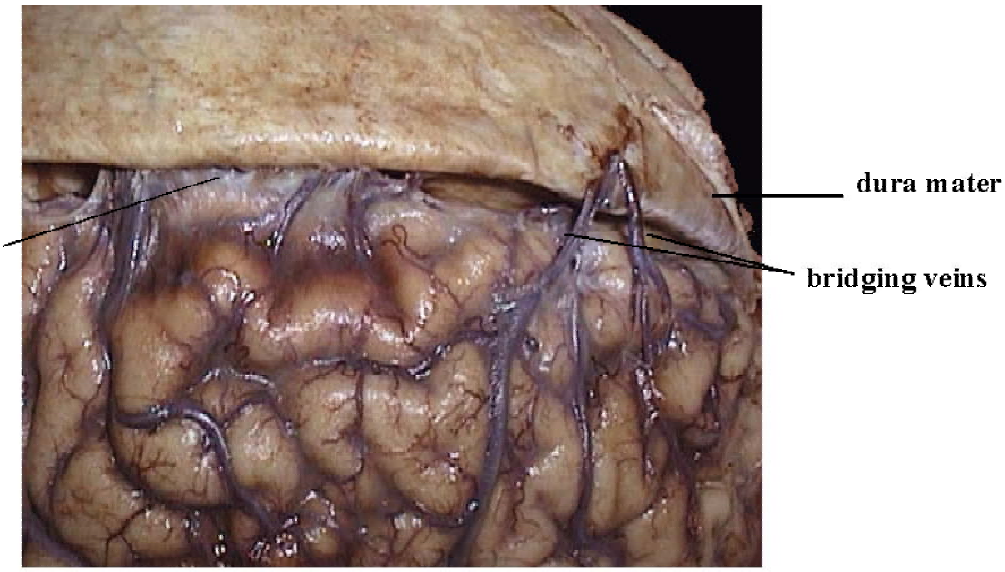

(b)

Figure 12- a) Bridging veins emptying into the superior sagittal sinus (Netter 1997). Cerebral veins, such as the superior cerebral vein shown here, transverse the subarachnoid space to reach the subdural space and enter the venous sinuses. These are called bridging veins. In this cartoon illustration the superior cerebral bridging vein is shown emptying into superior sagittal sinus. Also shown are the arachnoid granulations, where CSF enters into the venous blood. Notice the extensive trabeculae (shown in red) of the subarachnoid space (Netter 1997).

b) Cadaver photograph of bridging veins. In this image the dura mater if pulled back so that bridging veins can be seen piercing through the arachnoid mater into the subdural potential space. In ASDH these veins are torn, due to the relative motion between skull and brain, causing blood to fill the subdural space (www-medlib.med.utah.edu).

The sinuses located in the upper back region of the skull are the superior sagittal, inferior sagittal, straight, occipital and the two transverse sinuses (Figure 13). The superior sagittal sinus runs anterior to posterior. It is triangular in section, narrow in front and increases in size as it courses backwards. Most superficial veins, which collect blood from the cerebral surface, empty into the superior sagittal sinus through the bridging veins, as discussed above. These bridging veins, for the most part, run obliquely forward and open at the back part of the sinus (Nolte, 1999). Arachnoid granulations project into these sinuses allowing the regulated exchange of venous blood and CSF shown in Figure 12. At its posterior end, the superior sagittal sinus becomes dilated and gives rise to one of the two transverse sinuses (usually the right). The location of this switch is called the confluence of sinuses and is located near the bony internal occipital protuberance (Netter, 1997).

The transverse sinuses begin posteriorly, at the confluence of sinuses. Each transverse sinus passes laterally and anterior, tracing a convex up curvature. They pass through the temporal bones and then course downward and medial to reach the jugular foramen and become continuous with the internal jugular veins. The two transverse sinuses are frequently of unequal size with the larger one being the one that arose directly from the superior sagittal sinus (Nolte, 1999). They increase in size as they course forward.

The straight sinus bridges the superior and inferior sagittal sinuses (Figure 13). The great cerebral vein and superior cerebellar vein empty into the straight sinus. The straight sinus is triangular in cross-section and decreases in size as it

courses anteriorly. At its anterior end it connects with the inferior sagittal sinus (Figure 13). The occipital sinus is the smallest one. It commences at the foramen magnum (the large hole in the occipital bone in which the brainstem passes through), gives rise to several branches, and eventually joins the confluence of sinuses (Netter, 1997).

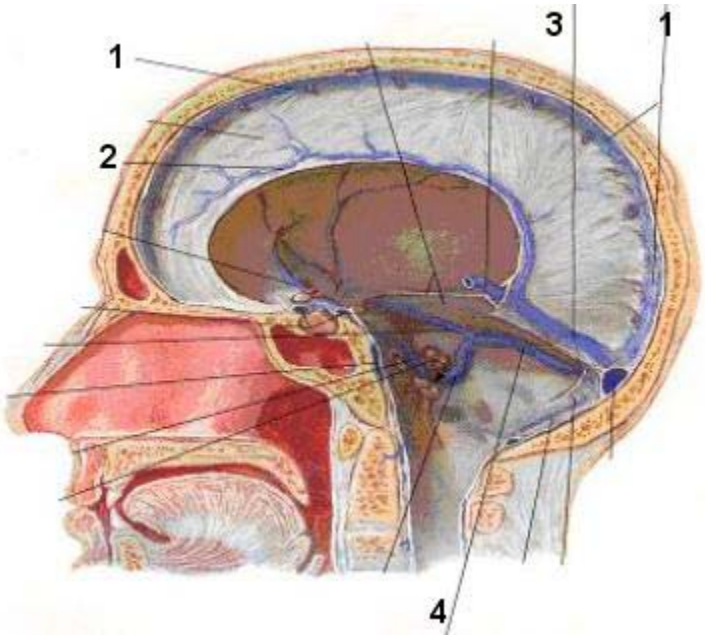

Figure 13- Dural venous sinuses. The main sinuses to notice are, 1) the superior sagittal sinus, which drain most of the bridging veins, 2) the inferior sagittal sinus, running a parallel course more inferior; 3) the straight sinus which connects the superior and inferior sagittal sinuses and 4) the transverse sinus running in the lateral part of the skull. The blood from all of these sinuses eventually drains into the internal jugular vein of the neck through jugular foramen of the skull shown here (Netter 1997).

3- LITERATURE REVIEW

Many research groups have investigated head injury through experimental, physical and numerical models. In this section a review of these works, in four categories, are presented: 1) experimental (including experiments on human cadavers and sub-human primates), 2) analytical models (including head impact modeling and validity), 3) physical models and 4) finite element models. Papers in each category are described below.

3-1 Experimental Studies

3-1-1 Abel et al. 1978

Abel et al. 1978, in a study evaluated the post-traumatic effects of applying angular acceleration to the heads of 40 Rhesus monkeys. The heads of the monkeys were subjected to a sagittal plane angular acceleration. The study was done to gain insights into the mechanical causes of loss of consciousness, cerebral concussion and ASDH. A maximum tangential acceleration of $7X10^3$ m/sec^2 was reported as the boundary separating the presence and absence of ASDH. The authors of this study concluded that the angular acceleration alone does not account for the incidence of concussion as predicted by Holbourn theory (Holbourn 1945). Both rotational and translational phenomena are important considerations for the occurrence of concussion and ASDH. The authors sacrificed 26 animals for pathological purposes, and their result showed that subdural hematoma (SDH) is more severe than subarachnoid hematoma (SAH).The results suggested that the governing mechanics are non-linear. Even

during the time course of the insult the mechanical coupling between the brain and the skull changes. Deformation mechanics are required for proper modeling. Therefore rigid structural models for the brain and the skull are not good assumptions. This limits the information that can be gained from experimental results. Simulations can pick up where experiments leave off and acquire more detailed insights for more accurate predictions.

3-1-2 Nahum et al. 1977

Another experiment done by Nahum et al. 1977, measured intracranial pressures during human cadaver head impacts. By varying the initial velocity of the impact (or impact magnitude), duration of the applied load and the mass of the impactor, these researchers measured the input force, changes in skull acceleration and in vivo intracranial pressure with time during the impact. These researchers performed two series of experiments on cadavers. Series I consisted of 8 individual experiments and series II, 7 multiple sequential impacts on a single specimen. Pressure changes were measured with transducers placed at the frontal, parietal and occipital bones as well as the posterior fossa and carotid siphon. One of the interesting results of this experiment was the linear relationship found between the peak pressure at the given locations and skull acceleration. All locations tested were found to be linear but with different slopes. The steepest slope was from the frontal location suggesting that the pressure in this region is most sensitive to head acceleration. This discovery simplifies the study of brain response during impact and provides data for model validations.

3-1-3 Lee and Haut 1989

Lee and Haut studied the effect of strain rate on tensile failure properties of human parasagittal bridging veins. The authors placed the cerebral parasagittal bridging veins, from eight unembalmed human cadavers, into a servo-controlled hydraulic testing machine. They stretched the specimens beyond failure under high and low strain rate conditions. They concluded that strain rate has no statistically significant effect on the measured failure properties (ultimate strain and stress). This is in contradiction with the hypothesis that the sensitivity of the ultimate strain of bridging veins to strain rate explains the acceleration tolerance data for SDH in primates (Gennarelli and Thibault 1982).

The most interesting result of their study is that the parasagittal bridging veins are more vulnerable to rupture in occipital rather than frontal impacts. They supported their idea by mentioning that most human parasagittal bridging veins have been documented to drain frontally into the superior sagittal sinus (O'Connell 1934, Copra and Anderson 1984 and Oka et al. 1985). For a frontal impact these veins are the first to be subjected to compression. For the occipital impact, they stretch immediately.

3-1-4 Monson et al. 2000, 2003

Monson et al. (2000, 2003) studied the static the dynamic material properties of cortical arteries and veins from the temporal lobes. They performed their experiment on 11 arteries and 11 veins from cadavers. They noticed a

significant difference between the material properties of arteries and veins, but not much difference between the static and dynamic properties.

The cortical arteries fail at approximately twice the stress level of cortical veins and about half the stretch. The venous data (bridging veins) properties from Lee and Haut 1989 differ significantly from Monson and his colleagues study. Lee and Haut 1989 found the bridging veins to be stiffer. These differences were likely due to the different specimen preparations.

3-1-5 Hardy et al. 2001 and Al-Bsharat et al. 1999

Using neutral density technology and high-speed biplanar X-ray, Hardy et al. measured the relative motion of the brain with respect to skull in human cadaver heads. A blunt head impact was applied to human cadavers and X-ray snap shots of the specimen's heads were taken to develop the 3D trajectory of the brain relative to the skull. They observed that brain undergoes displacement relative to skull on the order if +/- 5 mm, when impacted with an angular speed of 17 to 22 rad/s. Although such studies cannot be directly applied to real human head injuries, the mechanical responses observed can be used to develop finite-element models and further injury tolerance criteria.

In addition to obtaining experimental data Al-Bsharat et al. modified a finite-element model to better simulate this relative motion based on the trends observed in the experimental models. In the modified model a sliding element was introduced to simulate the interaction between CSF (modeled as a layer material with a low shear modulus). Good agreement between experimental and

computational results was obtained, thus validating the use of finite-element modeling for head impacts.

3-1-6 Miller's Group

A series of insightful studies was performed by Miller et al. in determining a constitutive model for the brain tissue as well as mechanical properties of brain tissue. These include Miller and Chinzei 1997, Miller 1999, Miller et al. 2000 and Miller and Chinzei 2002. They observed brain tissue responds differently under compression and tension. They proposed a hyper viscoelastic constitutive model, which did not account for blood and CSF. This model was able to account for the strong stress/strain rate dependence.

3-1-7 Gennarelli et al. 1982

The authors experimentally induced subdural hematomas in Rhesus monkeys by delivering short (on the order of milliseconds) rotational insults. Acceleration time histories were recorded and a mathematical model describing the biomechanics of ASDH was constructed. These researchers highlighted the importance of the pulse duration in causing ASDH. For a given deceleration of the head, the shorter the impact pulse duration (thus a larger impulse), the more likely ASDH is to occur. These important experiments helped to explain why ASDHs are observed more frequently in patients injured form a blow or fall (short duration head impacts) as opposed to an automobile accident (where the

occupants usually hit the dashboard, which deforms thus prolonging the impact duration).

3-1-8 Other Works On Sub-Human Primates

Ommaya et al. 1967 performed experiments on concussion-producing head rotations on the Rhesus monkeys. They developed a tolerance criterion for concussion in Rhesus monkeys. Ono et al. 1980, conducted three sets of experiments (translational acceleration, rotational acceleration and both at the same time) on live monkeys. They observed that translation alone cannot cause severe head injury. Rotational acceleration produced a higher rate of brain damage than translational due to there being more deformation of the skull and higher shear strains.

3-1-9 Other Cadaver Experiments

Lowenhielm (1974) studied the strain tolerance of the bridging veins. The tolerance criterion they developed was an angular acceleration with the threshold of 4500 rad /s2 or a threshold change in angular velocity of 50 rad /s.

Trosseille et al. (1992) carried out a series of cadaveric head impact tests to validate their FE model. The cadavers were suspended in a sitting position and were impacted by a 23.4 kg impactor at a velocity of 7 m/s. Intracranial and ventricular pressures were measured.

3-2 Analytical Studies

Analytical studies include the development of mathematical modeling as they relate the kinetic and kinematics parameters of impact to head injury. These studies can be used to guide and refine finite element models.

3-2-1 Anzelius, 1943

In his eloquent mathematical model, Anzelius determined the change of pressure with time within an inviscid liquid enclosed in a spherical vessel when subjected to a point impact on its surface. The results of this model showed that shortly after the impact a maximum pressure is reached near the center of the sphere with the same order of magnitude as the initial impact pressure. This maximum pressure is due to the superposition of two pressure waves originating at the counterpoles of the rigid sphere. The significance of this result in relation to head injury is that similar pressure waves are generated in the brain as a result of head impacts and these could cause brain damage (Engin, et. al. 1969).

3-2-2 Engin et al. 1969

The authors considered the viscoelastic behavior of the brain tissue in their mathematical model. With the assumption of steady-state oscillations and the brain being an incompressible material, this work extends the Anzelius model and looks at the viscoelastic response to head impacts (Anzelius 1943). Their theoretical analysis was based on the results from experimental studies on

Rhesus monkeys (Fallenstein et al. 1969). Their model determined the shear modulus of the brain as a function of oscillation frequency.

3-2-3 Newman 1980

In this study the Head Injury Criteria (HIC) was critically analyzed and reviewed. It was concluded that there is no general correlation between internal head injury and measurable kinematics. This conclusion lead to the invalidation of the anthropomorphic test dummies being used at the time to simulate human head injuries in automobile accidents. This study highlighted the need for better, more physiologically relevant, methods to simulate human head injury.

3-2-4 Newman et al. 2000

This study proposed a new hypothesis in which the threshold for head injury is related to the rate of change of kinetic energy (power). Thus, the maximum power input to the head can serve as the index to determine the probability of head injury. Based on this research a new and improved head injury assessment function was proposed that incorporated the scalar sum power for all six degrees of freedom. Combining this function with finite element models of brain could make the function more sensitive to the direction of impact.

3-2-5 Young 2003

Young's analytical model of blunt head injury simulated the head as a fluid-filled shell with geometric and material properties similar to those of the human head. This study is distinguished among other analytical and FE models in that the author focused on the dynamic contact problem in order to predict global impact characteristics. This is in contrast to previous models in which experimentally determined or assumed force-time histories are applied. Using this approach only global impact parameters can be predicted. One interesting conclusion from this study is that the fluid bulk modulus has no effect on the pressure response of the fluid-filled shells. Another conclusion from this study is that the peak pressure response is not a good criterion for head injury, especially for impacts with lower mass projectiles. This agrees with the general conclusion that injury correlates better with strain and strain rates rather than pressure.

3-3 Physical Models

Physical models have long been used to investigate the biomechanics of head impact and brain injury in the human and other animals. These studies help to compensate for the lack of experimental data. Physical models, in combination with studies on mechanical property of tissues are useful for simulated brain deformations. Results from impacts on physical models can also be used to refine and/or validate finite element models of brain displacement and deformations upon impact.

3-3-1 Margulies et al. 1990

In this study human and baboon skulls filled with surrogate brain tissue were subjected to rotational impacts. The surrogate brain tissue was a gel with a Young's modulus within the range of reported values for the brain (Margulies, 1987). The resulting deformations were compared to those found on autopsies and animal studies. Rotational impacts were used here because earlier physical models by Holbourn in 1943 (Holbourn 1943) determined that rotational impacts caused the greatest amount of deformation.

3-3-2 Viano et al. 1997

These researchers developed a parasagittal physical brain model that included a thin liquid paraffin layer for CSF. The inclusion of CSF caused a more complicated pattern of displacement and deformation.

3-3-3 Ivarsson et al. 2000

This study employs physical models to determine the role of the brain ventricles during rotational impacts. They concluded that the lateral ventricles (in the cerebral hemispheres) played a role in relieving strain and may act as natural protectors against brain injuries including ASDH.

3-3-4 Bradshaw et al. 2001

The authors modeled the cerebrum with silicone gel, CSF with paraffin and trabeculae with elastic membranes. The use of these elastic trabeculae reduced the local strains of the brain tissue. ASDH and DAI (diffuse axonal injury) were simulated with their physical model. When impacts in the coronal plane were used they found that bridging veins were more likely to tear on the contra-lateral side of their model. Lastly these authors found a positive correlation between the presence of brain sulci and the incidence of ASDH. They suggested that sulci decrease the acceleration threshold for ASDH.

3-4 Numerical Studies using FE Method

3-4-1 Nahum et al. 1977

To simulate the results of their own experiment, Nahum et al. 1977 constructed a three-dimensional linear FEM model of the human brain. The model describes the response of the skull to blunt impact. Different bulk moduli were used to account for pressure responses of the brain. This parameter provides incompressibility and was varied to best fit the data. Incompressibility reduces the correlation between experiments and simulations. A 20% damping factor for the brain was found to significantly improve the correlation.

3-4-2 Huang et al. 1999

Huang et al. 1999 designed a 3D model of the entire human head to examine the thresholds of angular and tangential acceleration required to tear the bridging veins. The CSF was not explicitly included in the model. Backwards and forwards rotations about the neck (using the first cervical vertebra as a pivot point), pure rotation about the center of mass of the brain and pure translation were tested and compared. Results were validated against Nahum experiments (described above).

The results also computed the tensile and compressive deformations of the bridging veins directly branching from the superior sagittal sinus. Occipital impacts were used because the veins affected by frontal impacts are rare in humans. Upon an occipital impact, the maximum stretch deformation occurred in veins draining anteriorly into the sinus at an angle of about 40 degrees with respect to the sinus. The maximum compression occurred in veins that drained posteriorly at about the same angle.

Strain-time relationships due to occipital impacts were also computed for the three types of motion described. Pure rotational motion caused the greatest amount of strain. Rotation is, therefore, an important factor for causing ASDH. Rotational acceleration contributes to brain motion to a greater degree than does translational motion. This is because the brain tissue has a very low shear modulus as compared to its bulk modulus. This is why the main focus in the current study is pure rotation.

One interesting result from this model showed that when an occipital impact was simulated by forward rotation of the head about the first cervical vertebra, the motion of the brain lagged that of the skull. However, the opposite was found when the frontal impact was simulated by backward rotation. Since the CSF did not play a role in these simulations, it will be instructive to compare these results to a 3D model that accounts for CSF. If a difference in the amplitude of this relative motion between brain and skull occurs due to the presence of CSF and the SAS trabeculae, it can be concluded that CSF plays an important role. Furthermore, the fact that there was a difference in the relative motion for occipital and frontal impacts gives more data for comparison. With models of the current study the CSF response can be determined. It is expected that if the CSF and SAS are properly modeled, the brain will lag the skull under both conditions.

The main conclusion of this study is that both the orientation of the veins as well as the direction and location of the impact play a role in causing ASDH. The pattern and magnitude of brain displacements (relative to the skull) vary because the structural properties of the head are not uniform in all directions. Currently, there is no definitive data linking the injury severity with impact direction and location.

3-4-3 Wayne State University Brain Injury Model (WSUBIM)

The Wayne State University brain injury model (WSUBIM) has been developed and revised over the last several years (Ruan et al. 1993, Zhou et al.

1995, Al-Bsharat et al. 1999, Zhang et al. 2001). This is a 3D FEM model of the human head that has been validated by experimental data published by Nahum et al. 1977. In the latest, 2001, version of the model improvements were made so that the model was able to simulate direct and indirect impacts with combined translation and rotational accelerations of the head. The main advantages of this model are the simulations of bone fractures in the face and skull.

The CSF and subarachnoid trabeculae were simulated in this model with solid elements. The material properties for these solid elements were the bulk modulus of water and a very low shear modulus for better representation of the fluid nature of the area. An additional frictionless sliding interface between the outer arachnoid and inner dural membranes was incorporated to better mimic real anatomy. This friction-free slip condition prevented separation between the brain and dura mater. Separation was not allowed so that tensile forces could be transmitted between the two contact surfaces. Due to these modifications, the model was better able to match intracranial pressure values obtained experimentally.

The ventricles were modeled as solid elements with shear modulus lower than the CSF. The calculated pressures matched well with intracranial and ventricular values obtained from experiments for the first 14ms. After 14ms the simulated pressures dropped to zero while experimental values remained high. The authors claimed that this discrepancy was due to the fact that the fluid-filled ventricles were modeled as solid elements.

Modeling with fluid elements should, therefore, better match experiments. Solid modeling cannot simulate the mechanical and thermodynamic properties of CSF. This is especially true when very low negative pressures are reached. Negative pressures have been observed experimentally but their role in head injury cannot be addressed without the proper fluid mechanical model.

Another computational study at Wayne State (Zhang et al. 2002) incorporated vasculature to study the role of blood vessels in the mechanical response of the brain. Blood vessels make up a significant fraction of total brain mass. The compliance of blood vessels is less than brain tissue and hence the mechanical properties of the entire structure are significantly altered by their presence. A simplified 2D model was constructed because of the technical difficulties of constructing an arterial tree into a 3D mesh. The conclusion was that blood vessels significantly decrease deformations of the brain with a minimal affect on intracranial pressure.

The major cerebral arteries were modeled as solid elements with a characteristic cross-sectional area of $2.2mm^2$. When modeling blood vessels in the brain several things have to be considered. Blood vessels exhibit non-linear stress-strain behavior. Experiments have indicated that, cranial arteries are significantly stiffer than extracranial vessels and they fail at approximately twice the stress but half the stretch of other arteries and veins. These arteries exhibit high compliance (low stress) at low levels of stretch and an increased stiffness at high levels of stretch.

In the future, to improve the model, the pia mater will be included. Blood vessel walls were modeled as being directly connected to the brain tissue. This is because nothing is currently known about the mechanical interactions between vessel walls and brain tissue. This may have added greater stiffness to the model than what is physiologically relevant.

Principal strain responses to rotational and linear loading were tested. The results showed an overall 37% reduction in the maximum principal strain with the introduction of blood vessels. Shear strain in the x-y plane was also tested for both rotational and linear loading. The results showed a 33% increase in shear strain due to the presence of blood vessels. Finally, intracranial pressure was compared and it was found that blood vessels don't affect intracranial pressure in linear loading but have a small decrease in rotational loading.

3-4-4 Other Mathematical Models

Lowenhielm (1975) studied the gliding contusion, which is a sub-cortical prevascular bleeding. In 1982, Gennarelli and Tribal developed a mathematical model to establish a tolerance criterion for the occurrence of ASDH. Another FE study of the head, analyzed the effect of inertial load, Tong et. al. 1989. In 1990, Nagashima and co-workers constructed a 2D model of vasogenic brain edema. They incorporated the physical properties of brain tissue and CSF. Chu et al. 1994, carried out a finite element analysis through a 2D model, to study the mechanism of cerebral contusion. Another 3D FE model of the human brain was conducted by DiMasi et al. 1995. They tested several head impact scenarios.

Due to the difficulties of modeling soft biological tissues, Mendis et al. 1995, discussed the use of a large strain constitutive relationship. Ruan and Prasad 1995, coupled a skull-brain finite element model of the human head with a multilink rigid body model of the Hybrid III dummy. In 1995, Willinger et al. performed a vibration analysis of the head and demonstrated that the head is not a solid non-deformable body, but a complex structure including deformable elements. To model the direct cortical impact experiments of Lighthall in 1988 and Lighthall et. al. in 1989, Ueno et al. 1995, built a 3D finite element model of the brain. Turquier et al. 1996, validated their 3D head model against five cadaver tests published by Trosseille et al. 1992. Nishimoto and Murakami in 1998 developed a 2D FE model of the head to analyze the occurrence of DAI, when direct impacts are applied. Miller and his group in 1999 developed a FE model to predict TBI. They validated their model with the experimental data from the animal study of Meaney et al. 1995. Anderson et al. 1999, coupled an experimental analysis with a numerical model of the sheep's head to evaluate the mechanism of DAI. In 1999, Willinger and his colleagues validated a 3D FEM against two sets of experimental data available in the literature (Nahum et al. 1977 and Trosseille et al. 1992).

4- TYPES OF HEAD/BRAIN INJURIES

Injuries to the cranial contents may result from a bone of the skull fracturing and being pushed inward (a depressed fracture), from the brain impacting the interior of the skull, or from the inertial stressing of the brain, i.e., shear, tension and/or compression. The resulting injuries reflect the diversity, and in some instance the subtlety, of the brain function, and may present a rather bewildering array of head injury consequences.

Head injuries are usually categorized into three major sets of criteria. These criteria are based on whether the injuries were due to sudden head movement, per se, or to head impact, whether the resulting lesion was focal (i.e., fairly localized) or diffuse (rather distributed), or whether the injury was primary or secondary. Primary refers to an injury, which occurs at the time of some initial injury-producing event, i.e., at the time of head impact or abrupt motion. In contrast to this, secondary refers to an injury which also results from some initial injury-producing event, but which does not develop until somewhat later.

Clinically there are four major categories of head injury: concussion, contusion, hematoma, and DAI (Diffuse Axonal Injury). Although these four categories overlap somewhat and therefore do not ideally partition head injury possibilities, the four categories provide a very useful basis for this research.

4-1 Concussion

Concussion may be defined as the loss of consciousness or as a diminution of mental process immediately following trauma. Typically, a

concussion will not be present as a localized brain injury, occurring at a single, identifiable site, and so, concussion is often referred to as a diffuse brain injury. Concussion is also included in the broad category of “Closed Head Injury” (CHI).

A major defining characteristic of concussion, which helps to distinguish it from other types of unconsciousness and losses of mental function, is the absence of a post-trauma “waiting period.” That is, concussion occurs at the instant of trauma rather than shortly thereafter. In general, the severity of a concussion is characterized by the duration of loss of consciousness (LOC).

4-2 Contusion

Brain contusion refers to a bruising of part of the brain, frequently the cortex (outer layer). A primary (impact) contusion may result from either head contact, or head acceleration without contact, and a secondary contusion may result from brain movement within the skull as the result of pathology secondary to the trauma. If due to head contact, the contusion frequently occurs at the site of impact, and is referred to as a “coup” injury. If, however, the impact also causes skull fracture at that site, the contusion may also be labeled a “fracture contusion.” A contusion may also occur opposite from the site of initial impact (or injury), in which case is referred to as “countercoup.” This type of injury is thought to occur due to brain movement with respect to skull. For example in the event of a frontal vehicle impact, the occupant’s head will move forward and then stop, but the brain may continue to move forward in its fluid bath, until it strikes the interior surface of the front part of the skull (coup injury), and then may bounce

backward, thereby striking the interior surface of the rear part of the skull (countercoup injury). Thus, either the front of the brain or the back of the brain (or both) may be injured by a single frontal impact.

4-3 Hematoma

Hematoma is commonly caused by a tear in a blood vessel, which leads to bleeding (hemorrhage) in the tissue. One of the most common methods of classifying a hematoma is based on its location with respect to meninges. More specifically, just about all classifications incorporate the distinction of whether the hematoma is outside (i.e., superficial to) or inside (i.e., deep to) the dura mater.

Figure 2 shows a simplified schematic of the structures of the head, including scalp, skull, meninges and brain. Intracranial hematomas occurring outside the dura, i.e., between dura and skull, are classified as epidural (extradural), while those within the dura are classified as intradural. The intradural category is further subdivided into subdural and subarachnoid. Generally, subdural is used to refer only to the region immediately below the dura (i.e., between dura and arachnoid) even though, in a literal sense, the other meninges, the space between them, and the brain itself are all subdural. Subarachnoid is used to refer on the region below the arachnoid mater, i.e., subarachnoid space (SAS).

The middle membrane, the arachnoid, is rather flexible, and there exists a potential space between the arachnoid and dura. This separation, however, should not be thought of as being a space in the sense of being empty. The dura

and arachnoid may be readily separated by a hematoma or other accumulation between them, at which point the potential space becomes an actual space.

The distinction between epidural and subdural has clinical significance. About 80% of epidural hematomas are associated with an impact to, and a fracture of, the temporoparietal region of the skull, as well as the tear of an underlying meningeal artery. It should be noted that epidural hematoma, although generally due to head contact, does not generally occur at the time of impact (primary), but rather is classified as secondary to impact. In fact, Hematomas are sometimes classified according to how long after the initial injury they become clinically evident. Typically, symptoms which develop within one day are considered **acute**, one day to two weeks, **sub-acute**, and longer than two weeks, **chronic.**

In contrast to the epidural hematoma, a subdural hematoma is more likely to be due to non-impact head trauma (deceleration trauma), which causes tearing of veins, which traverse the subdural space (referred to as parasagittal bridging veins, or just bridging veins).

One of the major functions of the CSF is to provide a buffer if a hematoma starts to form. The CSF is one of the three significant components if the intracranial volume (i.e., the intracranial contents). The other two are the brain and the blood. The interaction of these three is described by the Monro-Kellie Doctrine, which states, basically, that as long as the cranium remains intact, the total volume of the components will remain constant. It indicates that if there is an increase in volume of blood in cranium (such as would occur from intracranial

bleeding), the volume of CSF containing region (subarachnoid space) will decrease to accommodate it. As the hematoma increases in size, the SAS volume decreases, and these results in an increase in Intracranial Pressure (ICP), which is the pressure of the CSF, and not any other pressure within the cranium.

Two terms need to be explained: the cerebral perfusion pressure (CPP) and the cerebral blood flow (CBF). The CPP is basically the pressure gradient across the brain, i.e., the difference between the arterial pressure of the blood entering the brain (at the subarachnoid region) and the venous pressure of the blood leaving the brain (from the subarachnoid region). The CBF is the measure of the blood flowing to the brain per unit of time. It is typically about 750 ml/min for the entire brain, but can vary significantly for various sites within the brain. Therefore, the CPP is essentially the driving force for the CBF, analogous to any fluid flowing across pressure gradient, or an electric current flowing across the potential gradient. As mentioned above, hematoma formation can lead to an increase of ICP. Elevated ICP results in a decrease in CPP, which, in turn, results in decrease in CBF. It is the decrease in CBF, which results in neuronal death.

4-4 Diffuse Axonal Injury (DAI)

DAI is thought to result typically from extreme brain deformation and shear injury. Although DAI was originally used to describe a primary injury, it is sometimes also applied to injury, which results secondary to trauma. Regardless

of which category may ultimately be accepted, it is important to note that this is a very severe injury.

DAI may be characterized as mild, moderate, or severe, depending on the duration of associated coma and the presence or absence of signs of brainstem dysfunction. The least severe DAI, the so-called mild version, is characterized by coma of at least six hours (and as much as 24 hours) duration and has a fatality rate of about 15%. However, although survival is rather likely, some type of residual neurological deficit (i.e., some long term functional loss) is not uncommon. Moderate and severe DAI are both characterized by coma of more than 24 hours. Moderate DAI is associated with about 25% fatality. Severe DAI, in addition to a coma period of more than 24 hours, is associated with persistent brainstem signs. Severe DAI is associated with a rate of good recovery of only about 15%. Severe DAI also has associated with it a fatality rate of about 50%.

5- DYNAMIC SIMULATION OF HEAD INJURY

To quantify the real life blunt head impact forces and acceleration an accident involving the rider of a fork-lift truck has been simulated in this section. Specifically, an operator is assumed to ride the fork-lift truck and is tipped over or is fallen off a dock. Initially the truck and the operator are modeled as a rigid body and were analyzed dynamically. The purpose of this model was to obtain parameters relevant to head impact injuries and compare the results with the experimental results (Zoghi-Moghadam et. al. 2002(a)).

5-1 Experimental Testing Procedure

Experimental testing to measure operator injury potential variables during simulated tip-over (TO) and off-the-dock (OTD) accidents was performed by Crown Corporation, manufacturer of stand-up lift trucks (Crown Corp. New Berman, OH) using a Hybrid III, 50^{th} percentile male, pedestrian-modified ATD.

Right tip-over (RTO) and left tip-over (LTO) tests were performed slowly tipping the fork-lift trucks until their points of instability were reached and then allowing them to fall to the concrete covered ground. The OTD testing consisted of forks-trailing (OTD-FT) and forks-leading (OTD-FL) tests. In the forks-trailing tests, forward motion toward the dock edge was initiated by pushing the truck's with brakes disengaged at a speed of 3.2 to 4.8 km/h. In the forks-leading tests, the front wheels of the trucks were placed on a flat bed trailer parked at the dock. Motion was initiated by trailer pull away at approximately 4.8 km/h. The dock

height was 1.25 m. The concrete ramp below the dock had an upslope away from the base of the dock with a grade of 8.3 percent.

The ATD was instrumented with linear accelerometers positioned along each of three orthogonal axes in the head and in the thoracic spine, load cells for neck and lumbar spine loads, and a chest displacement transducer. The knee joints of the ATD were tightened so that it would stand by itself and the shoulder, elbow and hand joints were tightened to prevent movement under “one-g.” After calibration, the ATD was positioned in the operator compartment of the truck being tested with its hands taped to the controls. The operator compartment door was closed and latched. The truck was instrumented with accelerometers positioned along its three axes. The truck and ATD motions were videotaped and filmed with high-speed cameras. The acceleration, load and displacement signals were conditioned and filtered and then digitally recorded.

5-2 The Biodynamic Model

A multibody biodynamic model or simulation “mannequin” for the Hybrid III ATD and accurate rigid body SUR models were implemented in the mechanical event simulation software, MSC Visual Nastran Desktop 4D, (2002). The mechanics of rigid body collisions in this software are modeled through coefficients of restitution. Calibration of the biodynamic model and the capabilities and limitations of this type of simulation are discussed in Zoghi-Moghadam et al. (2002b).

The ATD simulation mannequin was a 50th percentile male, anthropomorphic model with multiple rigid body segments created by solid modeling in Pro/Engineer software, (2001). In its implementation in the simulation software, realistic physiological ranges of motion for joints were employed throughout. Except for the head and neck joints, all the joints contained an internal friction force, the coefficient of which was selected such that, analogous to the ATD, the body segment would not move when subjected to one-g acceleration, representing a standing posture.

The ATD was validated against a Hybrid III experimental test performed by Steffan et al. (2001). To validate the head and neck model, a simulation with the mannequin model restrained by a seat belt on a sled test undergoing the same deceleration as of the Hybrid III experimental test, reported in Steffan et. al. 2001 was performed (Figure 14). Specifically, as shown in Figure 15, the head acceleration of the model was approximately matched with the results of Steffan et. al. 2001, to determine the spring and damping characteristics of the head and neck connections.

For predominately forward or backward impact simulations, the neck/torso joint had flexion-extension with spring/damper connection. The head/neck (occipital condyle) joint had lateral flexion with spring/damper connection. The combinations of spring and damping coefficients for these two connections were modeled as being approximately the same, Zoghi-Moghadam (2002b). For predominately side impact simulations the neck/torso and head/neck joint

mobility connections were interchanged to permit more realistic lateral head motion response. Also, for simulations involving direct but oblique impact to the shoulder, rigid shoulder width was adjusted to compensate for shoulder rotational flexibility. The shoulder and hip joints had flexion-extension as well as lateral extension. The elbow had one rotation; the torso and upper torso had lateral extension; the torso and the hip had flexion/extension; and the knee had flexion/extension. The joint properties are summarized in Table 1.

Table 1- Joints used for the rigid mannequin with their motion characteristics.

Joint	Motion type	Range of motion
Head/neck (with spring and damper)	Lateral flexion	-40°/24°
Neck/torso (with spring and damper)	Flexion/extension	-50°/50°
Shoulder/torso	Flexion/extension	-70°/180°
	Lateral flexion	0°/160°
Hip/torso	Flexion/extension	-30°/10°
	Lateral flexion	-40°/40°
Elbow	Flexion/extension	-40°/90°

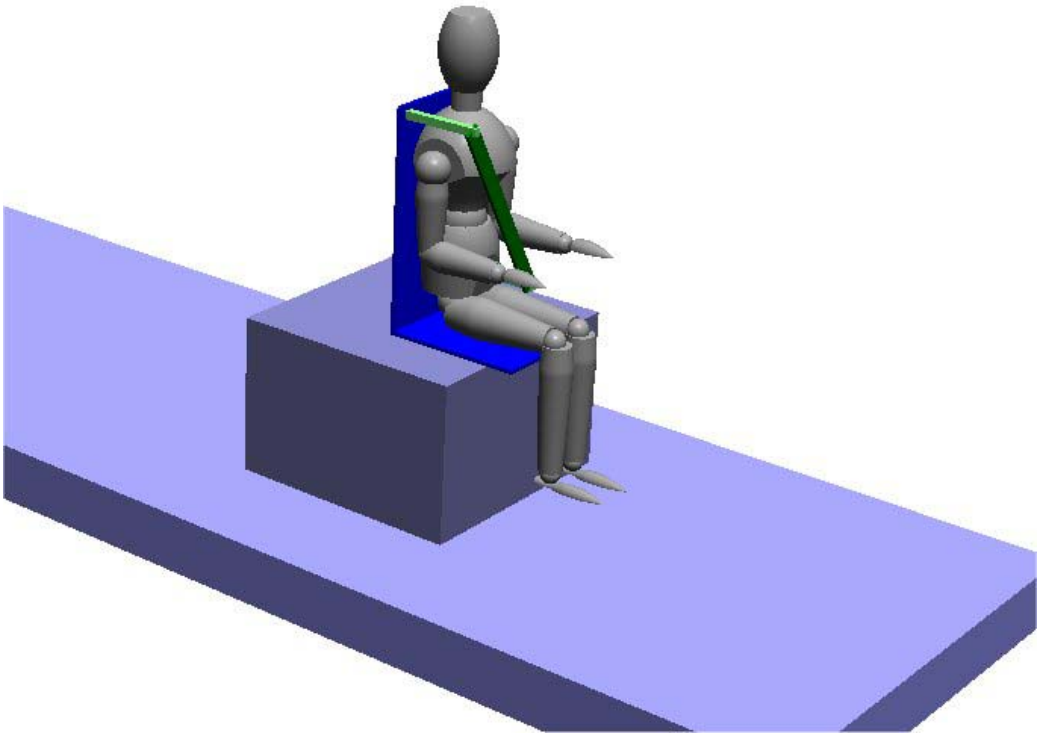

Figure 14. Validation of the model against the experimental data available on sled test.

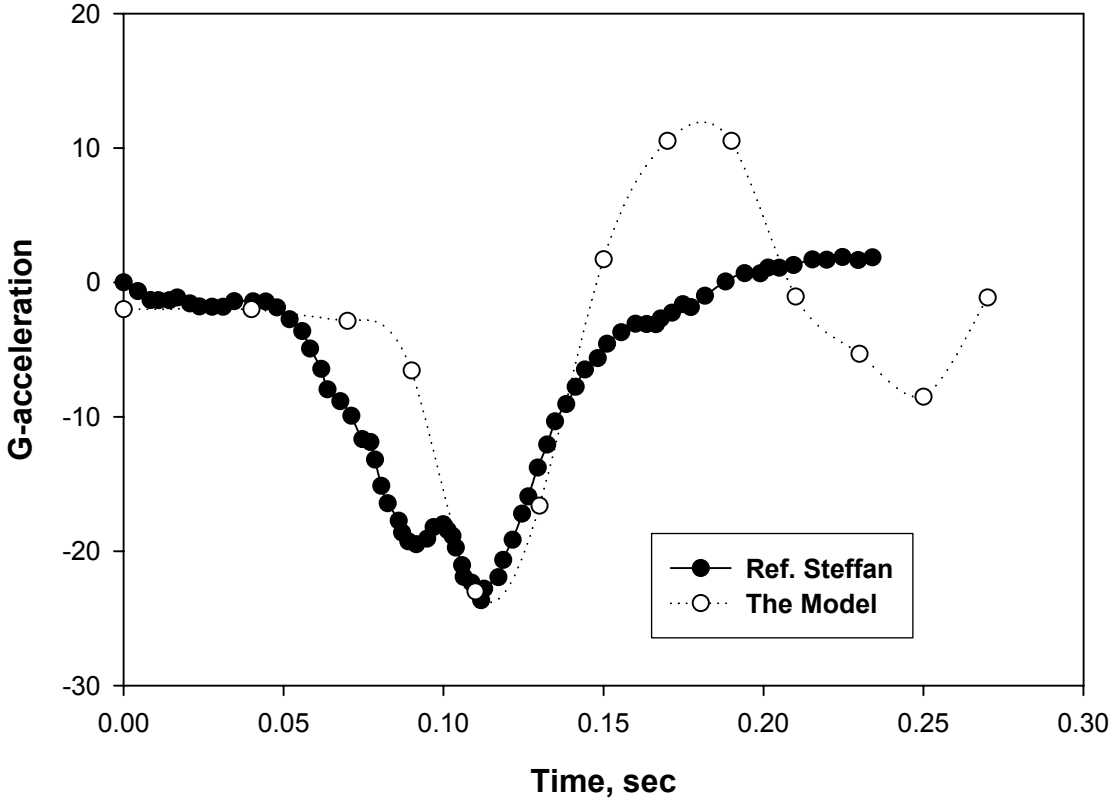

Figure 15. Validation of the model, head acceleration.

5-3 Simulation and Results

Using the same MSC software, rigid body models of the Crown RC and Crown RR lift trucks were created to have the physical dimensions and mass distribution of the tested trucks. The mannequin model was placed on the truck models in the normal, five-point side stance operator position as shown in Figure 16 and the mechanics of the various TO and OTD scenarios related to the testing were simulated. In each simulated case, the mannequin's hands were initially constrained to the truck at the two hand control locations and released at a point in time approximately corresponding to the observed tape breakage in the test of

that case. Table 2 compares the computed values of truck angular velocity and head impact velocity to those of the testing. The average head impact velocity was 4.5 m/s. The head impact results were employed into the FE models to evaluate the HIC value of the accidents. The results are shown in section 6-1-3. However in order to be more conservative the impact velocity of 5 m/s was selected. Figure 17 represents one of the off-the-dock accidents in three positions.

Table 2. Comparison of Computer Simulation with Tests

	Computer Simulation		Experimental Testing	
Case	Head Impact Velocity (m/s)	Truck Angular Velocity (rad/s)	Head Impact Velocity (m/s)	Truck Angular Velocity (rad/s)
RR RTO	3.81	2.37	4.11	2.0
RR LTO	3.63	2.65	2.47	2.25
RR OTD-FT	7.19	4.14	7.71	3.5
RC RTO	3.94	2.60	3.11	2.75
RC LTO	2.99	2.79	3.14	2.75
RC OTD-FT	6.12	3.23	6.74	4.0
RC OTD-FL	3.91	2.74	5.00	2.75

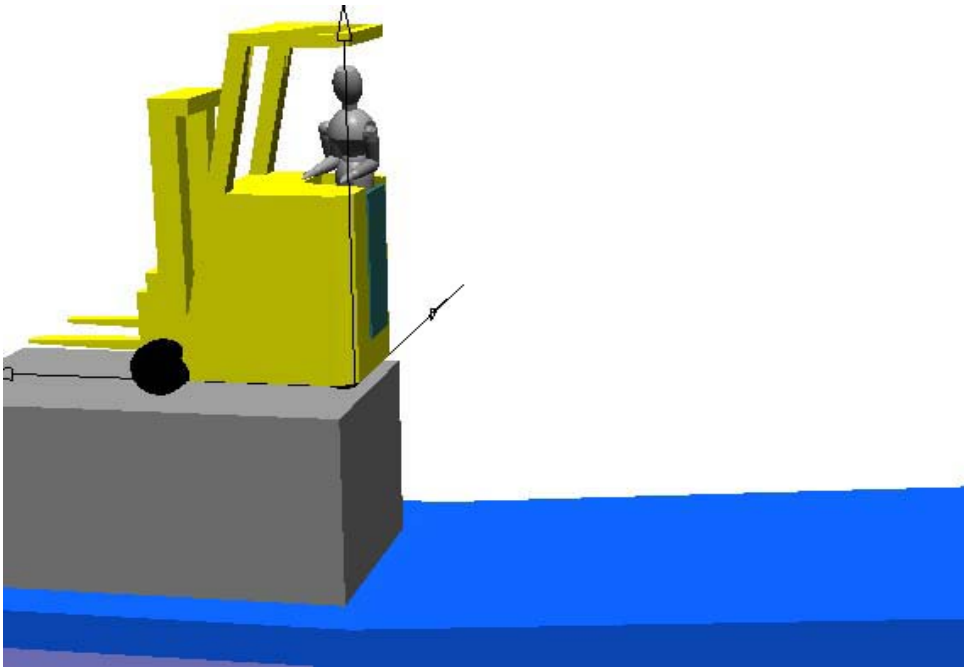

Figure 16. Mannequin placed in the truck.

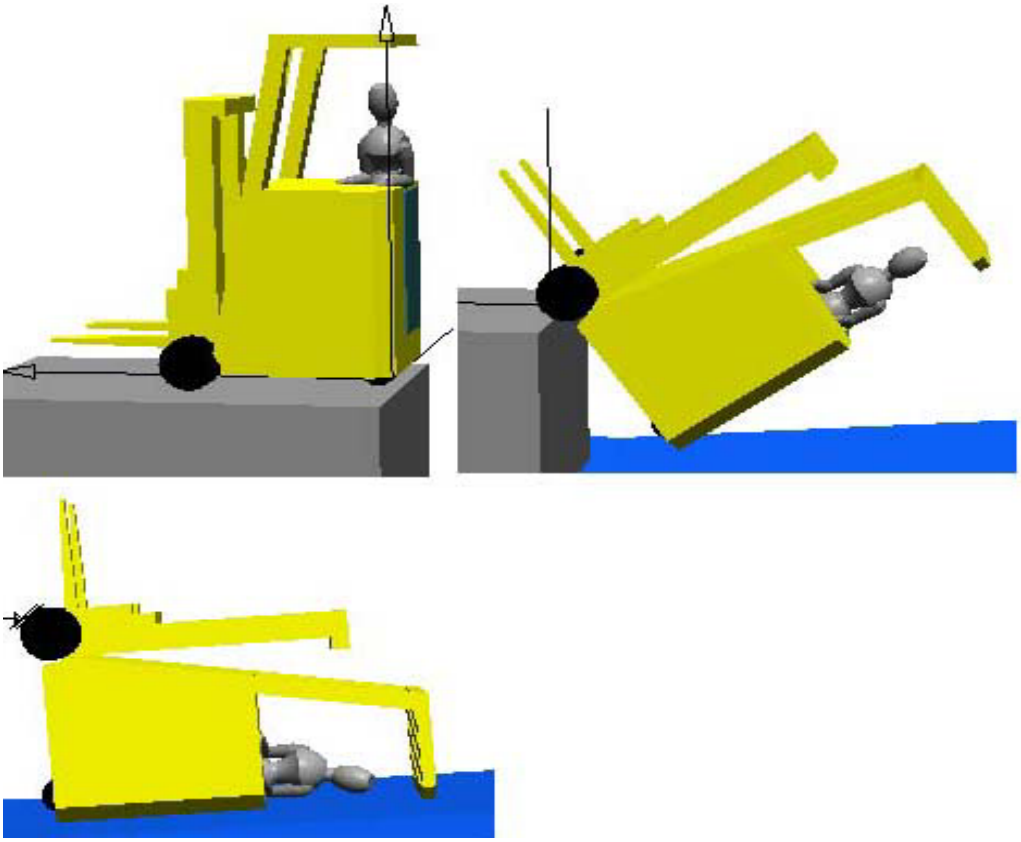

Figure 17. Simulation of an 0ff-the-dock accident.

6- TWO DIMENSIONAL HEAD MODELS

In this section, three detailed models of the head are described. Specifically, a 2D global solid model (Model-I) of the head and a (2D) global fluid model (Model-II) of the head, and a local model-III of the meningeal region were created.

The interactions of these models are described in the flow chart of Figure 18. The impact velocity of 5 m/s, obtained from the previous rigid model was utilized as one of the initial conditions for both models I and II.

The maximum displacement of the brain resulting from the first model-I, and the maximum pressure resulting from the second fluid model-II were incorporated into the third local model-III, as shown in the flow chart of Figure 18. The third Model was then analyzed. The details of these models are described below. The details of these models are described in Zoghi-Moghadam et. al. 2003.

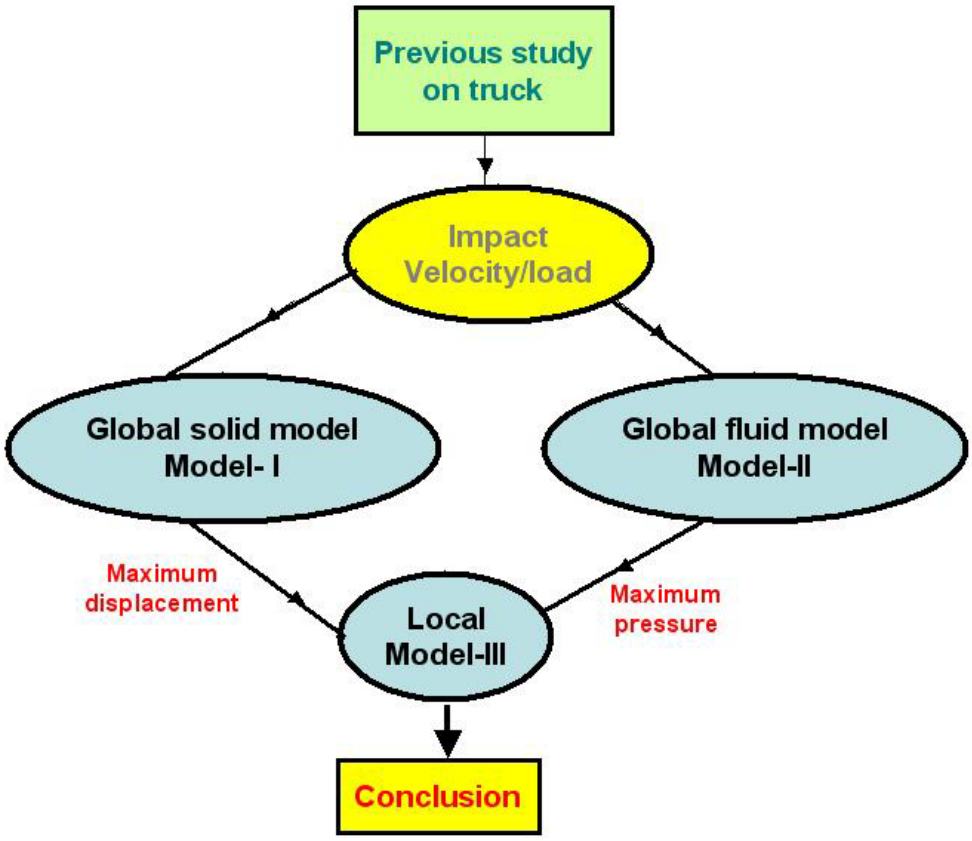

Figure 18. Schematic plan of the study. Starting with rigid analysis of the whole body and ending up with a local analysis of the head.

6-1 Model-I, global solid model of the head

To obtain the relative motion of the brain with respect to the skull, a 2-D global solid model (model-I) of the head in sagittal plane was created, as shown in Figure 19. The geometry of this model was taken from McGrath and Mills 1984. The model consists of three components: 1) the skull, 2) one layer to represent dura mater, arachnoid mater, SAS, CSF, trabeculae and pia mater, and 3) the brain. ANSYS software was used for pre-processor, post-processor, and the analysis of the model. The material properties of brain were assumed to

be isotropic, linear viscoelastic following Maxwell model. Table 3, summarizes the material properties used for this model, which was taken from Zhang et. al. 2002. Note that the commonly used Young modulus for the skull is 12.2 GPa, however, in order to include the effect of neck joint as well as the scalp, a lower Young modulus of 7 GPa was selected for the skull. This value was also chosen based on the fact that the neck region of the model is mainly consist of bone thereby is more rigid than the physiological neck. The plane strain condition was assumed for this model. For the skull and meningeal layer “Plane 82 Element” was used, and for the brain “Visco 88 Element” was used. The total number of elements was 1123 for “Plane 82” and 398 for “Visco 88”. No sliding was allowed between the components. The stiffness matrix multiplier of 0.001 was assumed to include the structural damping effects (Huang et. al. 1999).

6-1-1 Validation of Model-I

The model was validated against experimental data available in the literature (Nahum et. al. 1977). These researchers performed two series of experiments on cadavers. Series I consisted of 8 individual experiments and series II, 7 multiple sequential impacts on a single specimen. Experiment number 37 (experiment #2 from series I) was selected for this validation. In this experiment, a seated, stationary cadaver subject was impacted by a rigid mass of 5.59 kg with a constant velocity of 9.94 m/s. The impact was delivered to the frontal bone in the mid-sagittal plane, in an anterior-posterior direction. They recorded the dynamic measurement of input force and head acceleration and a

series of intracranial pressure-time histories, as explained in section 3-1-2. To simulate this data, the input force (shown in Figure 20) was applied to the frontal section of the model (Figure 19). Note that the load was converted to the proper load for plane strain assumption.

Table 3. Material properties used for solid models

Brain tissue	**Shear modulus at t=0 (G_0) (Pa)**	**$10.0*10^3$**
	Shear modulus at t=∞ (G∞) (Pa)	**$2.0*10^3$**
	Bulk modulus at t=0 (K_0) (Pa)	**$5.0*10^7$**
	Bulk modulus at t=∞ (K∞) (Pa)	**$5.0*10^7$**
	Relaxation time (λ) (s^{-1})	**16**
	Density (ρ) (kg/m^3)	**$1.04*10^3$**
Skull	**Young modulus (E) (Pa)**	**$7.0*10^9$**
	Poisson ratio (υ)	**0.22**
	Density (ρ) (kg/m^3)	**$2.12*10^3$**
Meningeal layer (in global solid model)	**Young modulus (E) (Pa)**	**$10*10^6$**
	Poisson ratio (υ)	**0.499**
	Density (ρ) (kg/m^3)	**$1.0*10^3$**
Dura, arachnoid and trabeculae	**Young modulus (E) (Pa)**	**$3.15*10^7$**
	Poisson ratio (υ)	**0.45**
	Density (ρ) (kg/m^3)	**$1.13*10^3$**
Pia mater	**Young modulus (E) (Pa)**	**$1.15*10^7$**
	Poisson ratio (υ)	**0.45**
	Density (ρ) (kg/m^3)	**$1.13*10^3$**

The stresses at frontal and occipital regions were plotted against frontal and occipital pressures reported by Nahum et al. 1977, see Figure 21. The

model seems to have approximately the same behavior as reported in the experiment. Figure 21 describes that the two peak pressures are almost the same (less than 5% difference) while the time lag in simulation is about one millisecond. The time lag is due to the difference in material properties of the meningeal region. As mentioned before, CSF has been modeled as a solid layer with low shear modulus and bulk modulus of water, which does not mimic the exact behavior of the fluid.

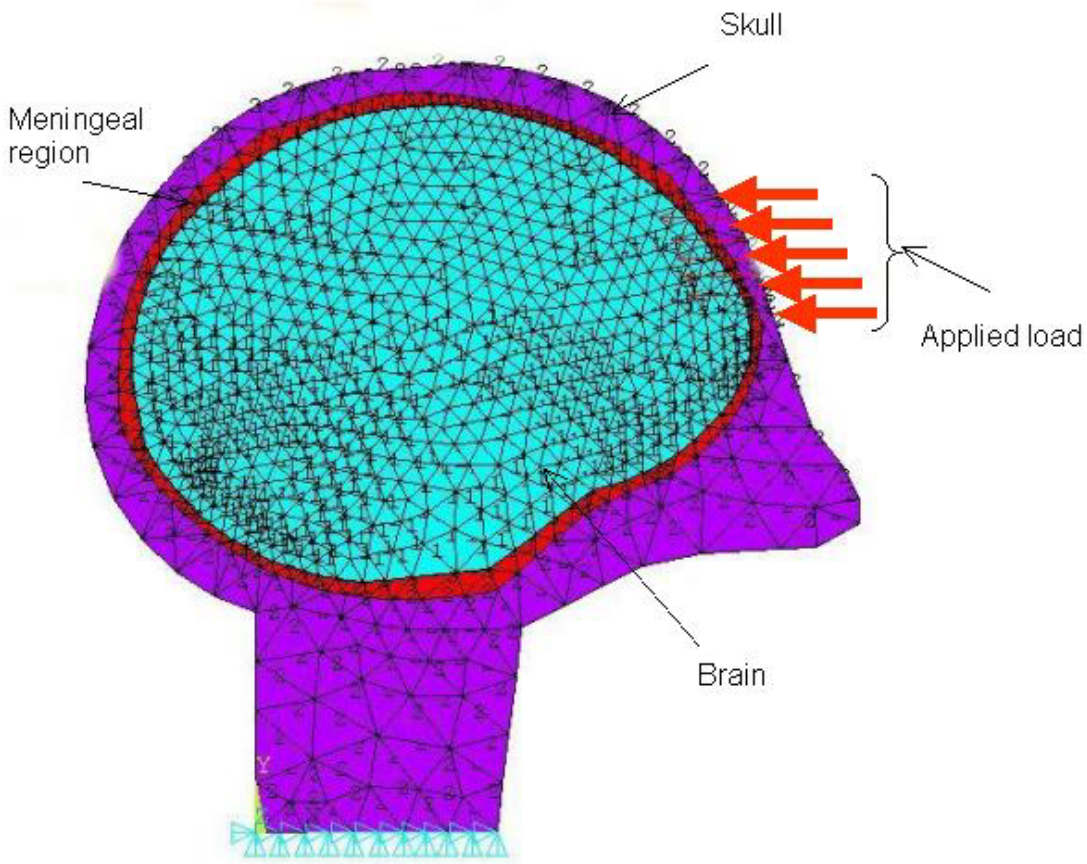

Figure 19. Global solid model with boundary conditions. Blue represents brain, red is the meningeal region including dura, arachnoid, pia, SAS trabeculae and CSF, purple represents skull. Plane strain condition was chosen.

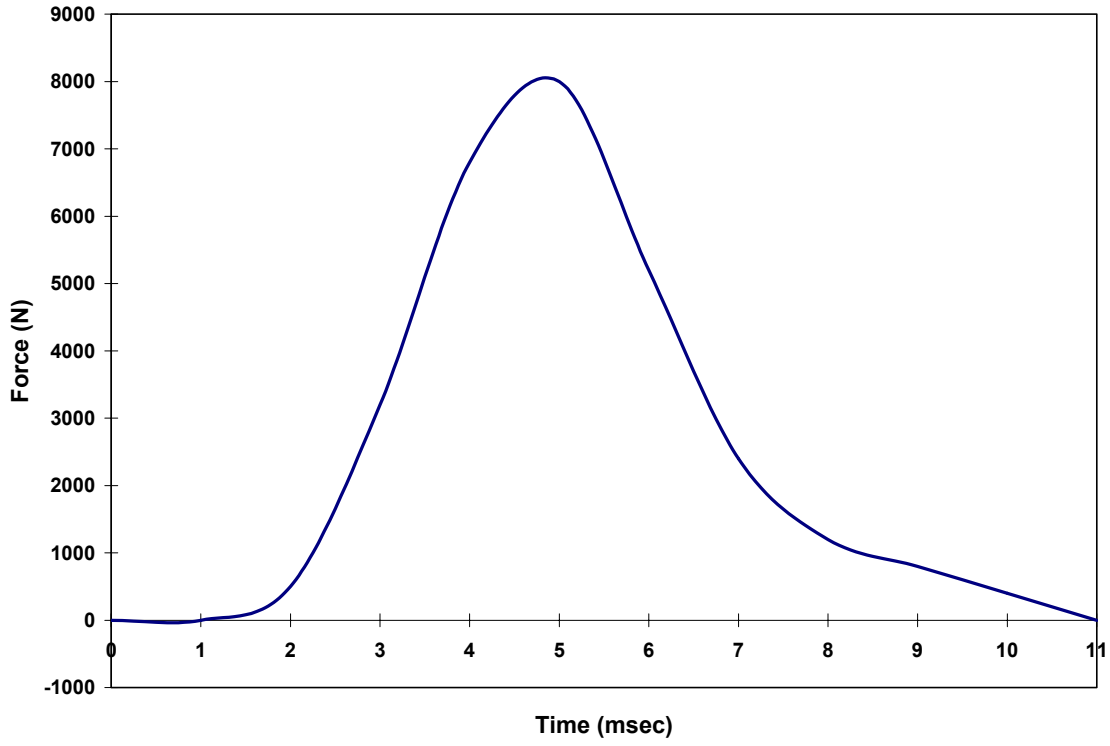

Figure 20- Input force (taken from Nahum et al. 1977) for the validation of Model-I.

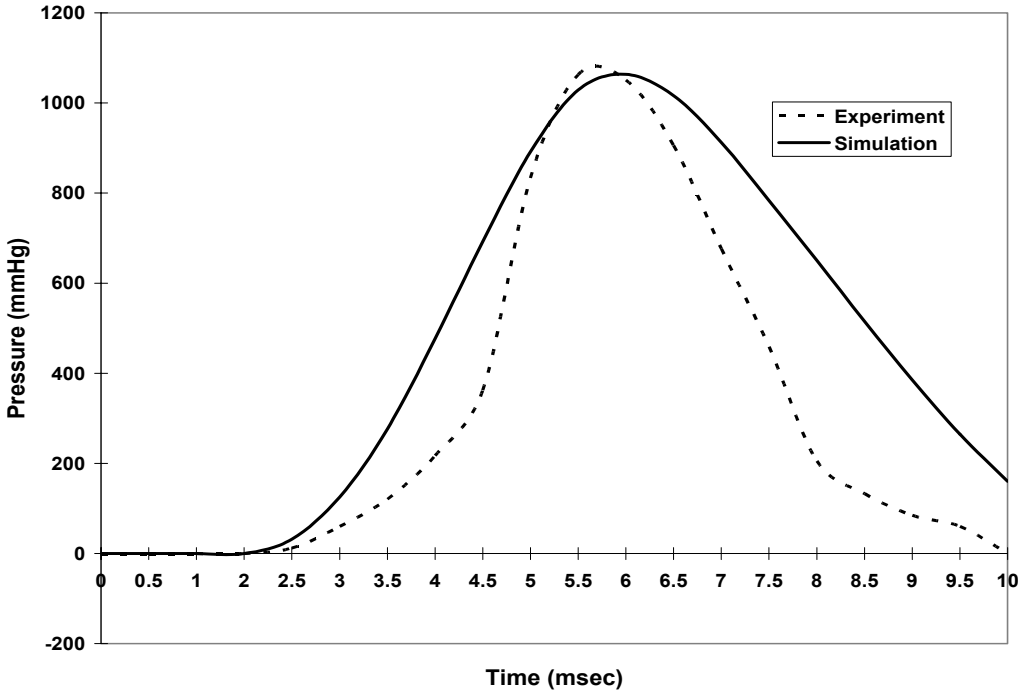

Figure 21- Validation of the Model-I against the experimental data for the frontal region.

6-1-2 Head Impact Simulation

The validated model was subjected to the frontal impact reported by Zoghi-Moghadam et. al. 2002 in the forklift truck accidents as described in section 5. The average head impact velocity was 5 m/s. An equivalent dynamic force corresponding to the impact velocity of 5 m/s was applied to the solid Model-I. This dynamic force was calculated using Ugural and Fenster (1995):

$$P_{dyn} = W \cdot \sqrt{\frac{v^2}{g \cdot \delta_{st}}}$$

where:

P_{dyn} is the dynamic force;

W is the head weight, 50 N;

v is the impact velocity, 5m/s;

g is the gravitational acceleration 9.81 m/s^2;

δ_{st} is the static deflection caused by the load W, being applied on Model-I , which is 1.8E-5 m.

The equivalent dynamic force of the impact was 750N, which was modified for the plane strain and was applied in a trapezoid shape over 40 m-sec as shown in Figure 22. Note that the plane strain condition was selected for the model and, the thickness of the model was assumed unity. The corresponding dynamic load for the unit thickness is 18,800 N. A dynamic analysis was

performed on the model using “Small Displacement Transient Analysis” option available in ANSYS software.

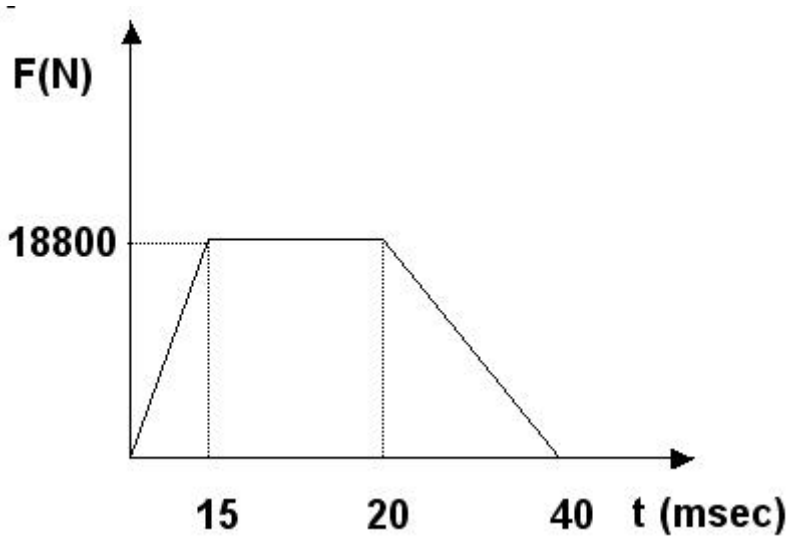

Figure 22. Dynamic input load for model-I relevant to the average head impact velocity of section 5.

6-1-3 Results of Model-I

As mentioned above, a dynamic analysis was performed on the Model-I. The model was subjected to the dynamic load of Figure 22. The stress and the displacement fields of the brain at each time step were determined and analyzed. Figure 23 shows the maximum displacement field of the brain at t=20 msec. As it was expected the maximum displacement occurred at 20 msec, corresponding to the peak of the load as shown in Figure 22.

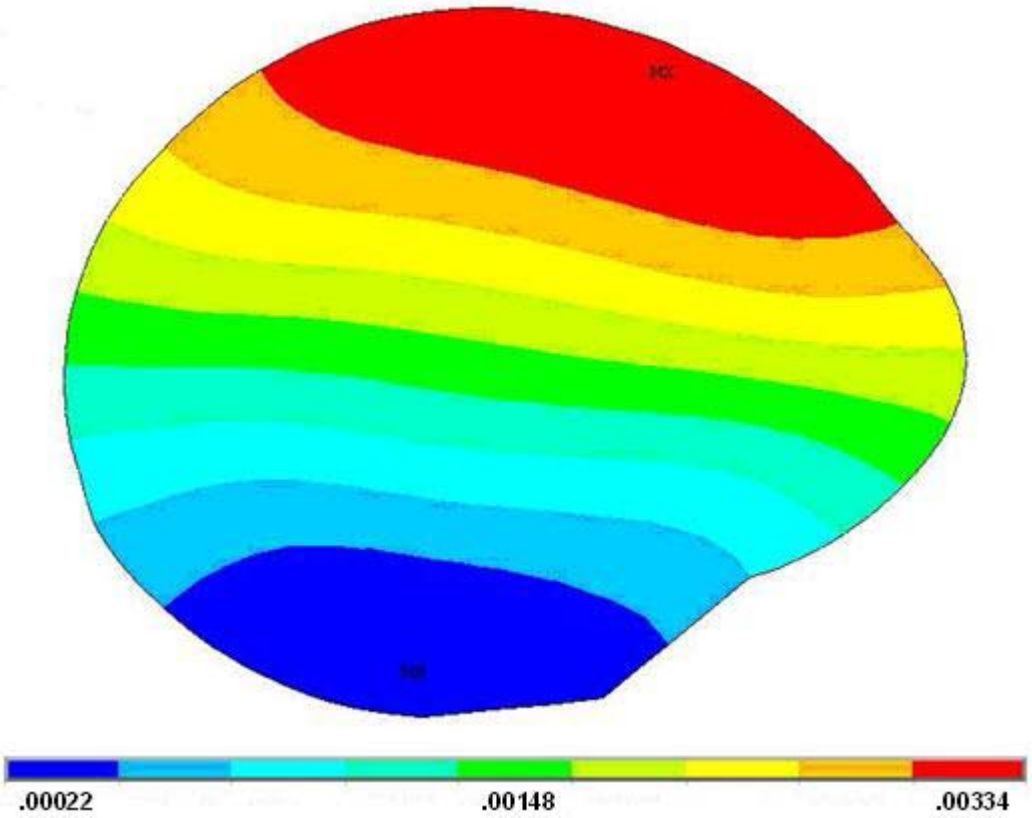

Figure 23. Displacement field for the brain in the global solid model at t=20 msec.

The model was also subjected to the impacts from the rigid body analysis (chapter 5). Table 4 shows the HIC values of the different tip-over cases of the lift-truck accidents. These values are compared with the experimental values (section 5-1).

Table 4. Comparison of Computer Simulation with Tests in terms of Maximum Head Acceleration and HIC

	Computer Simulation		Experimental Testing	
Case	Maximum head acceleration (g)	HIC	Maximum head acceleration (g)	HIC
RR-(RTO)	240	773	228	895
RR-(LTO)	229	686	229	596
RC-(RTO)	189	841	236	865
RC-(LTO)	249	423	274	494

6-2 Model-II, Global Fluid Model of the Head

One of the main goals of this research is to couple fluid dynamic analysis of the SAS region with the FE solid models. The coupling of solid/fluid analysis has not been addressed in the literature. In other words, the effect of SAS trabeculae in pressure distribution of CSF will be addressed in this part of the study. For this investigation two 2-D global fluid models (Model-II-a and b) were created. The GAMBIT 2.4 software was used as pre-processor and mesh generator. The meshed file was imported into the solver, the FLUENT 6.1 software. FLUENT 6.1 was used for the post-processing of the results. The geometries of the models II-a and II-b were taken from McGrath and Mills 1984. The geometry of both models is identical to the meningeal layer of Model-I.

Model-II-a and b are shown in Figure 24. The outer walls (boundaries) represent skull/dura and the inner walls (boundaries) represent brain/pia. The area between the walls is filled with CSF. In Figure 24, Model-II-a contains no SAS trabeculae, while Model-II-b has trabeculae. Arbitrary oriented indentations were added to simulate the SAS trabeculae. The 4-noded elements were used for both models. The number of elements was 3318 (2079 nodes), and 1950 (1309 nodes) for Model-II-a and Model-II-b, respectively. The outer walls of both models were subjected to the velocity impact of 5 m/s as a step function. An unsteady (dynamic) analysis was performed and the pressure of the fluid field was determined over a time period of 100 msec.

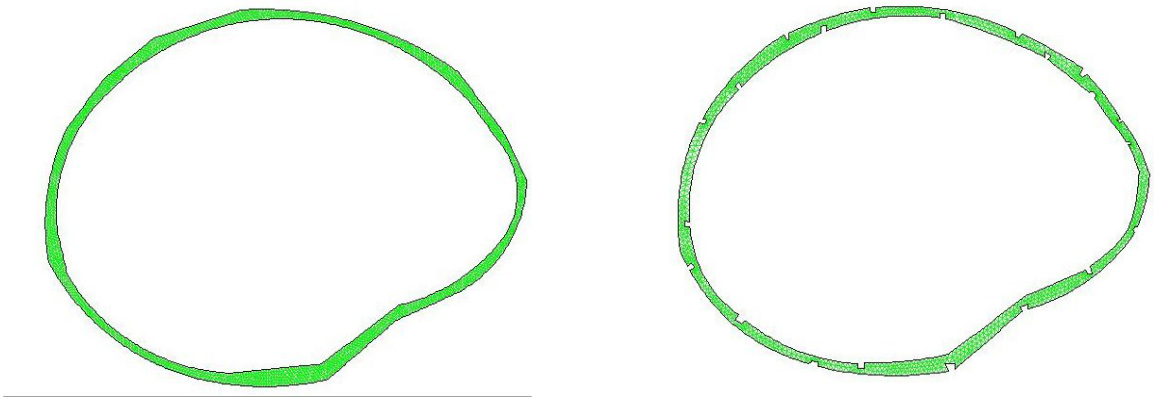

a **b**

Figure 24. Global fluid model (Model-II) , a) without trabeculae (Model-II-a), b) with trabeculae (Model-II-b).

6-2-1 Results of Model-II

The global fluid model (Model-II) was subjected to the impact velocity of the mannequin's head, presented in the rigid body analysis in chapter 5. In this

analysis the fluid characteristics of CSF were investigated. In particular, the CSF pressure distribution over time was determined. Figure 25 shows the pressure distribution of the CSF at the times 25, 50, 75, 100 msec for Model-II-a which contains no trabeculae, and Figure 26 depicts similar for Model-II-b, which contain trabeculae. Comparing Figures 25 and 26, the position of the peak pressure moves faster in the absence of trabeculae over a specific time period. The magnitude of the pressure is lower in the presence of the trabeculae. Pressure variation of CSF over the time period at the three locations of the head, frontal, superior and occipital, are shown in the Figures 27,28, and 29, respectively. These figures reflect that in the presence of trabeculae, the CSF pressure fluctuations have been dampened and the time lag for the peak pressure is longer. The maximum pressures of the three regions (frontal, superior and occipital) were employed as the input data for Model-III.

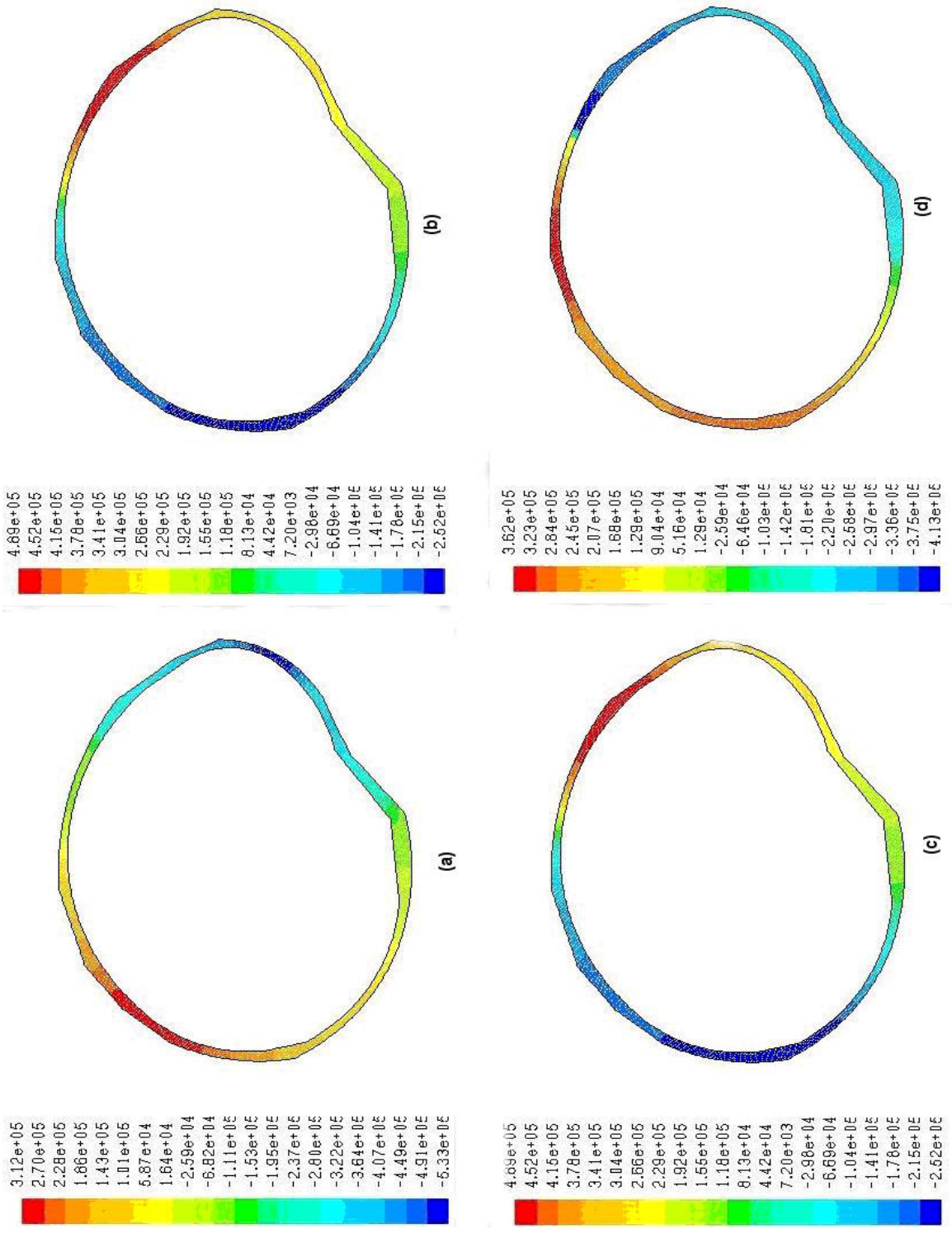

Figure 25. CSF Pressure distribution over time with no trabeculae. a) t=25 msec, b) t=50 msec, c) t= 75 msec, d) t=100 msec.

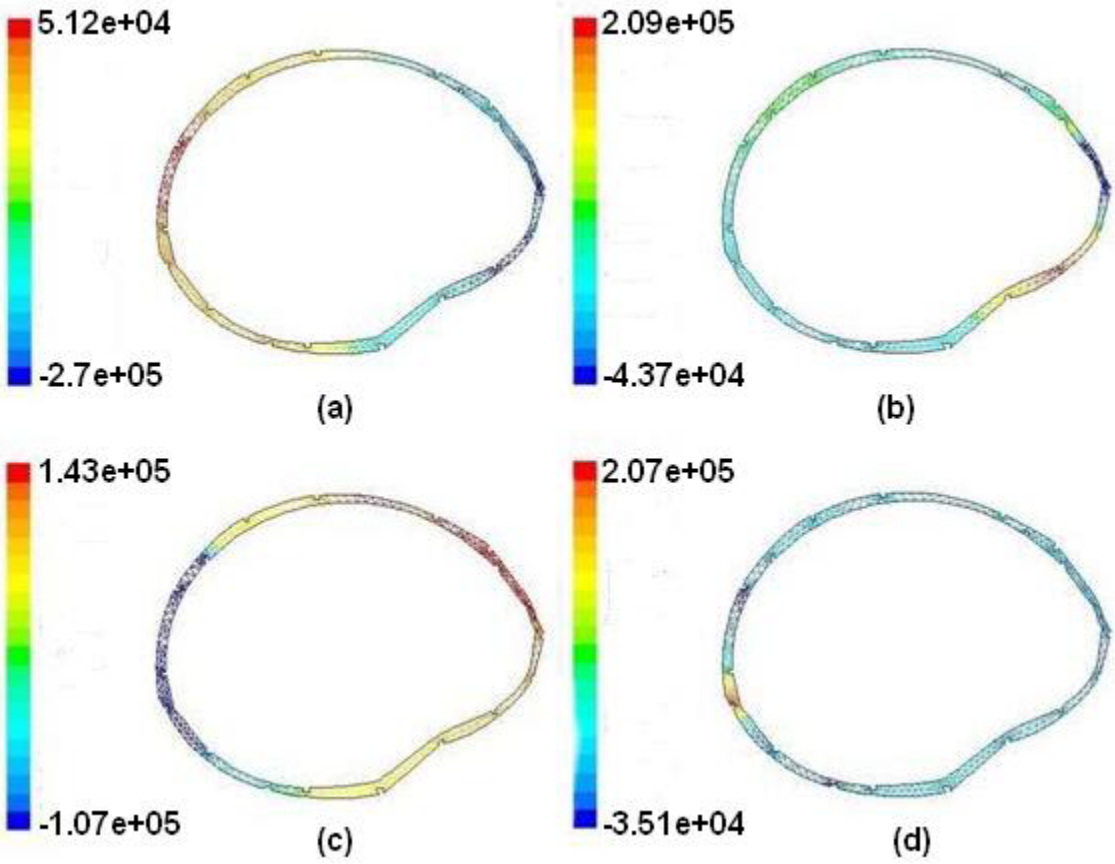

Figure 26. CSF Pressure distribution over time in the presence of trabeculae. a) t=25 msec, b) t=50 msec, c) t= 75 msec, d) t=100 msec.

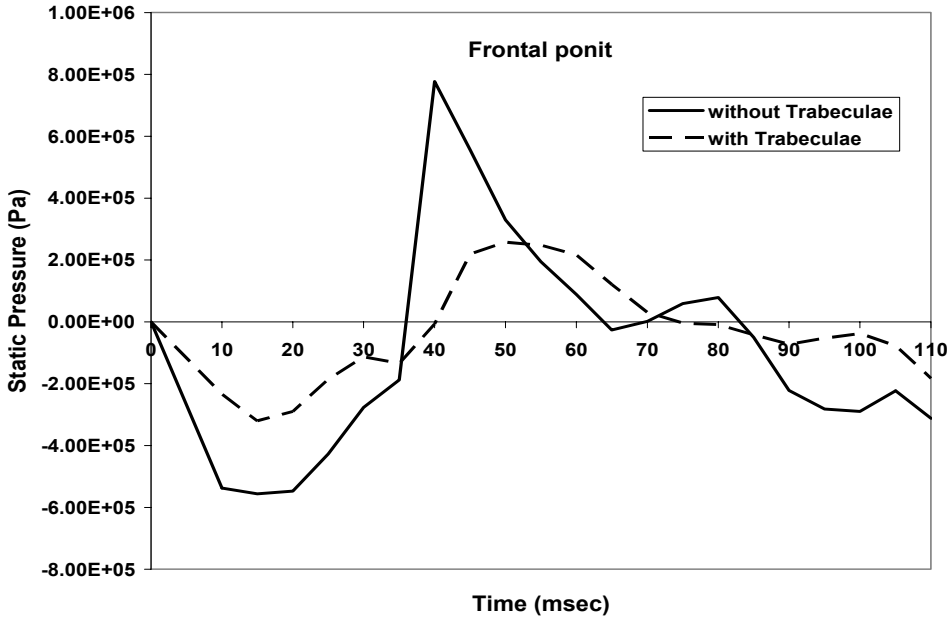

Figure 27. The CSF Pressure distribution in frontal region with and without trabeculae.

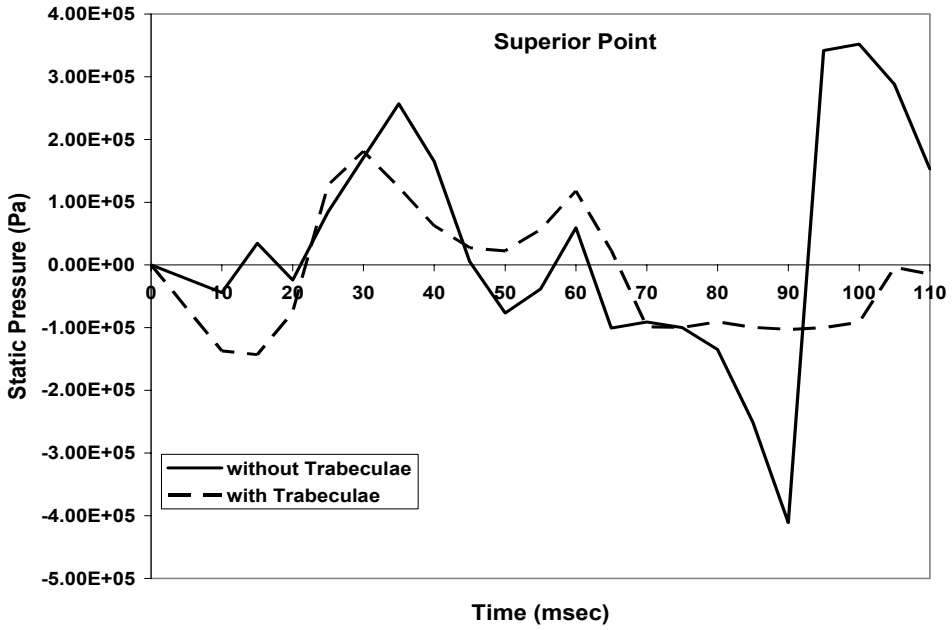

Figure 28. The CSF Pressure distribution in superior region with and without trabeculae.

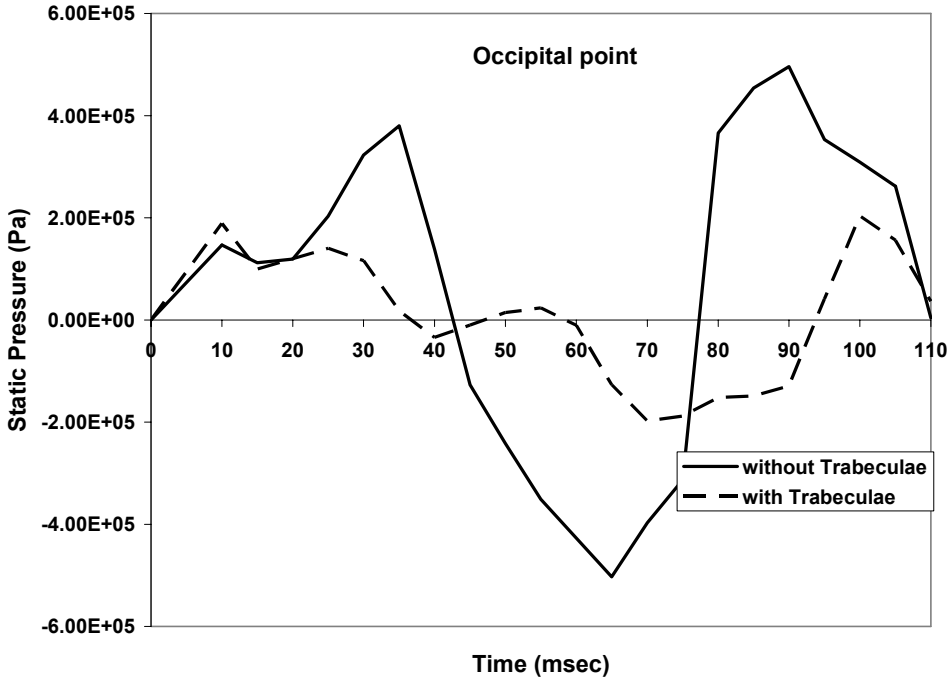

Figure 29. The CSF Pressure distribution in occipital region with and without trabeculae.

6-3 Model-III, Local Model of Meninges

As described in the flow chart, Figure 18, a local model (Model-III) was created to further analyze the results of Models-I and II. The objective of this model was to locally study the post-impact bucking and deformation of the trabeculae in the SAS. The output of the Models-I and II, i.e., the maximum displacement and the maximum pressure were employed as the input and the boundary conditions of Model-III. Model-III consisted of 6 layers representing the skull, dura mater, arachnoid, SAS, pia mater, and a portion of the brain (Figure 30). The geometry of the model is arbitrary but the thickness of the layers is

selected from the anatomy books (Gray and Netter). ANSYS was used as pre and post-processor, and as well as the solver for the analysis. Since the dura mater, arachnoid and the trabeculae are collagen based structures, their properties were assumed as the dura mater reported in Zhang et. al. 2002 (Table 2). All the internal surfaces in the SAS (region containing CSF) of the Model-III were subjected to the pressure calculated from Model-II. The lower boundary of the model was subjected to the displacements that were calculated from Model-I. For brain portion, 199 “VISCO 88” elements were used and for the rest of the components 1297 “PLANE 82” elements were used. A static analysis was performed on the model. In order to eliminate the effect of the side boundaries, the model was created as a long strip with no curvature, however, due to the space limitation, only the middle part of the model is shown in Figure 30.

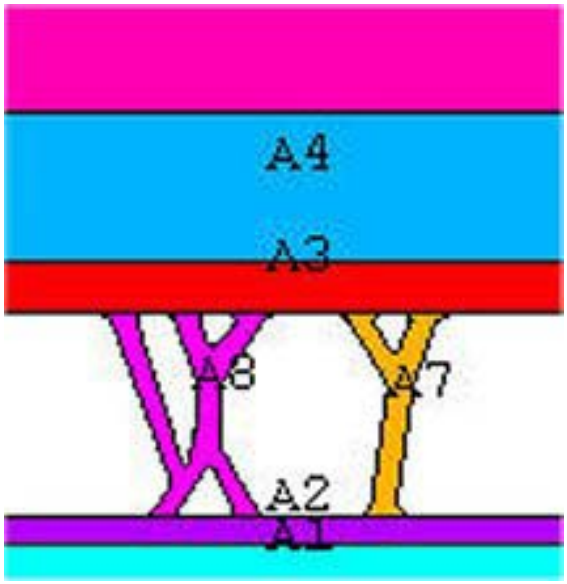

Figure 30. The Local model (Model-III). The whole model is wider than this picture, and only the area of interest is shown.

6-3-1 Results of Model-III

The outcomes of Models-I and II were employed as loading and boundary conditions of the Model-III. In particular, the maximum displacement of the brain, as shown in Table 3, along with the maximum CSF pressure of 2.58 MPa (as the maximum pressure of the three frontal, superior and occipital regions), were used as the input for the Model-III. Specifically, the inferior section of Model-III was subjected to the displacement while the maximum pressure was applied at the SAS region. Figure 31 indicates that the compressive force is the dominant load in the frontal trabeculae and that the trabeculae buckled and collapsed in the compressive mode. Figure 32 depicts the stress field of the trabeculae in the occipital region. This stress filed indicates the rebound (countercoup) pressure resulting in a compressive force and hence the trabeculae buckled. Figure 33 is the superior trabeculae subjected to the combined shear and tension. In first two cases the arachnoid trabeculae buckled and collapsed in the compression mode. Looking at the superior region, which shows the behavior of trabeculae in tension and shear it is observed that the SAS trabeculae restrain and anchor the brain.

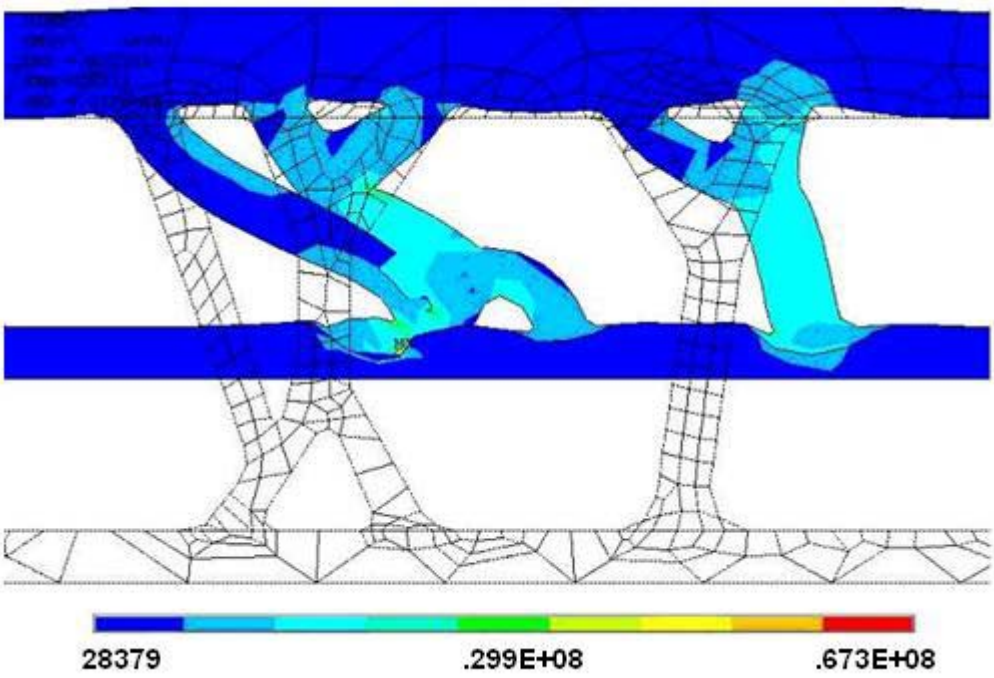

Figure 31. Stress field in the frontal trabeculae.

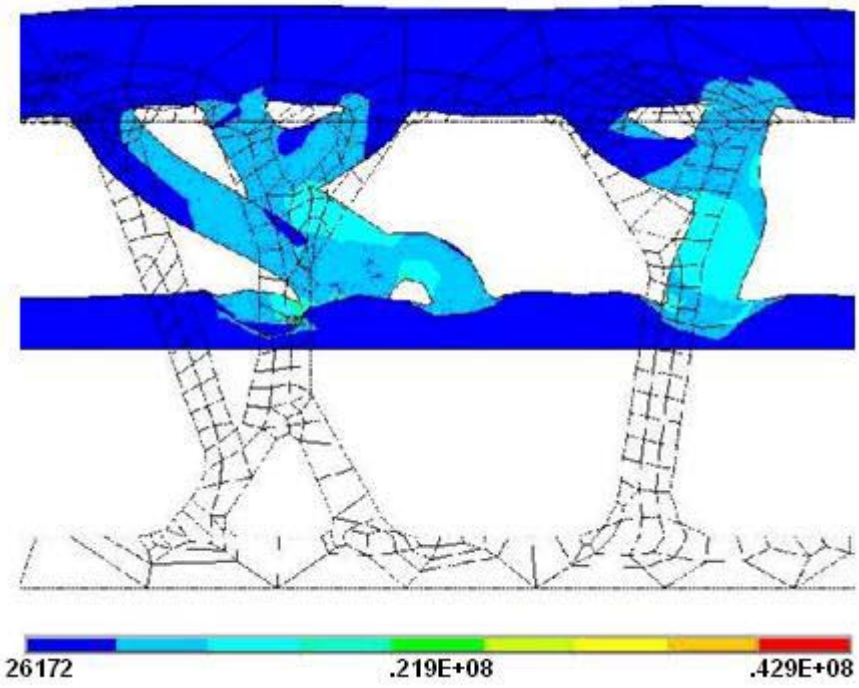

Figure 32. Stress field in the occipital trabeculae.

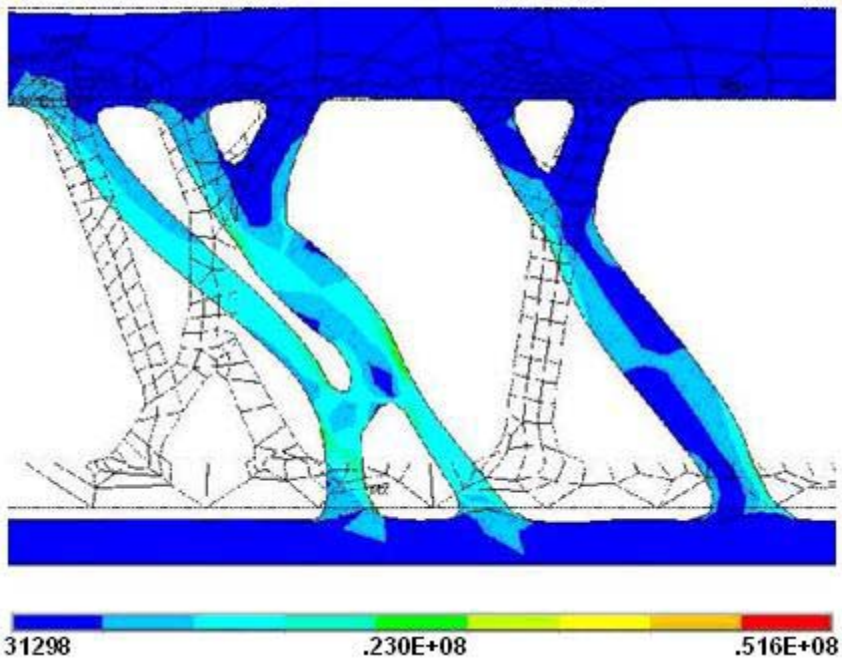

Figure 33. The stress field in the superior trabeculae.

The 2D models discussed in this chapter (Models I, II, III) followed the steps of the flowchart of the analysis, shown in Figure 18. That is, the analysis of the local model was performed using the displacement field from Model-I in conjunction with pressure distribution from Model-II. From Model II, it was concluded that the presence of trabeculae reduces the pressure distribution on SAS region. The effect of trabeculae is created by using random indentations in the inner and outer shell of Model II. In real anatomical case these trabeculae are connected to the two sides of SAS. Constructing the trabeculae in this manner for the 2D Model-II would stop the fluid flow, which is not desirable. That is, the role of the trabeculae can be better addressed in a three-dimensional (3D) model. The local analysis gives more information if blood vessels are included in it. Modeling the blood vessels in a 2D model will consider only a section of the

blood vessels, which cannot simulate the anatomical structure of them. A 3D model can include the blood vessels having their internal blood pressure. Therefore, to perform a more efficient investigation in head/brain injury, a set of 3D models is needed. These models will follow the same steps of the analysis shown in Figure 18 and are discussed in chapters 7, 8 and 9.

7- THREE DIMENSIONAL GLOBAL SOLID MODEL (GSM)

As concluded in chapter 6, the entire 2D analysis is to be extended into 3D analysis. This chapter explains how the 3D modeling of the global solid model (GSM) was performed. This is followed by the analysis of GSM under blunt and rotational impacts. The results will be shown and discussed. The relative displacement of the brain with respect to skull will be determined and will be used for the analysis of the local model.

7-1 Model Construction

The geometry of the model was takes from Horgan and Gilchrist (2003). They developed the model from computed tomography (CT) scans. The model was obtained in form of initial graphics exchange specification (IGES). To save computational time, due to the symmetry, only half of the head was modeled.

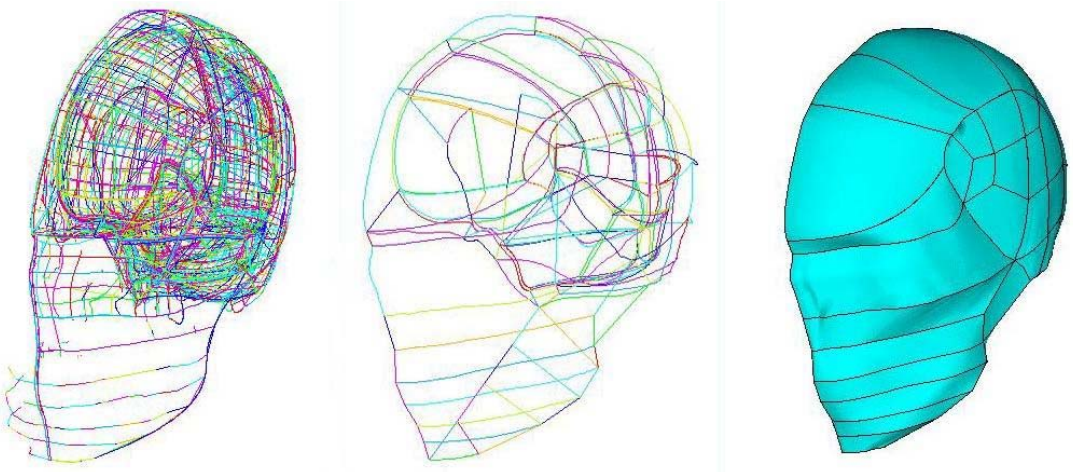

(a) (b) (c)

Figure 34. (a) The raw model needs to be cleaned up as shown in (b). (c) Areas are created by connecting the relevant lines.

Figure 34 shows the initial IGES model. As the figure shows there were a huge number of extra unattached lines in the crude model. That suggested that the model needed to be cleaned up. The process of cleaning up consisted of removing the overlying lines and attaching the disconnected lines. Once there was no unattached overlaying line (Figure 34-b), the areas were created by connecting the relevant lines together. The challenges in area creation were the areas not lying in a plane. Those areas needed to be formed by connecting 3 or 4 lines with each other. For the planar areas there was no limitation in the number of lines. Due to the complex geometry of the head the number of non-planar areas was very noticeable (98 non-planar areas out of 134 areas). Figure 34-c shows the areas of the face and skull. Followed by the area creation the volumes were constructed by connecting the relevant areas. There are 7 volumes in the solid model. They are skull, cerebrum, cerebellum, meningeal region around cerebrum, meningeal region around cerebellum, face and neck. Note that the geometry of the face, which has no effect on the analysis, was changed to look more realistic. Neck was added to the original model as well.

The next step was to generate the nodes and elements. ANSYS 8.0 software (ANSYS INC., PA) was used as preprocessor. Table 5 summarizes the mesh properties for the solid model.

The material properties of brain (cerebrum and cerebellum) were assumed to be isotropic, nonlinear viscoelastic following Maxwell model. All other components assumed to be linear, isotropic and elastic. Note that for the global solid model, meningeal region includes the three layers of dura mater, arachnoid,

pia mater, and cerebrospinal fluid (CSF) with SAS trabeculae. Table 6 tabulates the material properties of the different components used in GSM. The material properties are taken from Zhang et al. (2001) and Zhang et al. (2002). Since the different layers of skull has been modeled as a single layer, the average Young's modulus of the layers is used. The material properties of the meningeal layers in GSM is the average of dura mater, arachnoid and pia mater. Figure 35 represents the global solid model with its elements.

Table 5. The element properties and type used for GSM. The total number of elements is 78,252 and the total number of nodes is 76,940. Type I element is ANSYS-solid187 3D 10-node tetrahedral structure solid. Type II element is ANSYS visco89 3D 20-node viscoelastic solid.

	skull	cerebrum	cerebellum	meningeal region around cerebrum	meningeal region around cerebellum	face	neck
Element type	I	II	II	I	I	I	I
# of elements	15762	25603	14404	10512	8663	2392	916
# of nodes	14090	29735	16875	6882	6362	2320	676

Table 6- Material properties used in GSM.

Brain tissue (cerebrum and cerebellum)	Shear modulus at t=0 (G_0) (Pa)	$10.0*10^3$
	Shear modulus at t=∞ (G∞) (Pa)	$2.0*10^3$
	Bulk modulus at t=0 (K_0) (Pa)	$5.0*10^7$
	Bulk modulus at t=∞ (K∞) (Pa)	$5.0*10^7$
	Relaxation time (λ) (s^{-1})	16
	Density (ρ) (kg/m^3)	$1.04*10^3$
Skull	Young's modulus (E) (Pa)	$7.0*10^9$
	Poisson's ratio (υ)	0.22
	Density (ρ) (kg/m^3)	$2.12*10^3$
Meningeal layer (GSM)	Young's modulus (E) (Pa)	$10*10^6$
	Poisson's ratio (υ)	0.499
	Density (ρ) (kg/m^3)	$1.0*10^3$
Face and neck	Young's modulus (E) (Pa)	$0.5*10^9$
	Poisson's ratio (υ)	0.22
	Density (ρ) (kg/m^3)	$1.06*10^3$

7-2 Validation of the GSM

The model was validated against experimental data available in literature. Nahum et al. (1977) performed two series of impact test on human head cadavers. Series I consisted of 8 individual experiments and series II, 7 multiple sequential impacts on a single specimen. They measured intracranial pressures during human cadaver head impacts. By varying the initial velocity of the impact (or impact magnitude), duration of the applied load and the impactor's mass, these researchers measured the input force, changes in skull acceleration and in vivo intracranial pressure with time during the impact. Pressure changes were

measured with transducers placed at five different points: 1) the frontal bone adjacent to the impact contact area, 2) posterior and superior to the coronal and sequamosal sutures in the parietal bone, 3,4) inferior to the lambdoidal suture in the occipital bone (on both sides) and 5) in the occipital bone at the posterior fossa. The pressure was determined at these five points in GSM (Figure 35). It is worth mentioning that almost all the head/brain researchers have used Nahum et al. (1977) results to validate their models (Eppinger et al. (1995), Willinger et al. (1995), Zhou et al. (1995), Turquier et al. (1996), Claessens (1997), Al-Bsharat et al. (1999), Huang et al. (1999), Nishimoto and Murakami (1999), Willinger et al. (1999), Zhang et al. (2001), Kleiven and Hardy (2002), Kleiven and Von Holst (2002a), Kleiven and Von Holst (2002b), Kleiven (2003) and Sarkar et al. (2004)). As shown in Figure 20 the loading boundary condition used for validation was the input load from Nahum et al. (1977). The frontal region of the head was subjected to loading shown in figure 20. The areas located at the bottom part of the neck were subjected to fixed boundary condition.

ANSYS 8.0 software (ANSYS INC., PA) was used to perform a dynamic analysis on the model. It took 42 hours for a 2.4 GHz processor to complete the analysis.

The stress (as the pressure) in those five regions (shown in Figure 35-b) was compared with experimental intracranial pressure. Table 7 summarizes this comparison, which leads to a maximum difference of less than 7%. Figure 36 shows the validation curves of the locations shown in Figure 35-b.

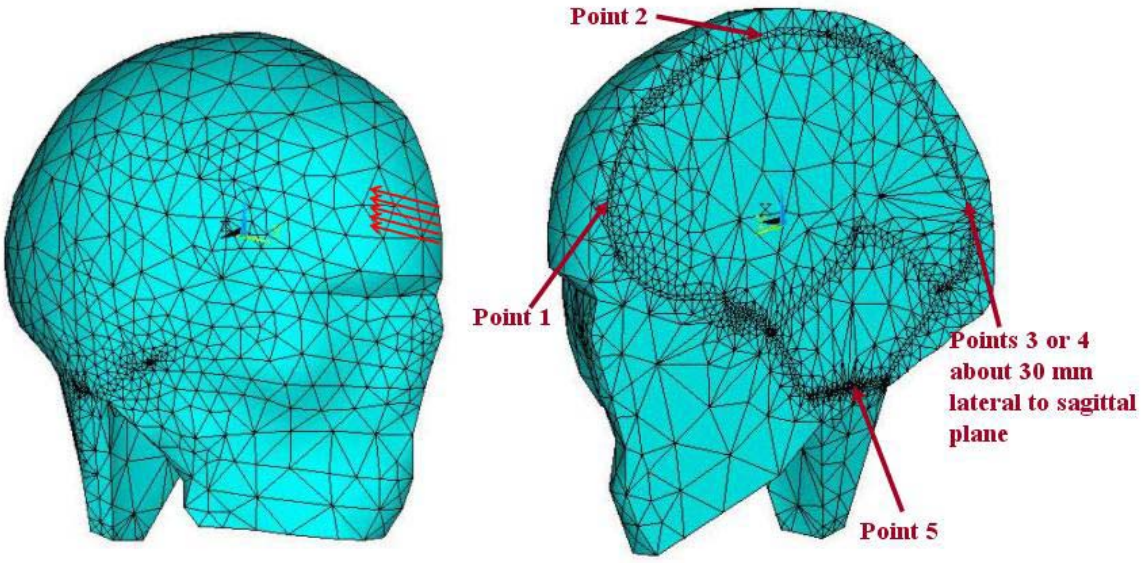

(a) (b)

Figure 35. (a) GSM under the loading. (b)The locations that validation was made against experimental data.

Table 7. Error and time lag of the GSM against the experiment (locations are shown in figure 35).

	Frontal (Point 1)	Superior (Point 2)	Occipital (Point 3 or 4)	Posterior fossa (Point 5)
Error %	0.7	-3.4	5.4	-6.8
Time lag (msec)	0.5	2.0	1.5	1.0

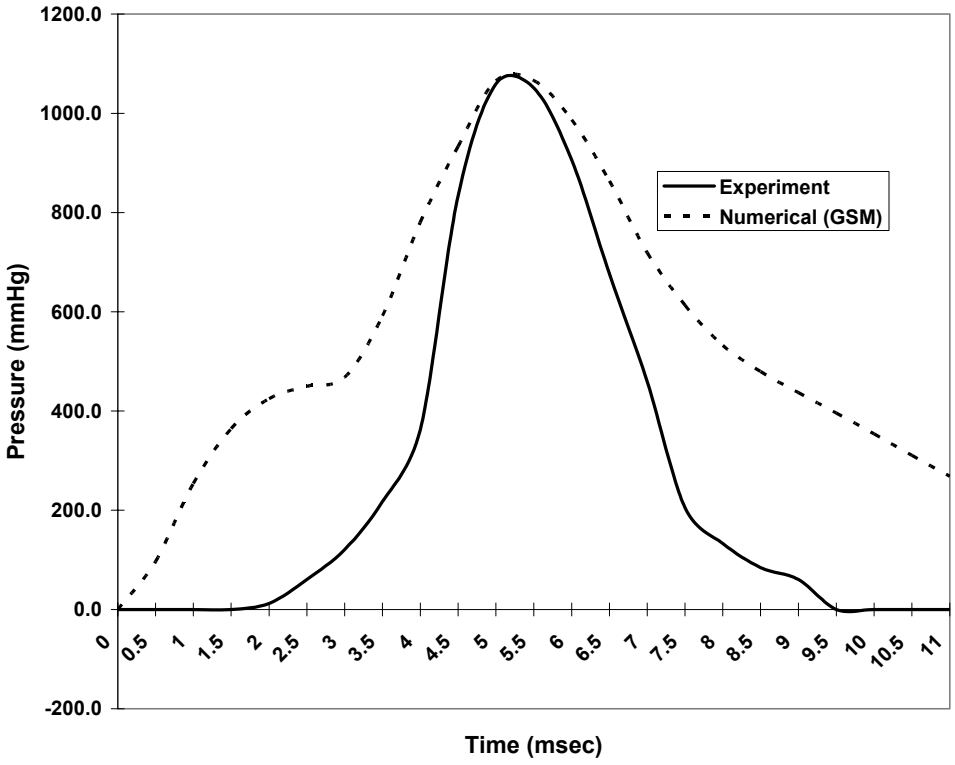

(a) frontal

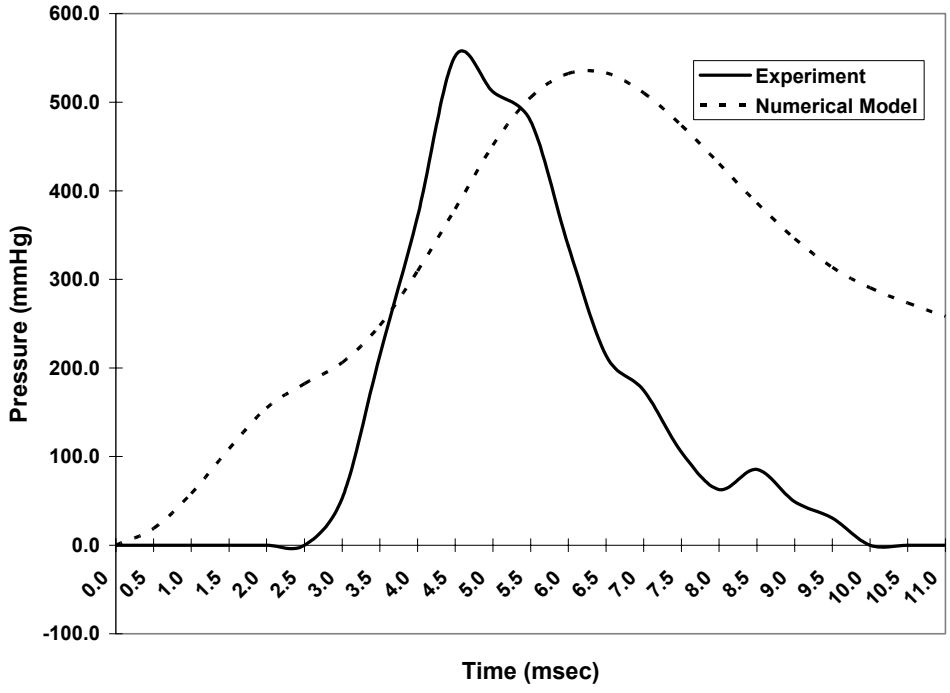

(b) superior

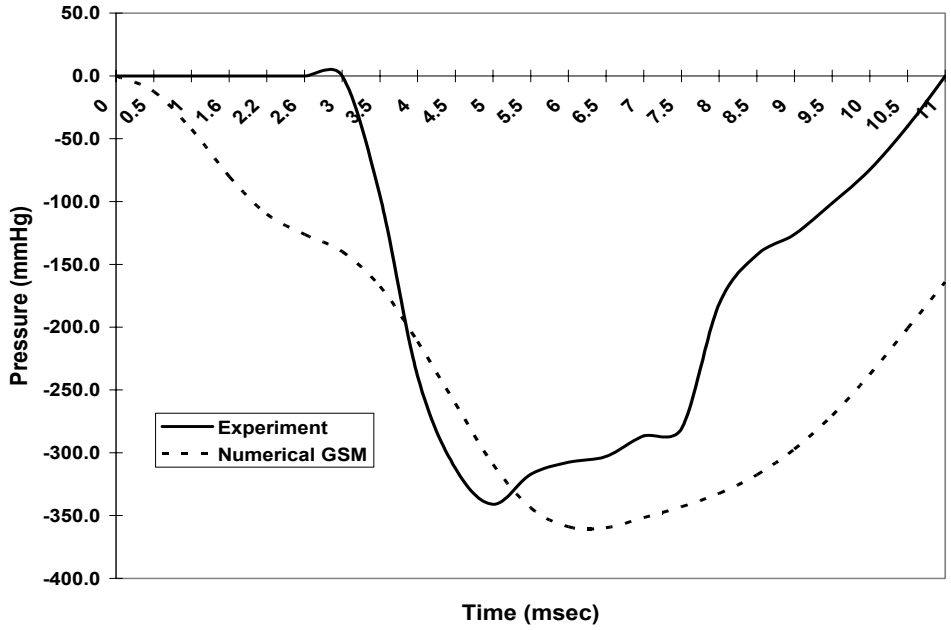

(c) occipital

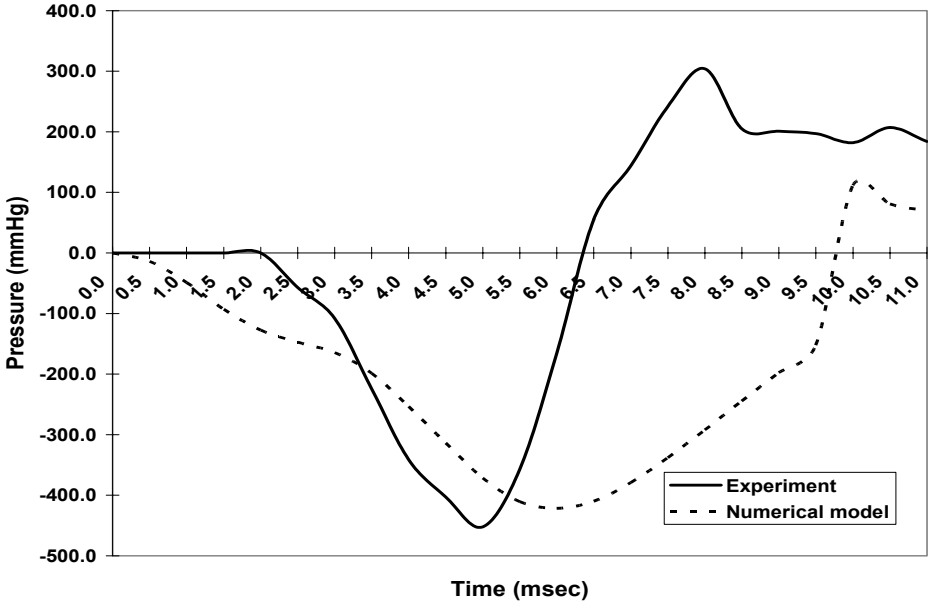

(d) posterior fossa

Figure 36- Validation of GSM against experimental data in the frontal (a), superior (b), occipital (c) and posterior fossa (d) regions.

7-3 GSM Blunt Impact

The model was subjected to two blunt head impacts. The first one was explained in validation section (7-2). The second one is similar to experiment 49 of Nahum et al. (1977) study, shown in Figure 37. This impact produces a HIC value of 1040, which is categorized to create severe injury. This load was applied to the frontal region of the head. To avoid stress concentration, the load was distributed equally on 10 nodes (Figure 35-a). The inferior section of the neck was restrained while a symmetric boundary condition was applied on the plane of symmetry. Due to the nature of the loading a dynamic analysis was performed.

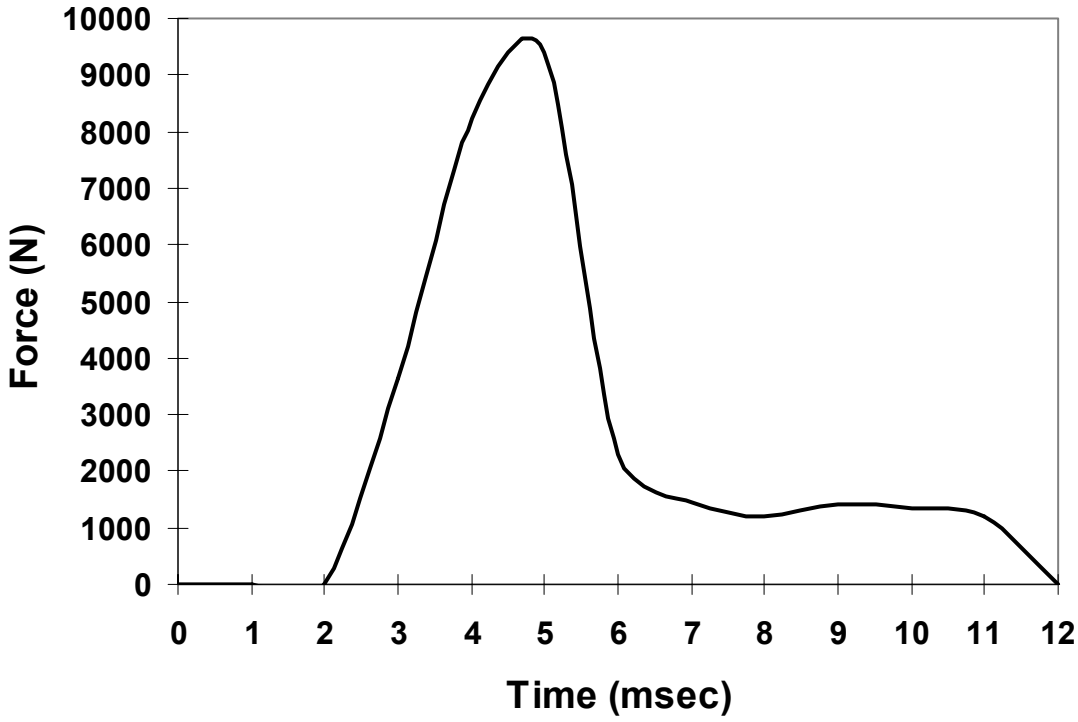

Figure 37- The input load for GSM under blunt head impact corresponding to a HIC value of 1040.

7-3-1 Results of GSM Blunt Impact

Figure 38-a shows the strain field of GSM under the loading of Figure 37. As shown in the figure the strain value is higher in the middle of the model where the brain is located. Note that the brain tissue is the most compliant component of the model, and Figure 38-b shows the strain filed of the brain. As shown in this figure, the maximum of the strain value is on the superior region. This is expected since the superior region is the farthest region from the center of rotation (inferior section of the neck), and thus the strain should be maximum in this region.

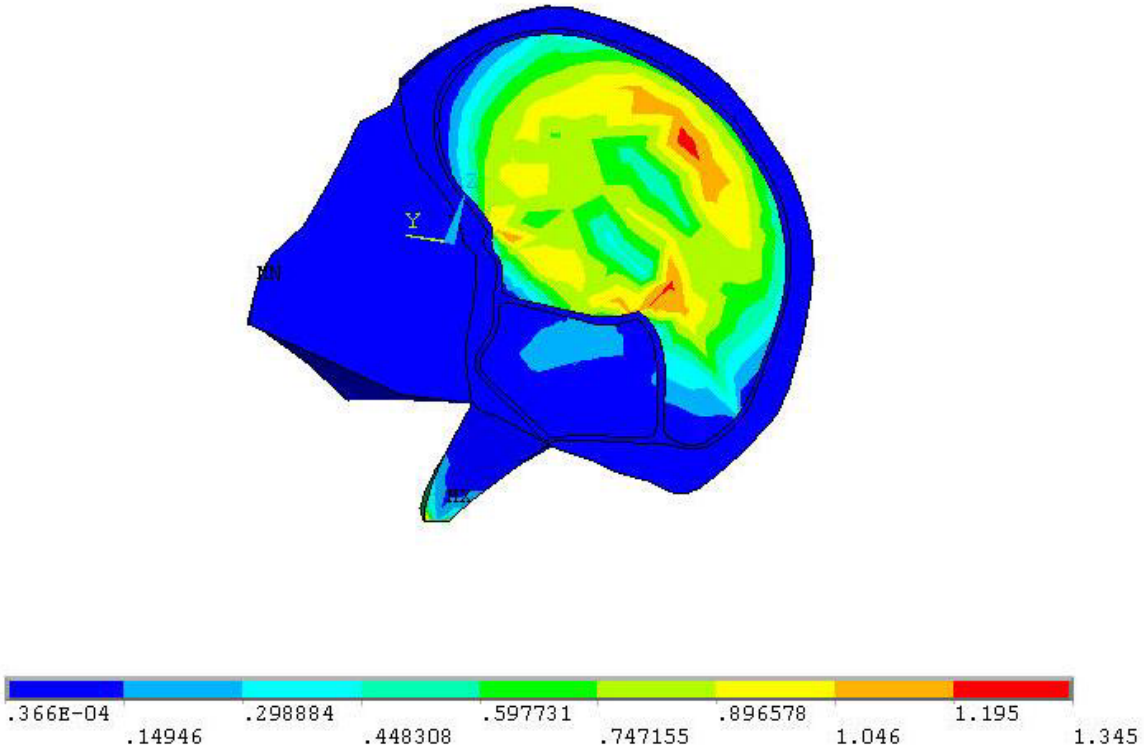

(a)

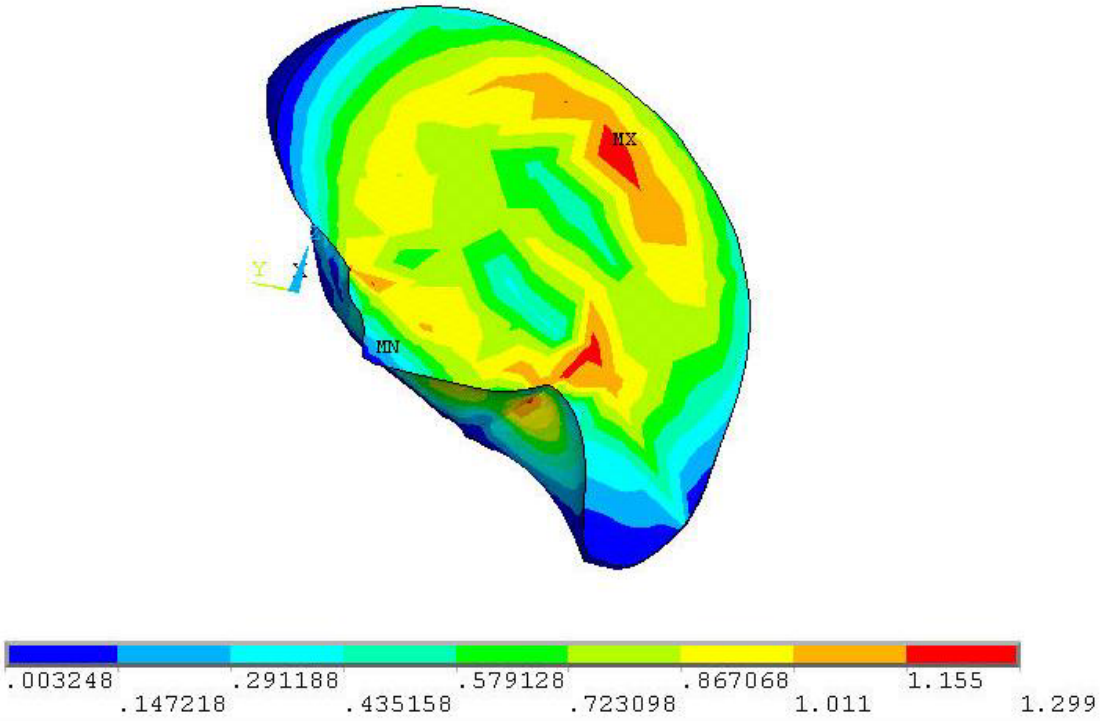

(b)

Figure 38- A typical result of GSM. Strain field at t=12.0 msec (a) entire model and (b) the brain.

Figure 39 shows a typical stress field in the meningeal layer. The significance of this region is that the stress field of the meningeal layer corresponds to the intracranial pressure.

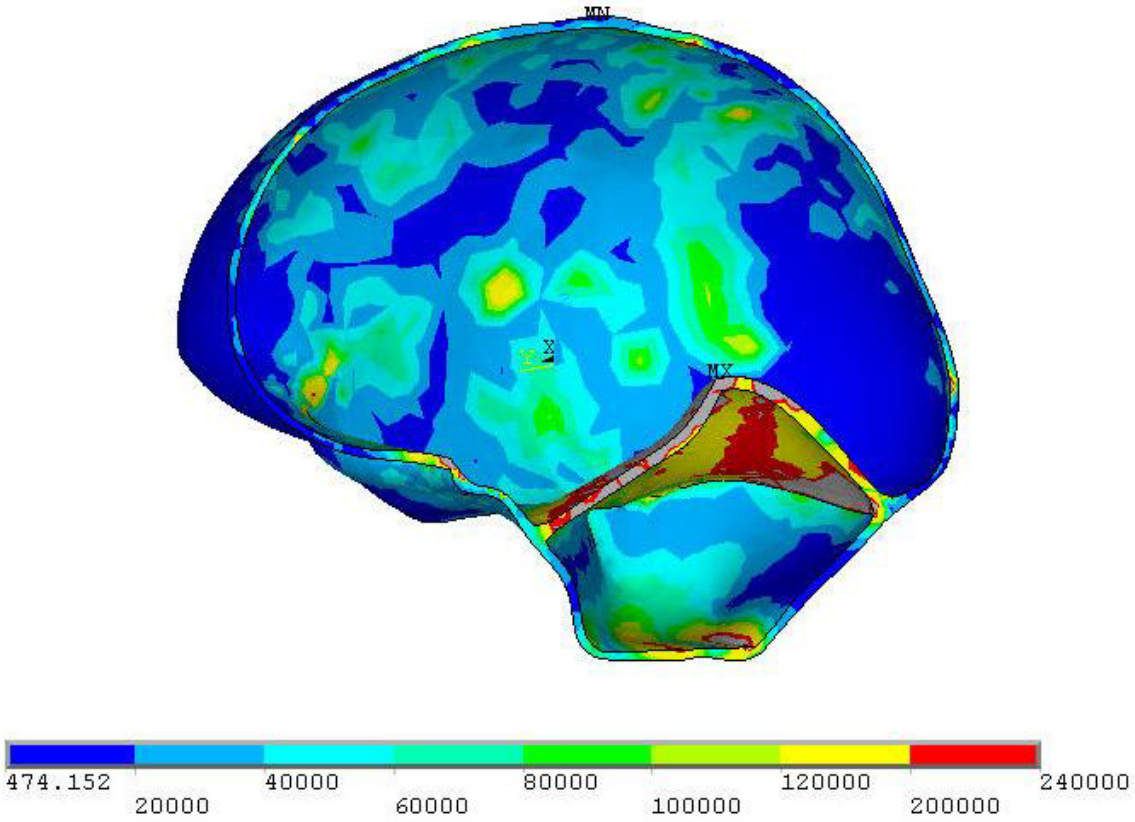

Figure 39- The stress field of the meningeal layers. The stress in this region corresponds to the intracranial pressure.

7-4 GSM Rotational Impact

The model was subjected into a rotational impact, shown in Figure 40a (Zhang et al. (2001)). This impact is known to create injury. The angular acceleration was in the form of a sine wave with peak value of 12,000 rad/s^2 over a period of 30 msec. The angular position of the head was determined from the angular acceleration assuming a rotation from zero degrees to 60° during the impact (Figure 40b).

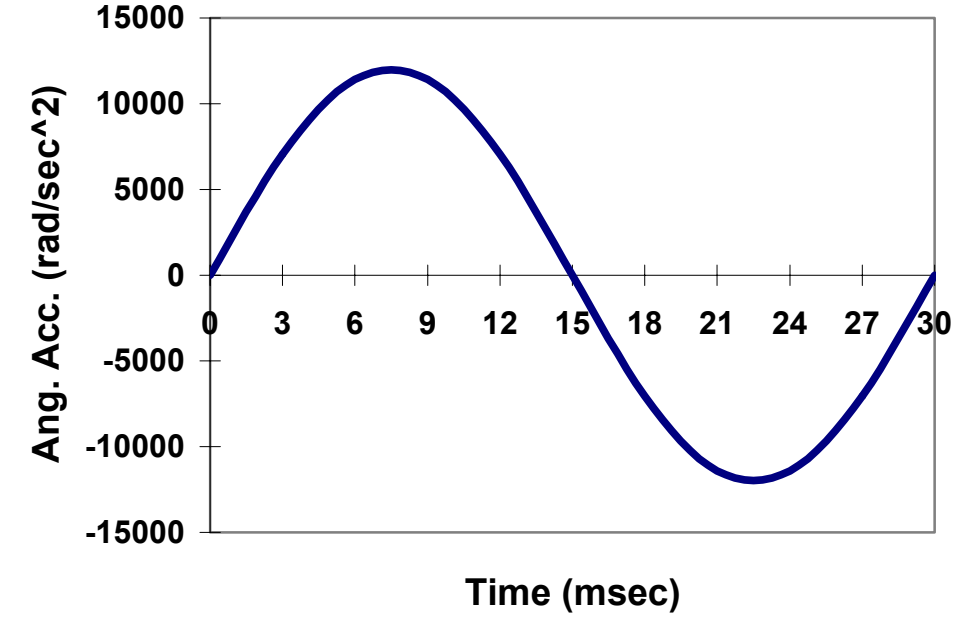

(a)

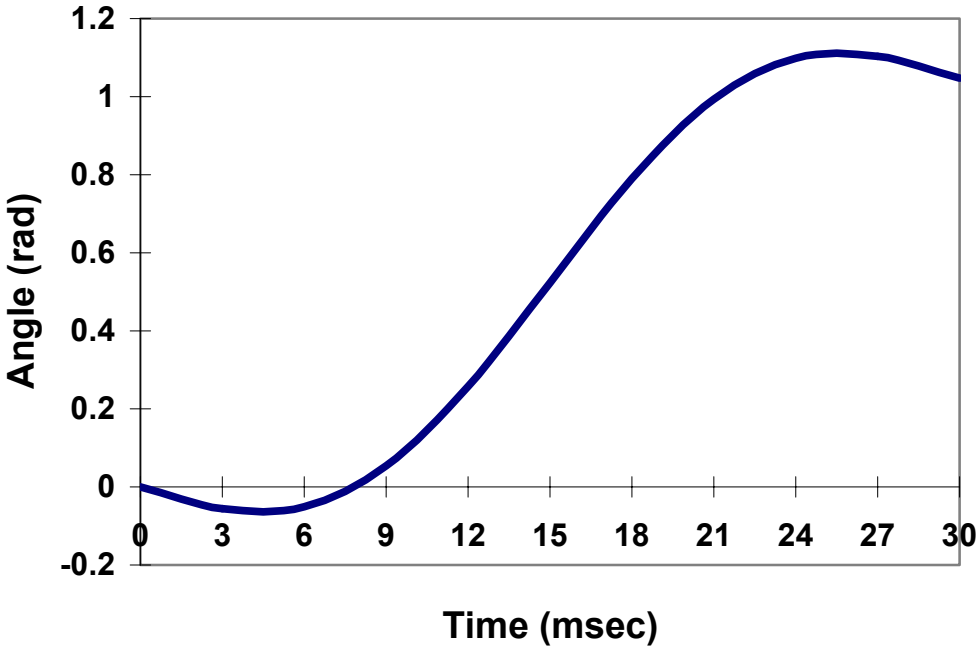

(b)

Figure 40. The impact load for GSM under rotational impact. (a) The angular acceleration taken from Zhang et al. (2001) and (b) the angular position driven from (a).

7-4-1 Results of GSM Rotational Impact

Figures 41a to 41d show the results of GSM under the impact of Figure 40 These results are the relative displacement between brain and skull in three regions of frontal, superior and occipital. Note that the positive Y direction is the direction from posterior to anterior, and positive Z direction is the direction from inferior to superior.

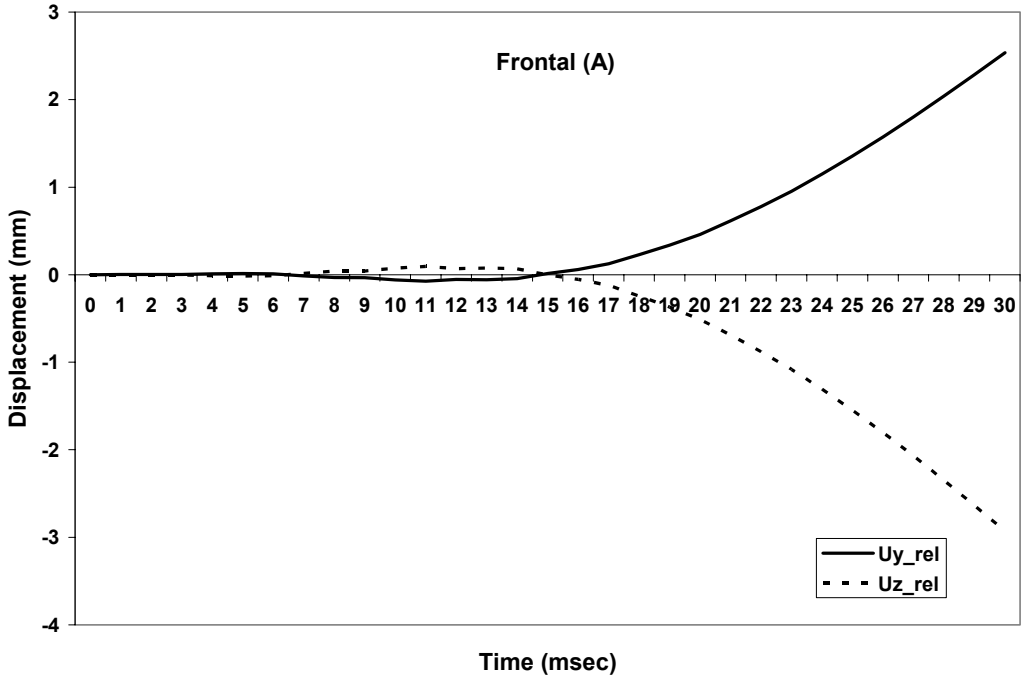

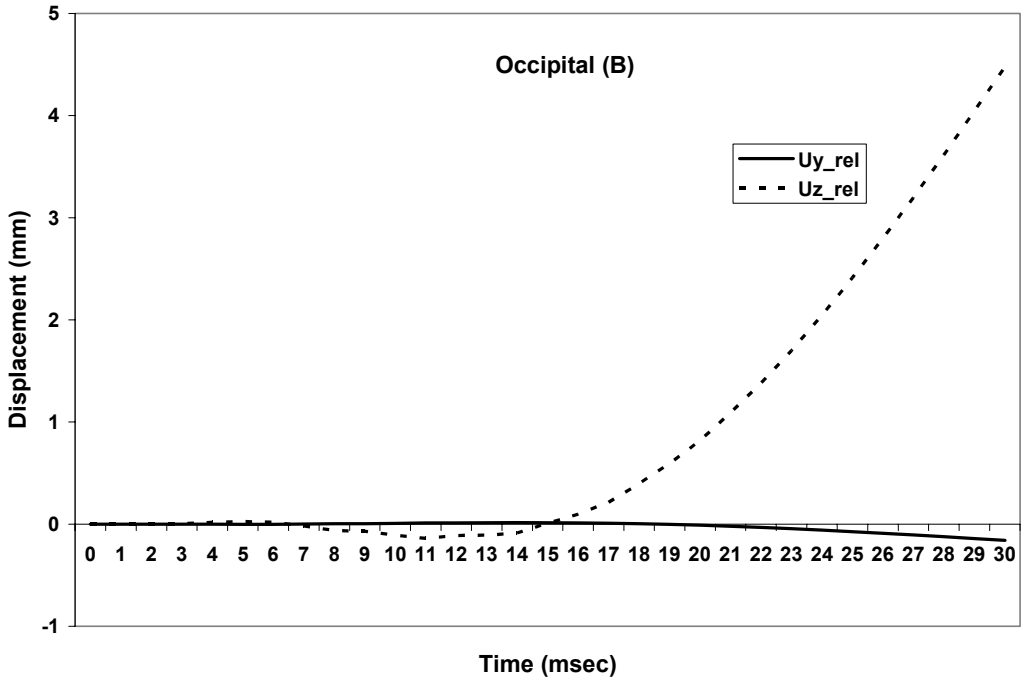
Occipital (B)
Uy_rel
Uz_rel
Displacement (mm)
5
4
3
2
1
0
-1
0 1 2 3 4 5 6 7 8 9 10 11 12 13 14 15 16 17 18 19 20 21 22 23 24 25 26 27 28 29 30
Time (msec)

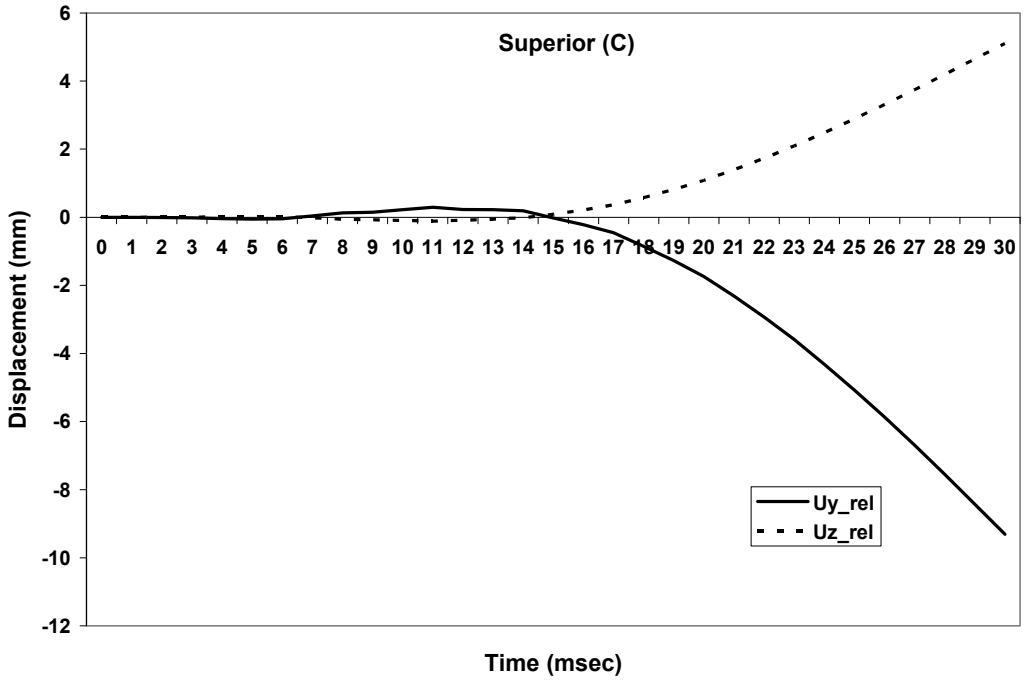
Superior (C)
Uy_rel
Uz_rel
Displacement (mm)
6
4
2
0
-2
-4
-6
-8
-10
-12
0 1 2 3 4 5 6 7 8 9 10 11 12 13 14 15 16 17 18 19 20 21 22 23 24 25 26 27 28 29 30
Time (msec)

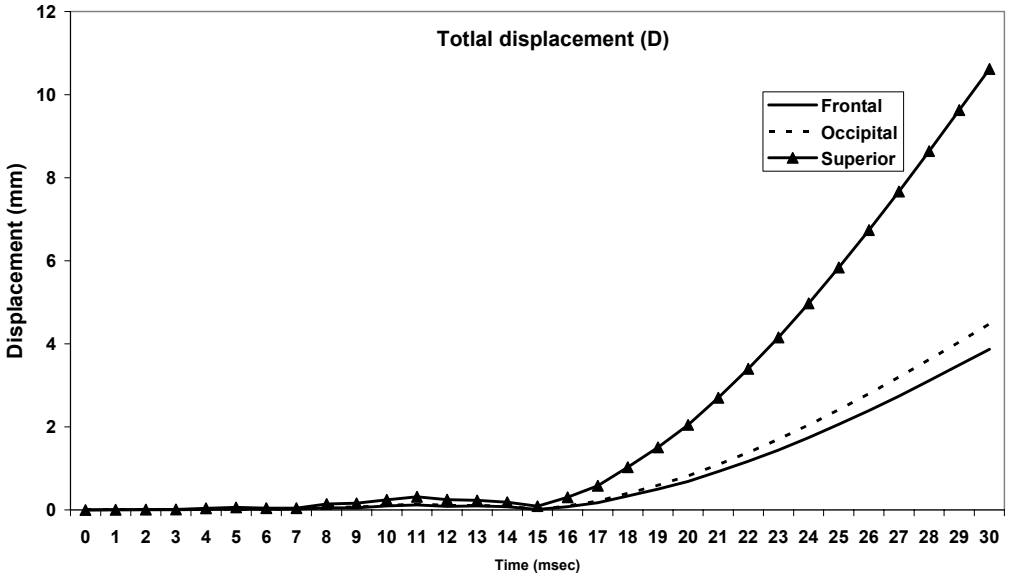

Figure 41. Results of GSM under rotational impact in three regions of frontal (A), Occipital (B) and Superior (C). The total displacement is shown on D. The superior has the largest relative displacement.

Figure 41d depicts the resultant of the relative displacement between the brain in Y and Z directions. As shown in this figure the relative displacement in the superior region is dominant among the others. This is in agreement with Gennarelli et al. (1982) and Huang et al. (1999). That is, in the sagittal plane rotation, the superior region has maximum relative displacement between brain and skull. Therefore the rupture and failure of the bridging veins are more likely in this region due to the abundance of the bridging veins in this region. Note that the rupture of the bridging veins is the causation of ASDH. In other words the rotational impact corresponds to ASDH.

8- THREE DIMENSIONAL GLOBAL FLUID MODEL (GFM)

GFM is basically the SAS region filled with CSF. As mentioned in anatomy section, there are trabeculae in SAS region. The interaction of CSF and SAS trabeculae creates an efficient damping system, in case of an impact. It is almost impossible to model the trabeculae individually in SAS, because of the abundance of them in SAS and also their non-uniform distribution. Thus the trabeculae were not included in the fluid model of this investigation. Instead, an equivalent viscous fluid was replaced for CSF and trabeculae system, which accounts for hydraulic resistance. That is, the solid /fluid interaction of trabeculae and the CSF, which has damping characteristics, was replaced with an equivalent viscous fluid with the same damping characteristics. This was accomplished by using experimental data of brain/head and using viscous shear flow analysis. Then the viscosity of the equivalent fluid was determined. Finally, the analysis of head impacts was performed using the equivalent properties.

8-1 Damping Characteristics

Hardy et al. (2001) used neutral density technology and high-speed biplanar X-ray to measure the relative motion of the brain with respect to skull. They applied 10 blunt impacts producing peak translational acceleration of 10 to 150 g and peak angular acceleration of 1000 to 8000 ras/s^2. These impacts were applied to 3 human cadavers while taking x-ray snap shots. Four of the impacts were made in the frontal region and the rest 6 impacts on the occipital region. The acceleration of brain was obtained from their results.

The logarithmic decrement method was used to determine the damping ratio of the head/brain system. That was calculated using two extreme values of acceleration X_1, and X_2 (Figure 42) measured from Hardy et al. (2001). The natural logarithm of the ratio of X_1 to X_2, δ, is:

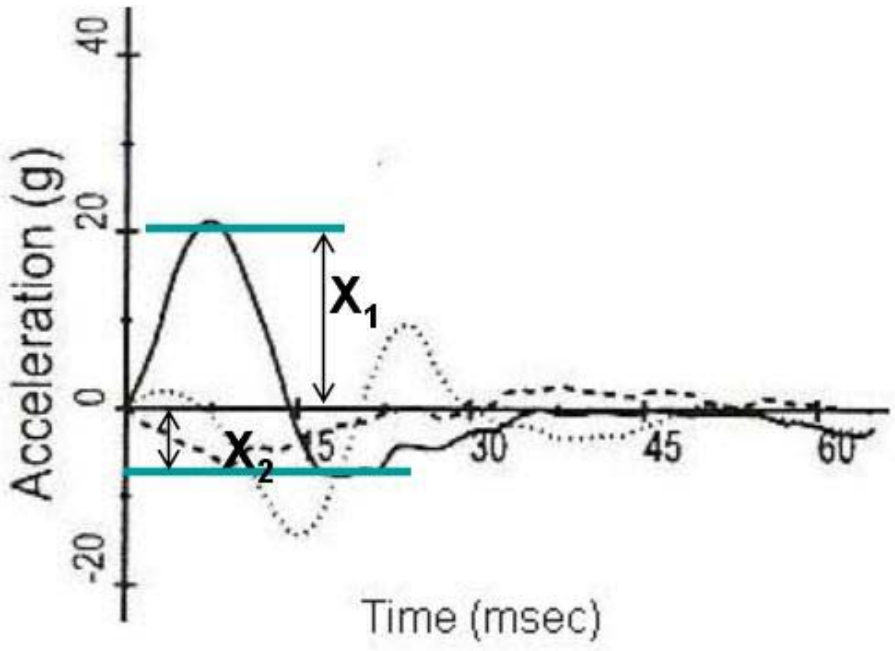

Figure 42- The acceleration graph. Taken from experiment C755-T2, Hardy et al. (2001).

$$\delta = \mathrm{Ln}(x_1/x_2) \qquad (1)$$

From δ, the critical damping ratio, ξ, is obtained:

$$\delta = (2.\pi.\ \xi)/(1 - \xi^2)^{0.5} \qquad (2)$$

Knowing the mass of the object (brain), m, and the natural frequency of the system, ω_n (from Figure 42), the critical damping, Cc, of the system can be evaluated as:

$$C_c = 2.m.\omega_n \qquad (3)$$

Therefore, by solving (2) for ξ and using (3), the damping coefficient, C is given by,

$$C = \xi . C_c \qquad (4)$$

The next step was to determine the damping force, F_{damp}, which is the product of the damping coefficient, C and the velocity of the fluid (CSF), v.

$$F_{damp} = C . v \qquad (5)$$

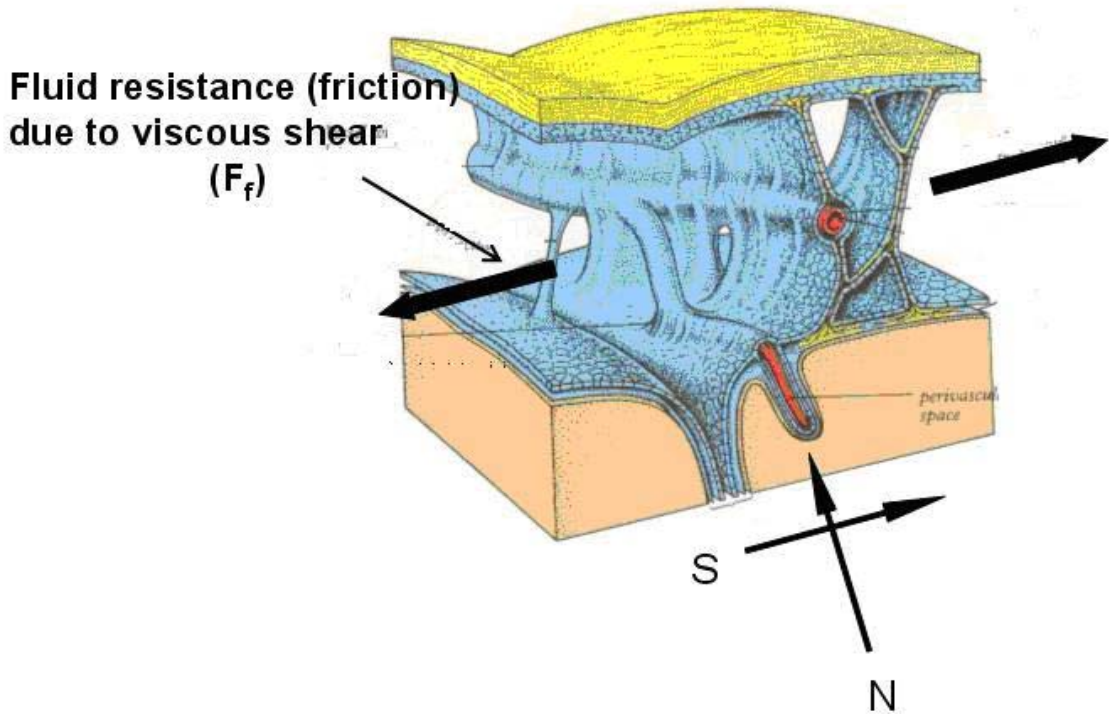

Figure 43- Regardless of the direction of the applied load, i.e., normal (N) and shear (S), the hydraulic friction is created. The cartoon is taken from Gray 1995.

To find the average value of the damping force the mean velocity of CSF needed to be defined. This was done using the angular velocity of the system given by Hardy et al (2001), which was depicted as a half sine wave. The effective (mean) value of the angular velocity was calculated ($w_{eff} = 0.707 w_{max}$) and multiplied by the average radius of the head (0.075 m) to determine the velocity, v.

As shown in Figure 43, during any head rapid movement, the brain moves with respect to the skull in tangential and normal directions. This would force the fluid (CSF), which is located in the SAS region, to flow in all directions while passing through the trabeculae space. Therefore, rapid head movement creates hydraulic friction due to the shear stress, τ between CSF and trabeculae. The

damping force calculated in (5) is the same as the friction force, F_f that is equal to:

$F_{damp} = F_f = \tau \cdot A$ (6)

To determine τ, the surface area of all trabeculae, A, which are in contact with CSF, needs to be calculated. Since there is no reference in literature regarding the specifics of the geometry of the trabeculae in SAS, the total area A has been approximated as follows.

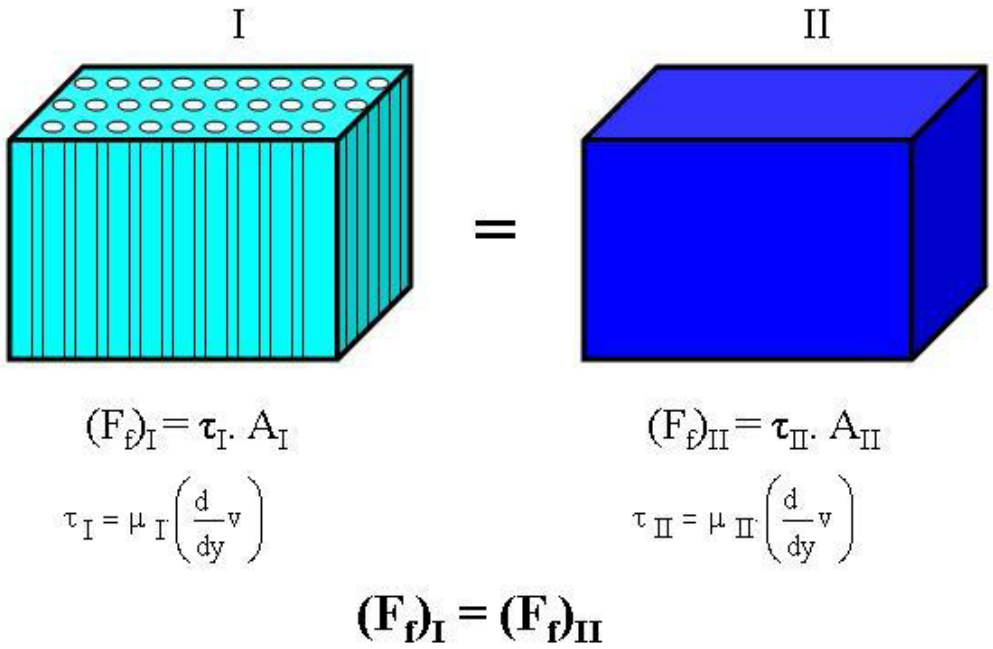

Figure 44- Schematic view of the damping model I, and the equivalent model without trabeculae, model II.

An arbitrary control volume of the SAS of the dimensions 4x4x3 mm^3 was selected. Based on the anatomy of the SAS and the abundance of the trabeculae in the region, it was assumed that the volume contains 121 trabeculae each having a cylindrical shape with diameter of 0.3 mm, as shown in Figure 44-I. The

total area of SAS consist of the total surface area of trabeculae that are in contact with the CSF was approximated to be 2 m^2. Therefore, using (6) the shear stress for the fluid model of Figure 44-I, τ_I, consisting SAS and CSF, was determined.

For CSF being a Newtonian fluid (Bloomfield et al. (1998), Brydon and Hayward (1995) and Ommaya (1968)), viscosity can be determined as:

$$\tau = \mu.(\Delta v/\Delta y) \qquad (7)$$

The velocity gradient was measured assuming changing the velocity from zero to its maximum over the maximum thickness of SAS that is 3mm, and assuming that one surface (skull) is moving with respect to the other surface (brain).

Therefore, the equivalent viscosity, μ, was calculated from (7), = 0.24 Pa.sec. Note that the idea is to determine the characteristics of an equivalent fluid model, as shown in Figure 44-II, which does not have any trabeculae and yet has the same damping characteristics to the one depicted in Figure 44-I. That is, the equivalent model of Figure 44-II eliminates the need to model each individual trabecula. Thus, we assume that the viscosity of the two models, I and II are equal as well as the two shear stresses τ_I and τ_{II}. To complete the material properties of the equivalent fluid, model of Figure 44-II, the density of the fluid was calculated as $\rho = 1100$ kg/m^3. This was based on the mixture of CSF (30%

with the density of 1000 kg/m^3) and trabeculae (70% with the density of 1130 kg/m^3).

The process in which viscosity of the CSF was calculated is described in a flow chart, as shown in Figure 45. That is, logarithmic decrement method was applied to the experimental results of Hardy, et al. 2001 and damping coefficient, damping force and the shear force was determined. Then, through a proposed geometry for the SAS and approximation of the area of the SAS the equivalent viscosity of the CSF in SAS was calculated. The equivalent viscosity was determined by relating the viscous shear into the damping force. The viscosity was validated, along with the fluid model, with the Nahum's experimental study as described in the next section.

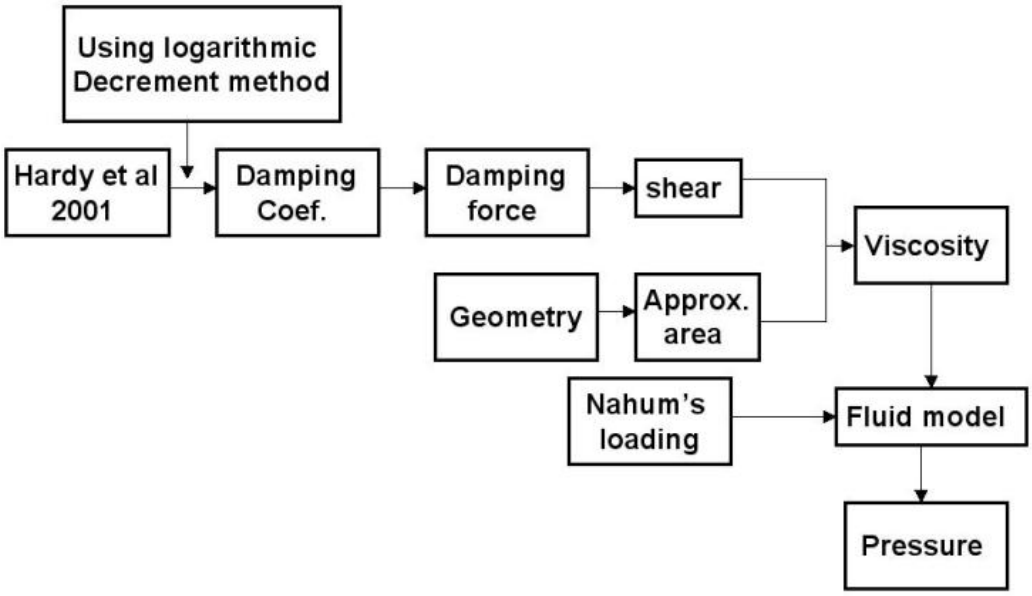

Figure 45. The steps taken to determine damping effect of the system of CSF and SAS trabeculae and the equivalent fluid model.

8-2 Model Construction

The head (including the skull and brain) solid model was constructed based on the geometry used by Horgan and Gilchrist (2003), Figure 46a. This model was extensively described in Zoghi-Moghadam and Sadegh (2006), however; only the SAS region was utilized for this analysis. That is, skull, brain, face and neck are not included in the current fluid model. Figures 46b to 46e show, the 3D fluid model, and other cross-sections including the frontal, sagittal and the transverse sections, respectively. Note that the three perpendicular sections of frontal, sagittal and transverse are passing through the center of the gravity (CG) of the brain. In the fluid model the skull and brain are assumed as rigid boundaries containing the equivalent fluid representing CSF and the trabeculae. The model was allowed to have relative displacement between the skull and the brain. Gambit software (Fluent Inc., NH, USA) was used as the preprocessor to generate the nodes and elements. There are total number of 500,316 tetrahedral elements and 154,687 nodes for this fluid model.

In performing the analysis of the model we faced two main challenges. The first challenge was due to the relative motion of the brain with respect to the skull. Up on the impact, as the brain moves toward the skull (or vice versa), the geometry of the fluid model (mesh) changes. Therefore, through out the analysis, the geometry of the fluid mesh (between the brain and the skull) was modified, to reflect the relative motion (displacement) of the brain and the skull. This process is called Dynamic Mesh Motion in the Fluent software. The software provides Dynamic Mesh Motion only for constant relative velocity of two objects. That is,

The Dynamic Mesh Motion is not a built-in function in the Fluent software for more complex functions such as nonlinear motion of brain and skull. A user-defined function was developed in C++ and was integrated into the solver, which described the motion of the skull and brain and created Dynamic Mesh as the analysis was proceed.

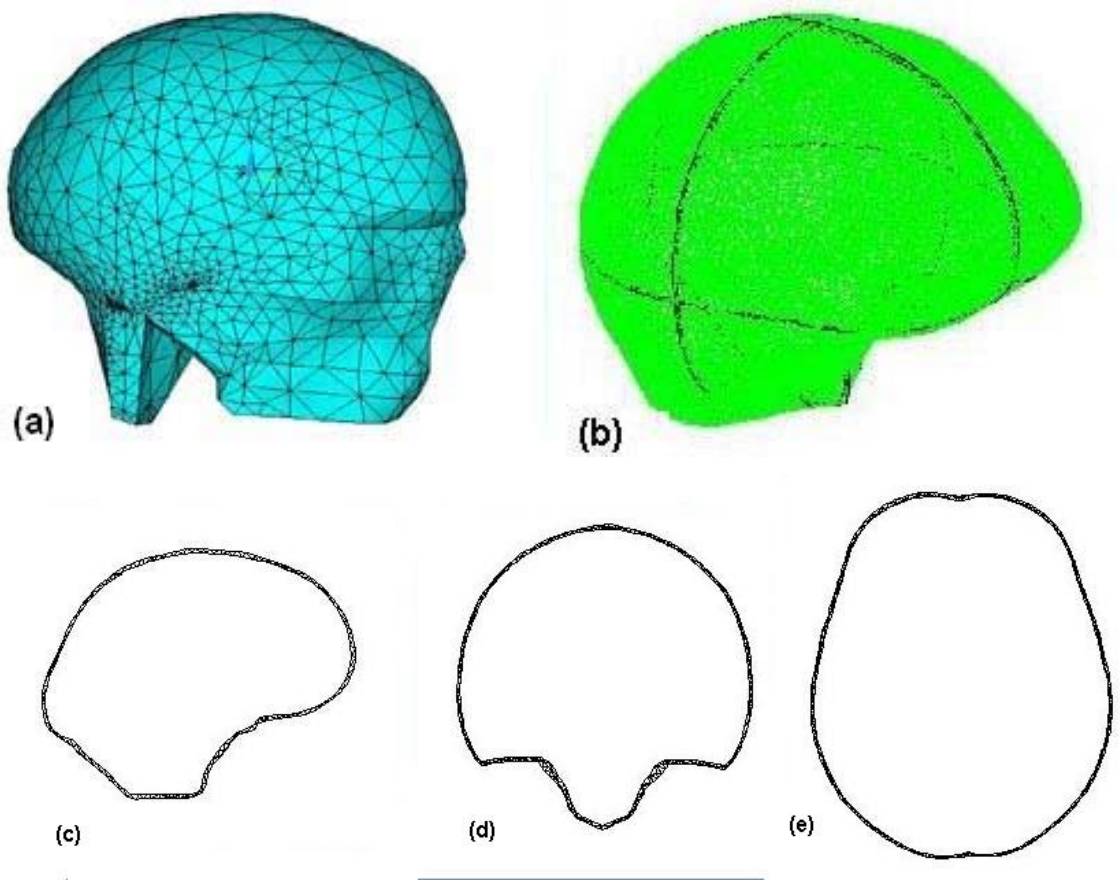

Figure 46- The 3D model. (a) original solid model, (b) isometric view, (c) sagittal section, (d) frontal section, (e) transverse section.

The next challenge was related to the collision of the moving boundaries (walls), i.e. skull and the brain. When they move toward each other, they may collide and Fluent software is unable to handle the collision of the walls. In the process of a head impact, the brain approaches the point of impact to the skull

and the trabeculae on one side collapse (buckle) while the trabeculae on the opposite site of the brain stretch. As the brain moves closer to the skull, the buckled trabeculae form a solid matrix of trabeculae, which reduces the brain movement. The collapse of the trabeculae prevents the direct contact of the brain with the skull. Due to the abundance of trabeculae in the SAS region it was assumed that the thickness of the solid matrix is about 80% of the thickness of the SAS region. Therefore, to overcome the collision of brain and the skull in this problem, a phase delay of 0.055 radians between the brain and the skull was used. This is based on the 2- mm average thickness of the fluid layer, or the length of trabeculae in the SAS region. Thus, the total distance that brain moves towards the skull is about 0.4 mm.

8-3 Validation of the GFM

The equivalent viscosity and the fluid model of the CSF and the SAS trabeculae were validated with available experimental results. Unfortunately there are a limited number of such studies. Nahum et al. (1977) performed two sets of impact tests on human head cadavers. They measured intracranial pressure changes during the impacts. Other studies include: Gennarelli et al. (1982) on the subhuman primates; Hardy et al. (2001) studied kinematics of head injuries using cadavers; and Trosseille et al. (1992) study on cadavers measuring the long term response of the brain to an impact. The experimental study of Nahum et al. (1977), which is the most frequently referenced study, was used to validate the fluid model.

The initial and boundary conditions used for this model were taken from the input load of Nahum et al. 1977, which is shown in Figure 20 as the time history of the applied force to the head. From this graph the velocity of the head was calculated over 6 msec (from 2 to 8 msec). This velocity was applied to the fluid model. The computational fluid dynamics (CFD) software, Fluent 6.1 software (Fluent Inc., NH, USA) was employed to perform an unsteady fluid dynamic analysis of the model.

In the process of applying the load history the brain was moved closer to the skull in the frontal region. As a typical result, shown in Figure 47, the cross section of the equivalent fluid layer (the distance between the brain and the skull) was reduced form d_1 at time step T_1=0 to d_2 at time steps, T_2=4.8 msec.

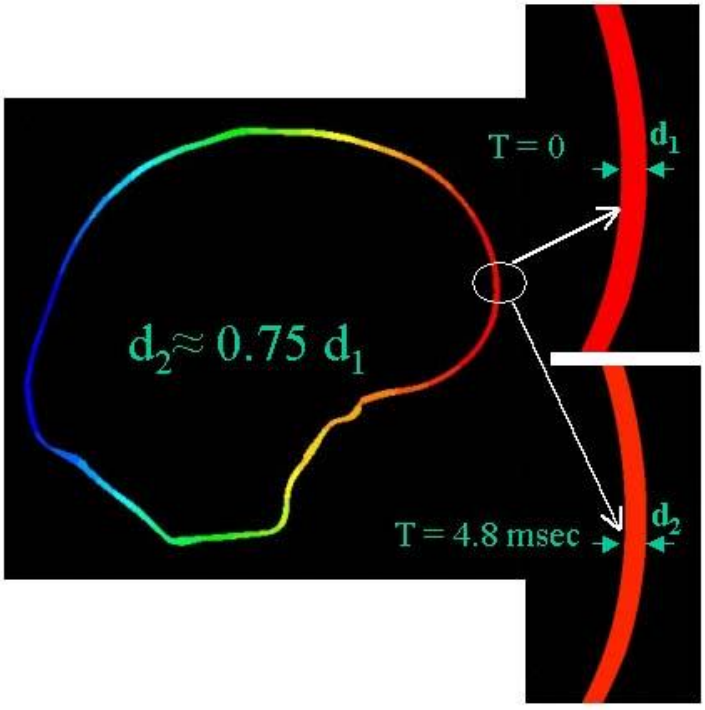

Figure 47. The relative motions between the brain and skull, d_1 and d_2, at two time steps, T_1=0 and T_2=4.8 msec, respectively, in the sagittal section of the fluid model.

The total pressure of the CSF was compared with the intracranial pressure reported by Nahum et al. (1977). As shown in Figures 48a and 48b the peak value of the pressure in the superior and frontal regions are about 5% more than that of experimental value.

8-4 GFM Blunt Impact

The GFM was subjected into a blunt head impact. The impact was taken from experiment 37 reported by Nahum et al. (1977). This is the same loading used for validation of the model (Figure 20), however it was applied in the form of velocity. Figure 49 shows the input of this loading, which is applied in the anterior to posterior direction (the positive value is from posterior to interior). As shown in the figure the motion of the brain is lagged by a value of 0.055 rad. As mentioned in section 8-2 this lag time is related to the collision of the boundary on the CFD code. Fluent software is unable to handle collision of the walls, therefore a phase lag was included in the motion of the brain.

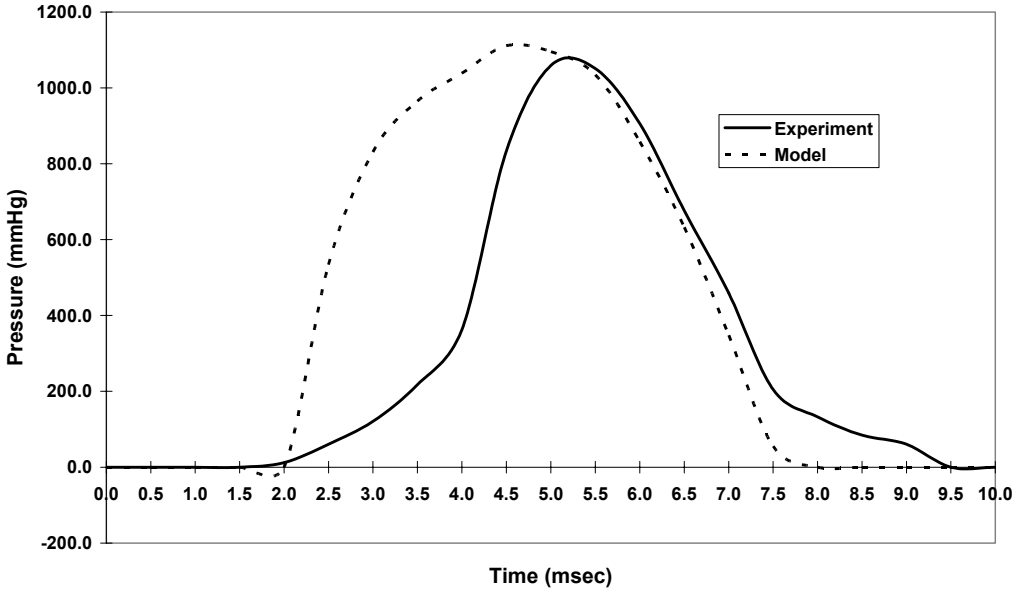

(a) frontal

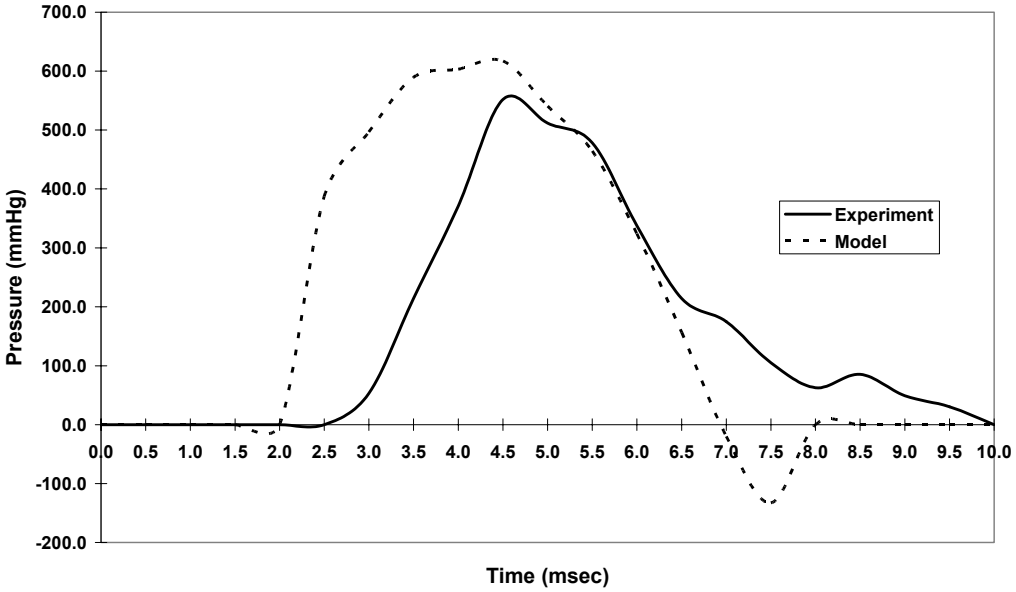

(b) superior

Figure 48. Validation of the numerical model against cadaveric experimental data (a) in frontal and (b) superior regions.

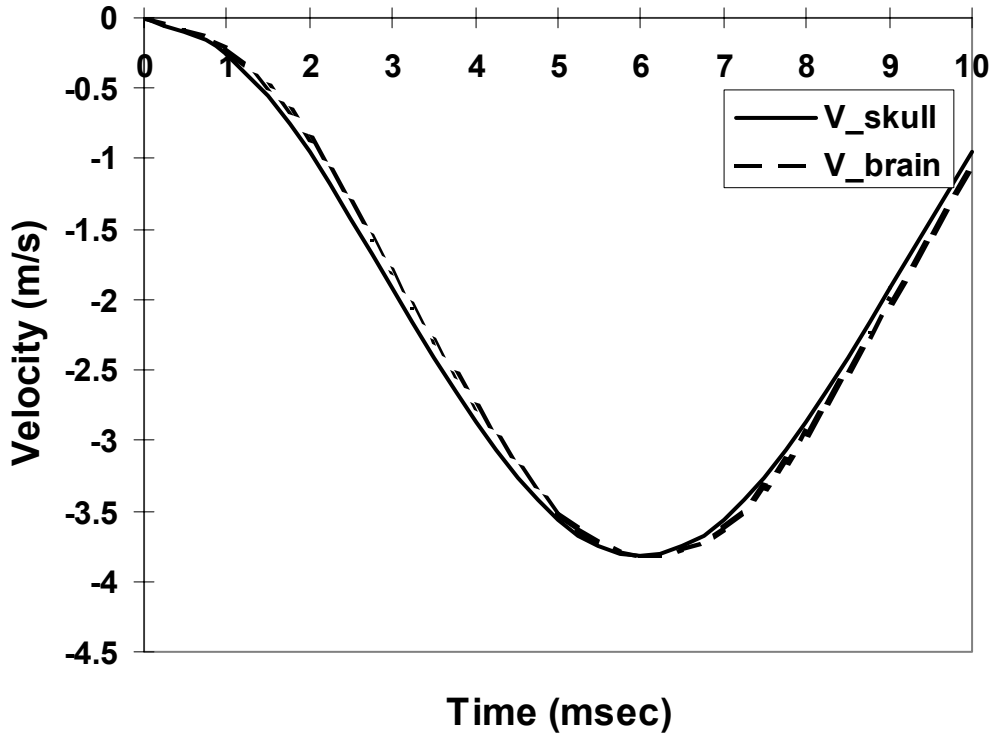

Figure 49- The input load for GFM under blunt head impact. Note that there is a 0.055 rad lag for the motion of the brain.

8-4-1 Results of GFM Blunt Impact

Figures 50 to 52 show typical series of pressure contour of the GFM under blunt head impact at two time steps of t = 5.0 msec and t = 8.0 msec. As shown in Figure 50, at t = 5.0 msec, the maximum pressure (the red zone) is in the frontal region and the minimum (the dark blue zone) is in the occipital region. As time passes the pressure drops in the frontal region and increases in the occipital region. At t = 8.0 msec, as seen in Figure 50, the pressure is more uniform. That is the pressure damps as time passes.

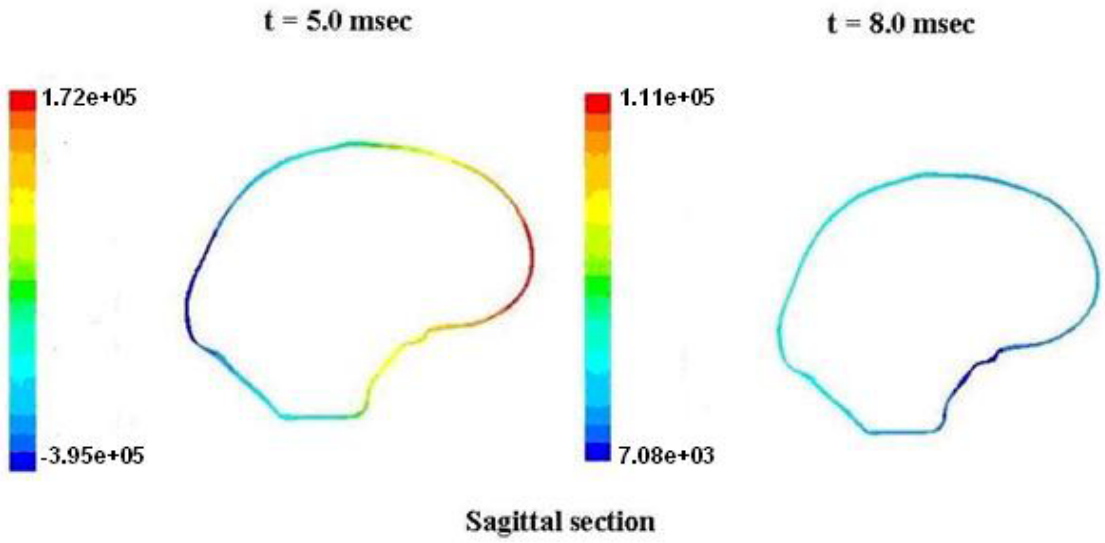

Figure 50- The pressure contour of the GFM under blunt head impact in the sagittal plane at t = 5.0 msec and t = 8.0 msec.

As sown in Figure 51, at both time steps the pressure is almost uniform. The reason for uniformity is that the impact is an anterior-posterior one and is perpendicular to the frontal plane, therefore it is expected that pressure be uniform in the frontal sections. The difference between these two time steps is that the pressure is lower at t = 8.0 msec. This difference is because of the damping qualities of the bran/skull system. Note that the geometry of the model has altered at t = 8.0 msec. This change is due to the relative motion between brain and skull.

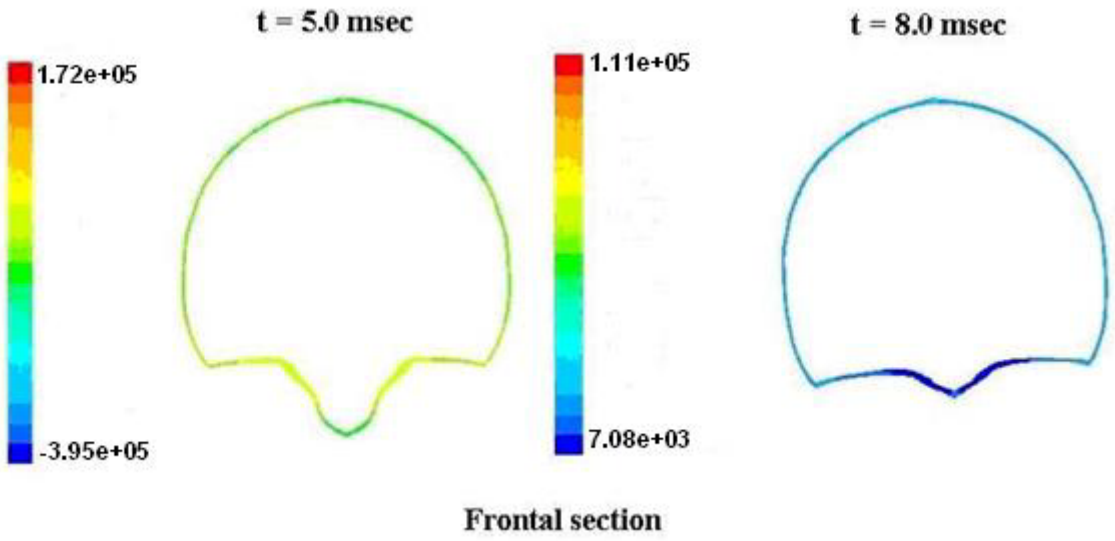

Figure 51- The pressure contour of the GFM under blunt head impact in the frontal plane at t = 5.0 msec and t = 8.0 msec.

As shown in Figure 52, at t = 5.0 msec, the maximum pressure (the red zone) is in the frontal region and the minimum (the dark blue zone) is in the occipital region. As time passes the pressure drops in the frontal region and increases in the occipital region. At t = 8.0 msec, as seen in Figure 52, the pressure is more uniform. This behavior is similar to the one in sagittal section. The reason for similarity is that the applied impact is parallel to these two sections.

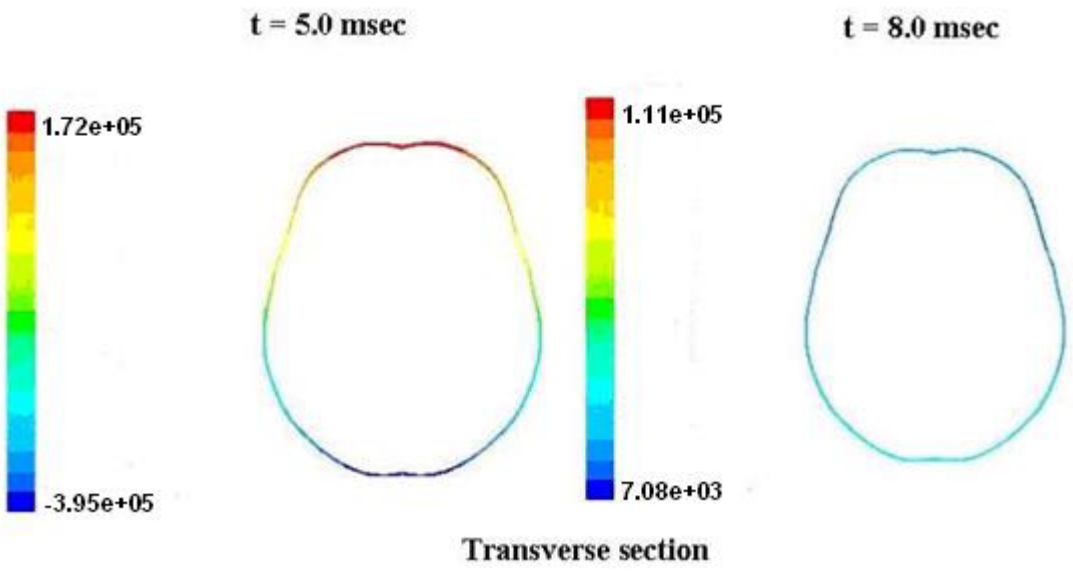

Figure 52- The pressure contour of the GFM under blunt head impact in the transverse plane at t = 5.0 msec and t = 8.0 msec.

8-5 GFM Rotational Impact

The same loading used for GSM was applied on the GFM in form of angular velocity. The angular velocity was determined by integrating the angular acceleration shown in Figure 40a over a range of 0 to 60° rotation. This impact is shown in Figure 53 and applied on the CG of the head/brain model.

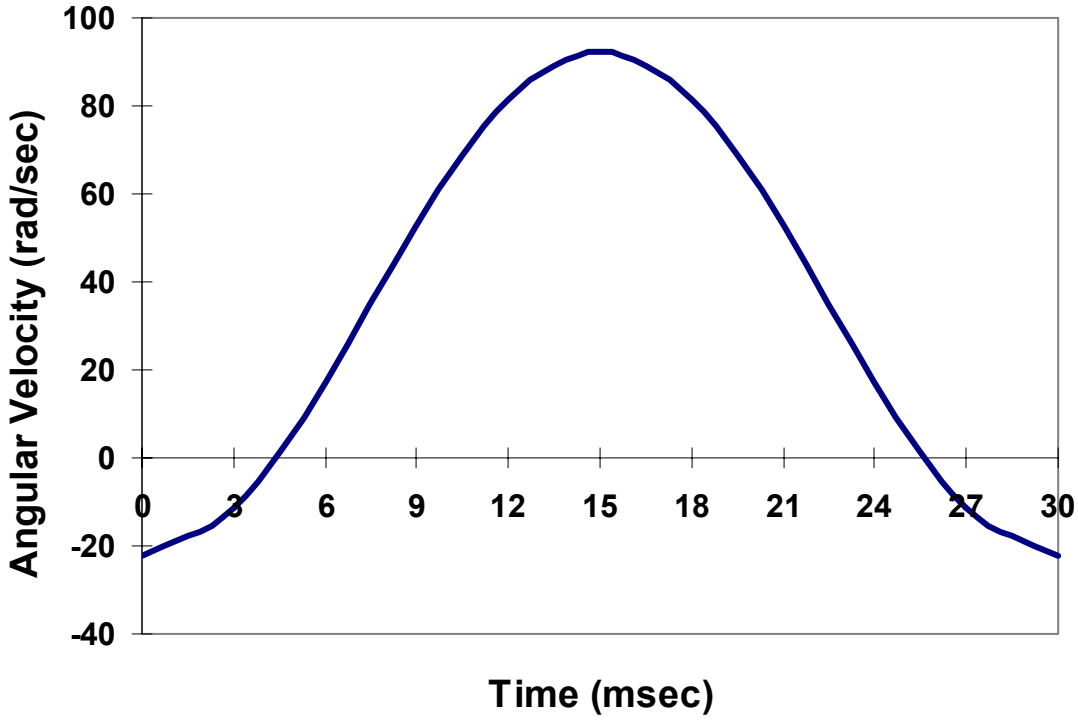

Figure 53- The loading used for GFM under rotational impact. The angular velocity was determined from the angular acceleration taken from Zhang et al. (2001) shown in Figure 40a with the initial angular velocity of –31.3 rad/s.

8-5-1 Results of GFM Rotational Impact

Figure 54 shows the pressure contour of the GFM in three perpendicular planes. As shown, the maximum pressure in the sagittal section is in the occipital region, where as time passes, it shifts to the frontal region. Figure 55 shows the pressure distribution of the CSF in three regions of frontal, occipital and superior. As shown in this figure the changes of the pressure in the frontal and occipital regions are relatively sharp while it is smoother in the superior region.

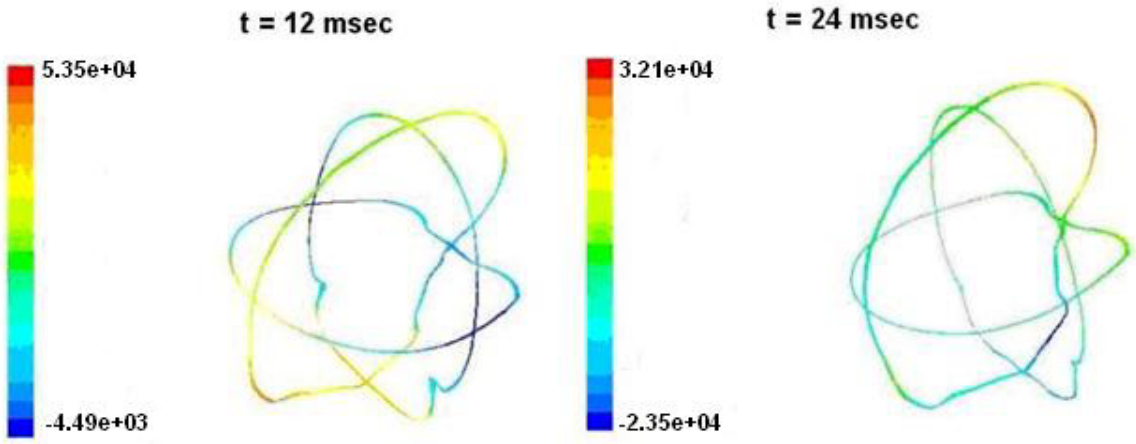

Figure 54- Pressure contours of GFM in three perpendicular planes at two time steps of t = 12 msec and t = 24 msec. As shown the maximum pressure at t = 12 msec is in the occipital region and it has been shifted to the frontal region at t = 24 msec.

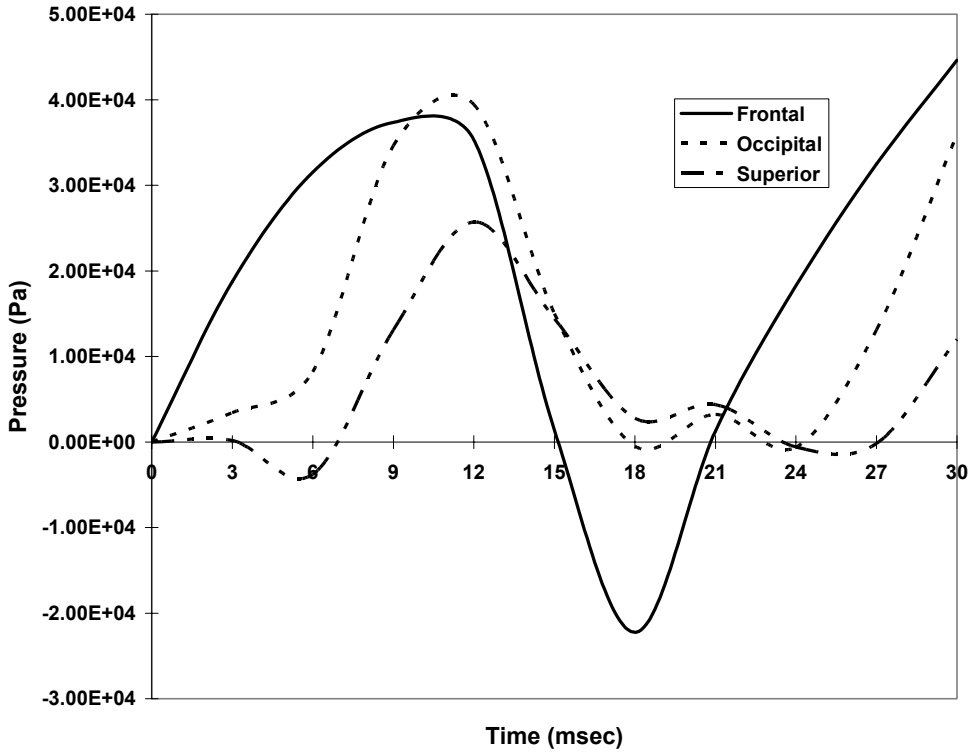

Figure 55- The pressure distribution of GFM under rotational impact in three regions of frontal, occipital and superior.

8-6 The Effect of the Surface Area and Viscosity Changes on the GFM

To evaluate the reliability of the current model a parametric study was performed where the variation of the CSF pressure distribution in the fluid model was determined as a function of the viscosity of the equivalent fluid and the surface area of the trabeculae. In the process of determining equivalent viscosity, through equation 6, the trabeculae surface area, shown in Fig. 44-I, was estimated (assumed) for the fluid model.

In this section, the sensitivity of the estimated surface area of the trabeculae and the change in viscosity with respect to the pressure distribution of the fluid model is presented. Specifically, through a curve fitting, an analytical relationship between the pressure and the viscosity was determined. Then, utilizing equation 6, the variation of the pressure with respect to the change in the estimated surface area was examined.

The fluid model was subjected to the same boundary condition used for validation (as shown in Figure 20), however, with different viscosities. The viscosity changes ranged from : =0.001-Pa.sec (viscosity of water) to := 0.30-Pa.sec, with the total number of 11 cases. Figure 56 shows the pressure distribution of all the 11 cases for the frontal region. As shown in Figure 56, the pressure rises nonlinearly as the viscosity increases. Since brain injuries generally occur at about the time where the maximum CSF pressure occurs, only the relationship between the peak pressures and the viscosity was explored. A statistical analysis was performed on the peak values of the pressure curves,

shown in Figure 56. A nonlinear model was curve fitted on the data and a satisfactory equation,

$P = P_0 + a \cdot e^{b\mu}$, (8)

was determined, where the constants of the equation were determined through the curve fitting, with $R^2 = 0.9998$ as,

$P_0 = 535{,}846$ (Pa), a= 614,878 (Pa) and b= 0.5132 $(Pa.Sec)^{-1}$.

Figure 57 shows the exponential growth of the pressure as a function of viscosity.

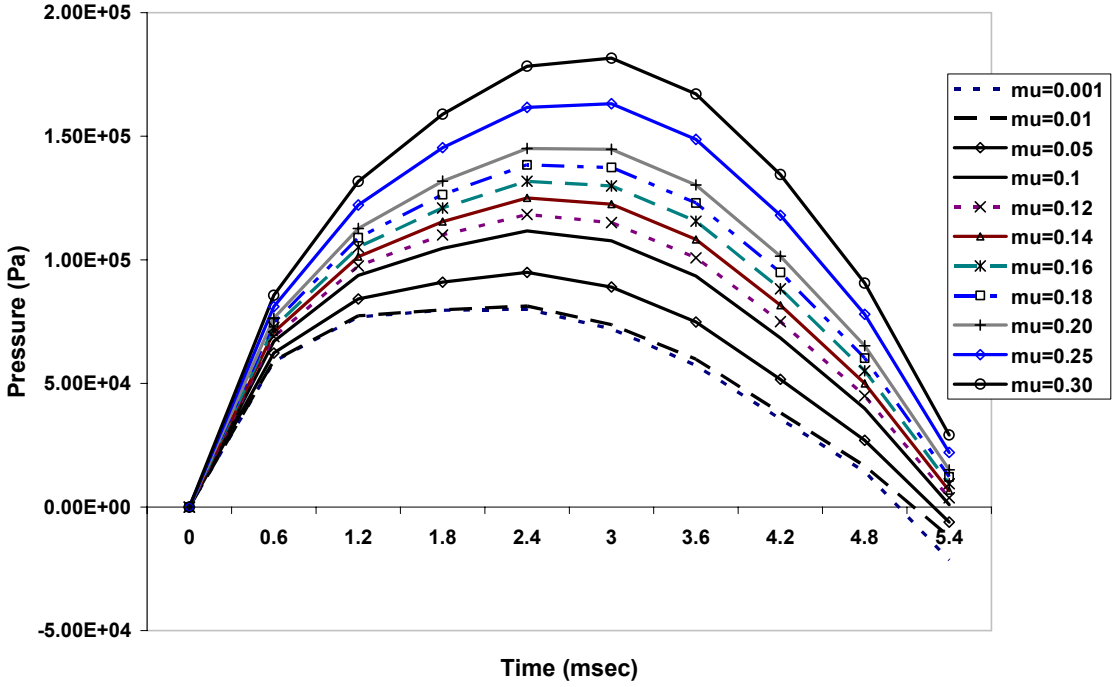

Figure 56- Variation of pressure with respect to viscosity in the frontal region.

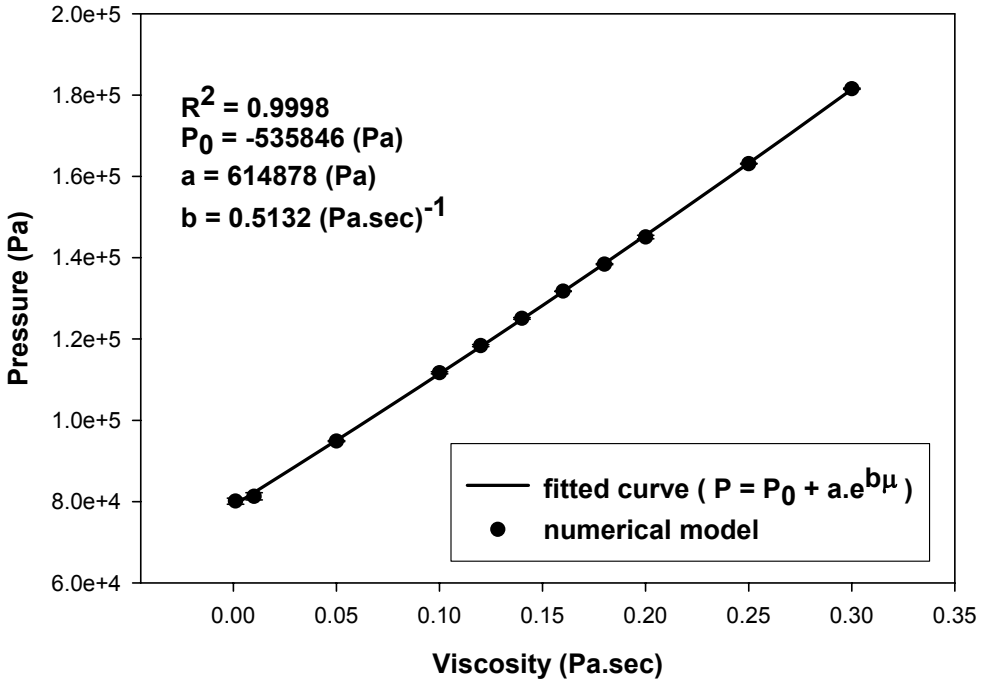

Figure 57- The pressure with respect to viscosity follows an exponential growth.

Having an analytical function for the maximum pressure with respect to viscosity, equation 8, the sensitivity of the fluid model to the variation of the estimated area was studied. The estimated trabeculae surface area of 2 m^2 was varied (+/- 15%) and the change in viscosity and the CSF fluid pressure were calculated. The upper and lower limits of the surface area (i.e., 2.3 m^2 and 1.7 m^2,) respectively, resulted in the viscosity change of 0.20 Pa. sec to 0.27 Pa. sec., and are given in Table 8. The viscosity values were substituted into equation 8 and the peak pressures were determined. Figure 58 shows the relative changes in pressure with respect to the relative area change. Figure 58 and Table 8 indicate that for +/-15% change in the trabeculae area resulted in the peak pressure changes from -6.7 to 9.3 %, respectively.

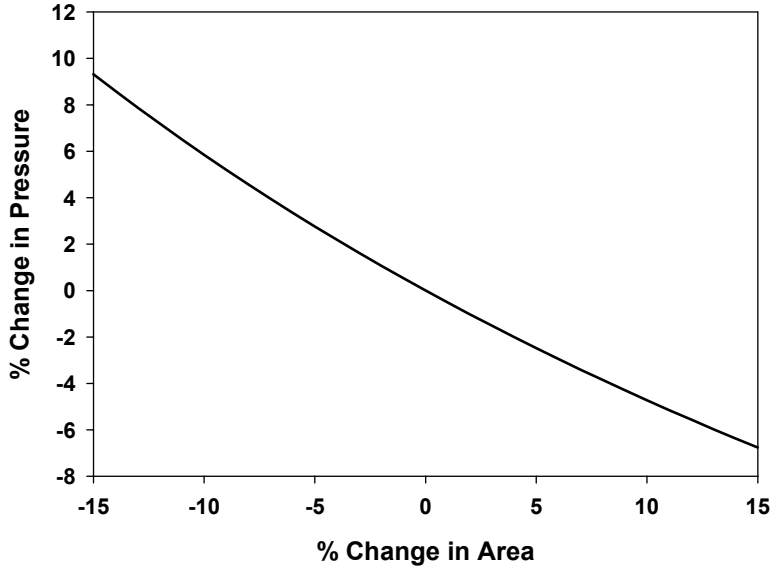

Figure 58. Percent change of the pressure with respect to percent change of area. For +/-15% area change, pressure varies within 9.3% and – 6.7%.

Table 8. The variation of the pressure as the viscosity changes to ±15% of its initial value.

	μ_1 = 0.27 Pa.sec	μ_2 = 0.24 Pa.sec	μ_3 = 0.20 Pa.sec
Relevant area (m^2)	1.7	2.0	2.3
Pressure (Pa)	170,409	155,881	145,336
% error (pressure)	9.3	0	-6.7

8-7 Damping Analysis Discussion

The main objective of the GFM was to quantify the damping characteristics of the SAS trabeculae and to establish an equivalent fluid model for SAS region, representing the cerebrospinal Fluid (CSF) and the SAS trabeculae. To accomplish this goal, first, the effective viscosity of the CSF and

SAS trabeculae was calculated using the cadaver study of Hardy et al. (2001). Following the steps of logarithmic decrement method, the damping force of the system was calculated. Since the CSF is a Newtonian fluid (Bloomfield et al. (1998), Brydon and Hayward (1995) and Ommaya (1968)), then the damping force is related to the viscosity through $\tau = \mu (\partial v/\partial y)$, where the shear stress, τ, is the damping force divided by the surface of the SAS trabeculae.

There is no specific data in the literature regarding the geometry of the SAS trabeculae. Perhaps that is due to the abundance of the trabeculae and also their random orientation in the SAS region. Based on the anatomy of the SAS trabeculae (Gray Anatomy 1995) a structural model was introduced and the surface area of the trabeculae was estimate 2 m^2. This led to an equivalent viscosity value of 0.24 Pa.-sec. This viscosity represents the CSF fluid and the trabeculae interactions. In this section, a 3D fluid model of CSF, without trabeculae was created and was validated with the experimental results of Nahum et al. (1977).

While efforts were made to accurately estimate the surface area of the trabeculae, the estimated surface area of 2 m^2 was varied (+/- 15%) and the change in viscosity and the CSF fluid pressure were calculated. Figure 58 and Table 8 indicate that the peak pressure changes from -6.7 to 9.3 % (within +/- 10%) range as a result of the +/-15% change in the trabeculae area.

GFM introduced a new method of accounting for the hydraulic damping characteristic of the CSF in the SAS region. Using the equivalent viscosity eliminates a tedious and time-consuming process of modeling the trabeculae,

and would reduce computation time for running a head/brain model significantly. In addition, using the equivalent viscosity safeguards the accuracy of the results. Even a very elaborate and detailed model of CSF may not lead to accurate results since the material properties of the SAS trabeculae are not well established in the literature and more experimental studies are needed. That is, more experimental studies are needed to determine the geometry and mechanical properties of the meningeal layers. Although Hardy et al. (2001) performed experimental studies on human cadavers, still more experiments on human cadavers specifically for the purpose of determining the damping characteristics of the head/brain system are needed.

In light of the fact that the fluid (CSF) and solid (SAS trabeculae) interaction plays an important part of the damping head impacts and thereby protecting the brain from injuries, using this method could enable the researches to create more realistic models for the study of head/brain injuries.

9- THREE DIMENSIONAL LOCAL SOLID MODEL (LSM)

To locally study the mechanism of injury a local 3D model of meningeal region is to be created in this section. This model works with the other two global models GSM and GFM.

9-1 Model Construction

The local model was constructed using the base geometry model. A section of 6mm*6mm was cut and prepared for the modeling. The emphasis of this model is on the meningeal layers and SAS region. The model consists of (from outer to inner) skull (a thin layer), dura mater, arachnoid, SAS region, randomly oriented trabeculae, blood vessels (one artery and one vein), pia mater and brain. As shown in Figure 59 this model is a multi-layered model. Since this model is a local model and is cut from the real size model, the boundary conditions at the planes of cut were carefully considered. To suppress the effect of boundary condition, the edges of the model were extended twice as the model size. Due to Saint-Venon principle there is no effect of boundary condition far from loading sight. The model with its extensions is shown in the Figure 59.

ANSYS 8.0 software (ANSYS INC., PA) was used as preprocessor to generate the model and the elements. The total number of elements is 183,612 and the total number of nodes is 132,259. The mesh details for the components of LSM are summarized in Table 9. The material properties used for this model was taken from Zhang et al. (2001, 2002). Table 10 shows the material

properties used for this model. ANSYS 8.0 software (ANSYS INC., PA) was used to perform the analysis.

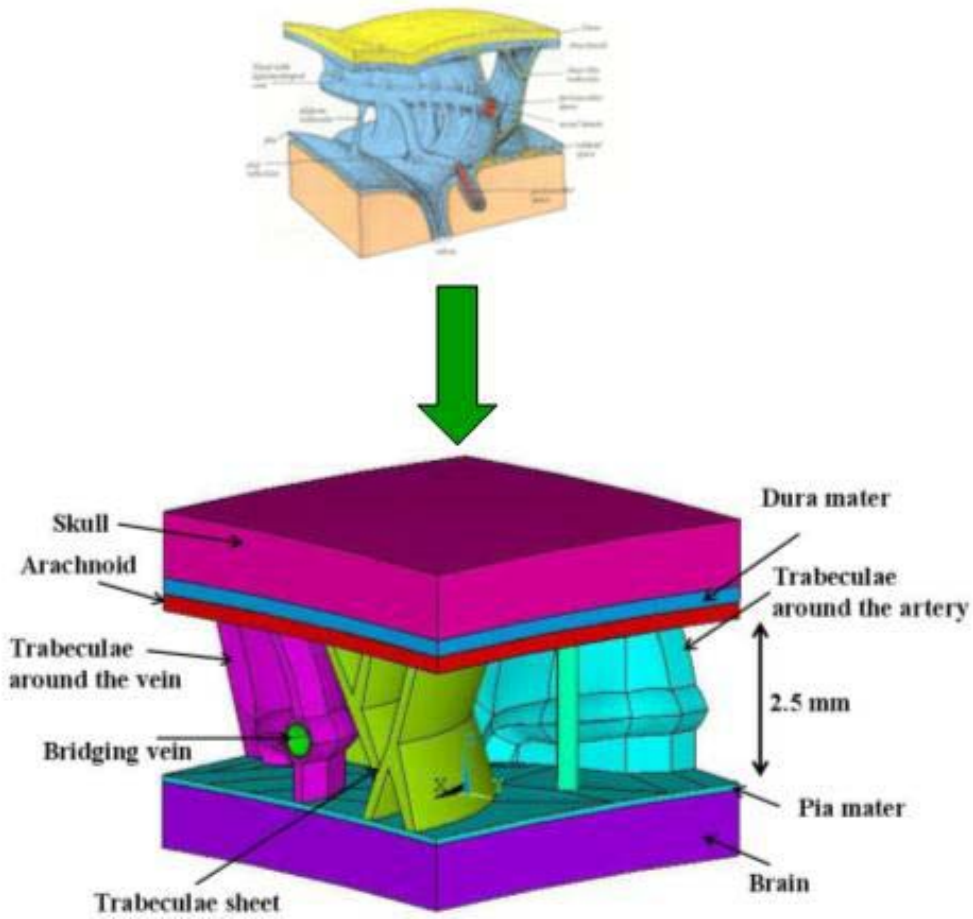

Figure 59. The local model and its components. The cartoon is taken from Gray, 1995.

Table 9. The element properties and type used for LSM. The total number of elements is 183,612 and the total number of nodes is 132,259. The information for the extended region is not tabulated (23,024 elements and 15,248 nodes). Type I element is ANSYS-solid187 3D 10-node tetrahedral structure solid. Type II element is ANSYS visco89 3D 20-node viscoelastic solid.

	Skull	Dura mater	Arachnoid and trabeculae	Artery	Vein	Pia mater	Brain tissue
Element type	I	I	I	I	I	I	II
# of elements	2536	1806	45602	39644	41479	9806	19715
# of nodes	2357	1137	32166	26231	27505	6308	21127

9-2 LSM Blunt Impact

In this study a global/local approach have been employed. That is, the desired loadings were applied on the two global models (GSM and GFM). The outputs of GSM, which was relative displacement between brain and skull, and also the one for GFM, which was the pressure distribution of CSF, were employed as boundary condition and loading of LSM.

LSM was subjected to two sets of blunt impacts. These are the loadings producing HIC values of 744 and 1040, respectively. The first blunt impact is the one used for validation of the global models. Since Nahum et al. (1977) data was used for validation of the two global models, the output of those analyses was used as the input for the current analysis. As mentioned above this impact produces a HIC value of 744. Figures 60 and 61 show the relative displacement

and the pressure, respectively. The second impact is taken from experiment number 49 of Nahum et al. (1977). This impact produces a HIC value of 1040.

Table 10- Material properties used for LSM. The properties of the brain tissue is the same as the ones shown on Table 6.

Skull	Young's modulus (E) (Pa)	$12.2*10^9$
	Poisson's ratio (υ)	0.22
	Density (ρ) (kg/m^3)	$2.12*10^3$
Dura mater	Young's modulus (E) (Pa)	$31.5*10^6$
	Poisson's ratio (υ)	0.45
	Density (ρ) (kg/m^3)	$1.13*10^3$
Arachnoid and trabeculae	Young's modulus (E) (Pa)	$21.5*10^6$
	Poisson's ratio (υ)	0.45
	Density (ρ) (kg/m^3)	$1.13*10^3$
Pia mater	Young's modulus (E) (Pa)	$11.5*10^6$
	Poisson's ratio (υ)	0.45
	Density (ρ) (kg/m^3)	$1.13*10^3$
Artery	Young's modulus (E) (Pa)	$15.0*10^6$
	Poisson's ratio (υ)	0.48
	Density (ρ) (kg/m^3)	$1.04*10^3$
Vein	Young's modulus (E) (Pa)	$4.6*10^6$
	Poisson's ratio (υ)	0.48
	Density (ρ) (kg/m^3)	$1.13*10^3$

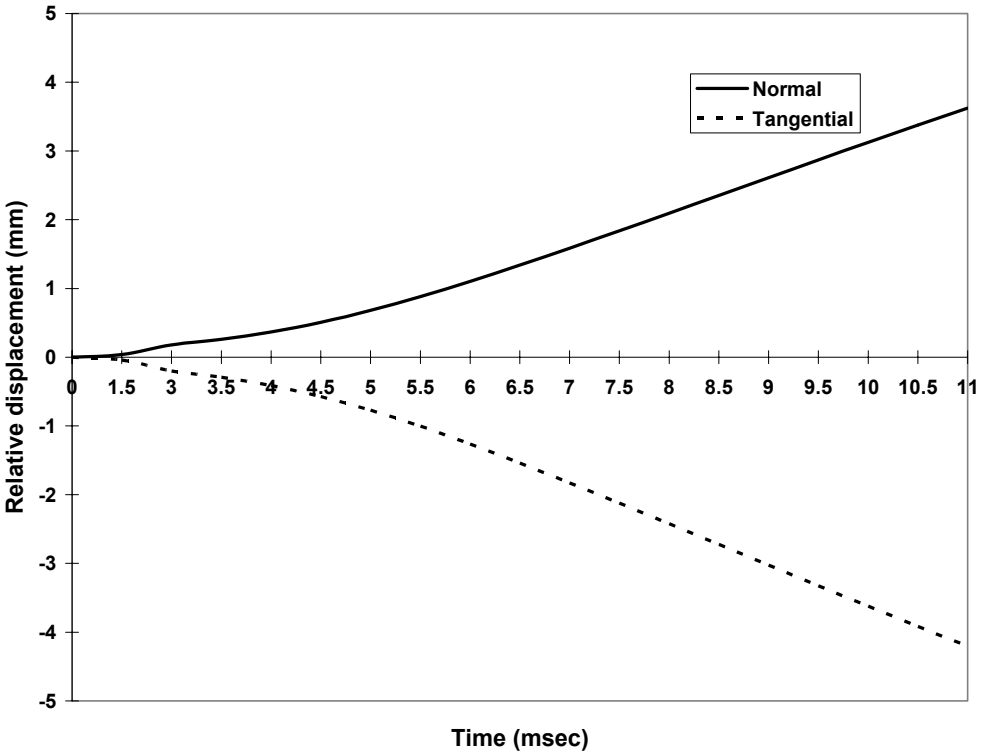

Figure 60- The relative displacement between brain and skull determined from the frontal region of GSM (point 1 of Figure 35). This was applied to LSM. Note that the positive normal direction is compression.

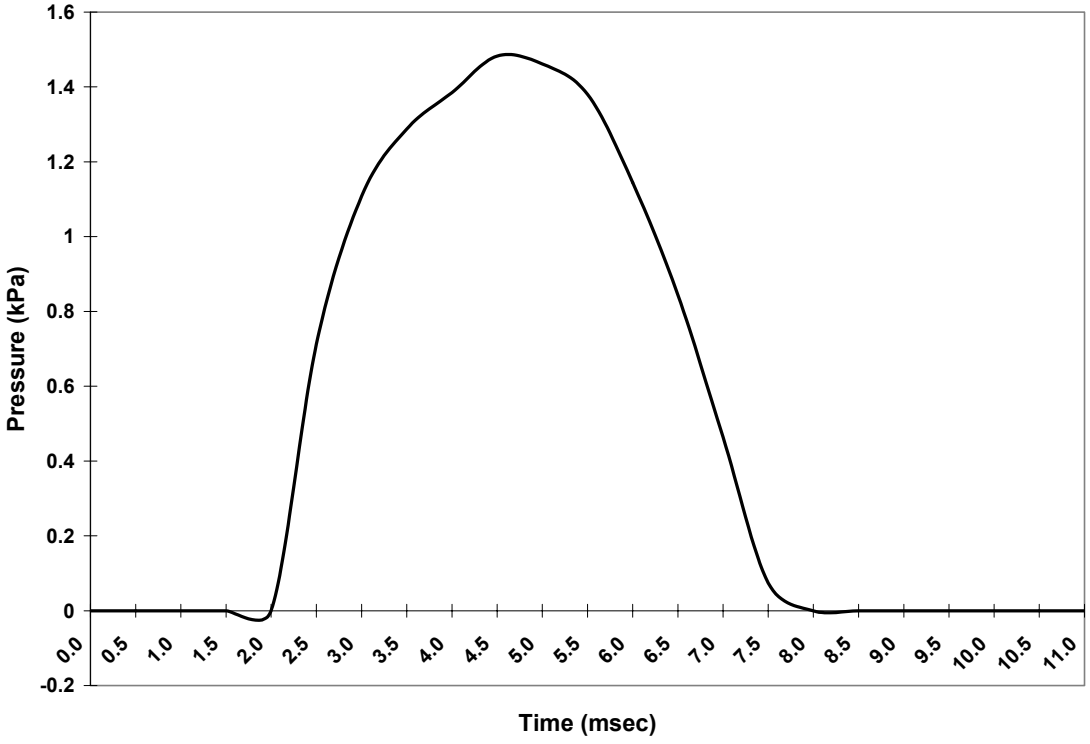

Figure 61- The pressure distribution over time in the frontal region of GFM. This was applied on LSM.

ANSYS 8.0 software (ANSYS INC., PA) was used to solve the local model. As the boundary conditions shown in Figures 60 and 61 suggest, a dynamic analysis was performed on LSM. It took 40 hours for a 2.4 GHz processor to complete the analysis.

9-2-1 Results of LSM Blunt Impact

The goal of LSM is to introduce a tool for quantifying ASDH and subarachnoid hemorrhage (SAH). In order to do that the blood vessels in LSM should be carefully studied. The strain fields of the blood vessels will be

compared to the experimental values of the ultimate strain for cerebral vessels reported by Monson et al. (2000, 2003).

The strains of the blood vessels of LSM subjected to the second loading set (HIC = 1040) are shown in Figure 62. The two selected incidences are t = 5.5 msec (the time of the peak pressure) and t = 11.0 msec (the end time).

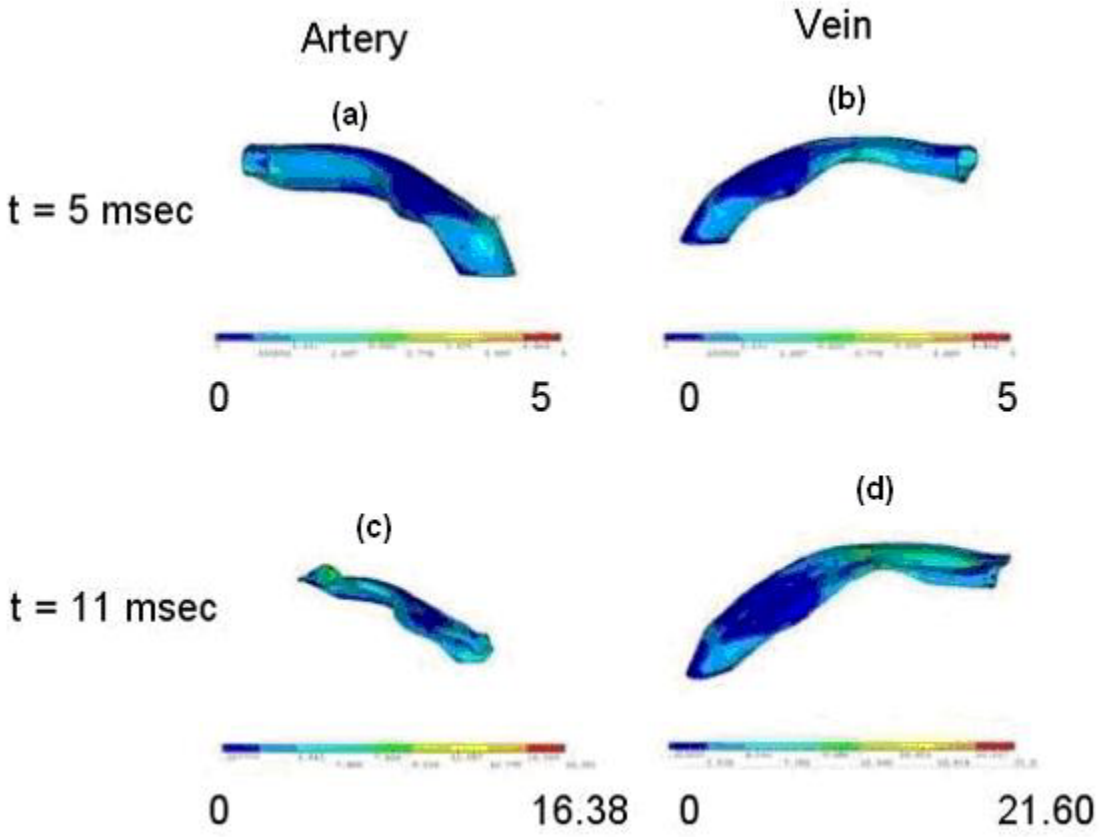

Figure 62- Strain distribution of LSM (mm/mm) under the second loading set (HIC = 1040) (a) in the artery at t = 5.0 msec, (b) vein at t = 5.0 msec, (c) artery at t = 11.0 msec and (d) vein at t = 11.0 msec.

Figure 63 shows the average strain of the blood vessels in four incidences of t = 3.0 msec, t = 5.0 msec, t = 8.0 msec and t = 11.0 msec for the first loading set (HIC 744). The average strains are drawn with respect to the normalized

value of the position to length. These results are compared to the experimental results of Monson et al. (2000, 2003).

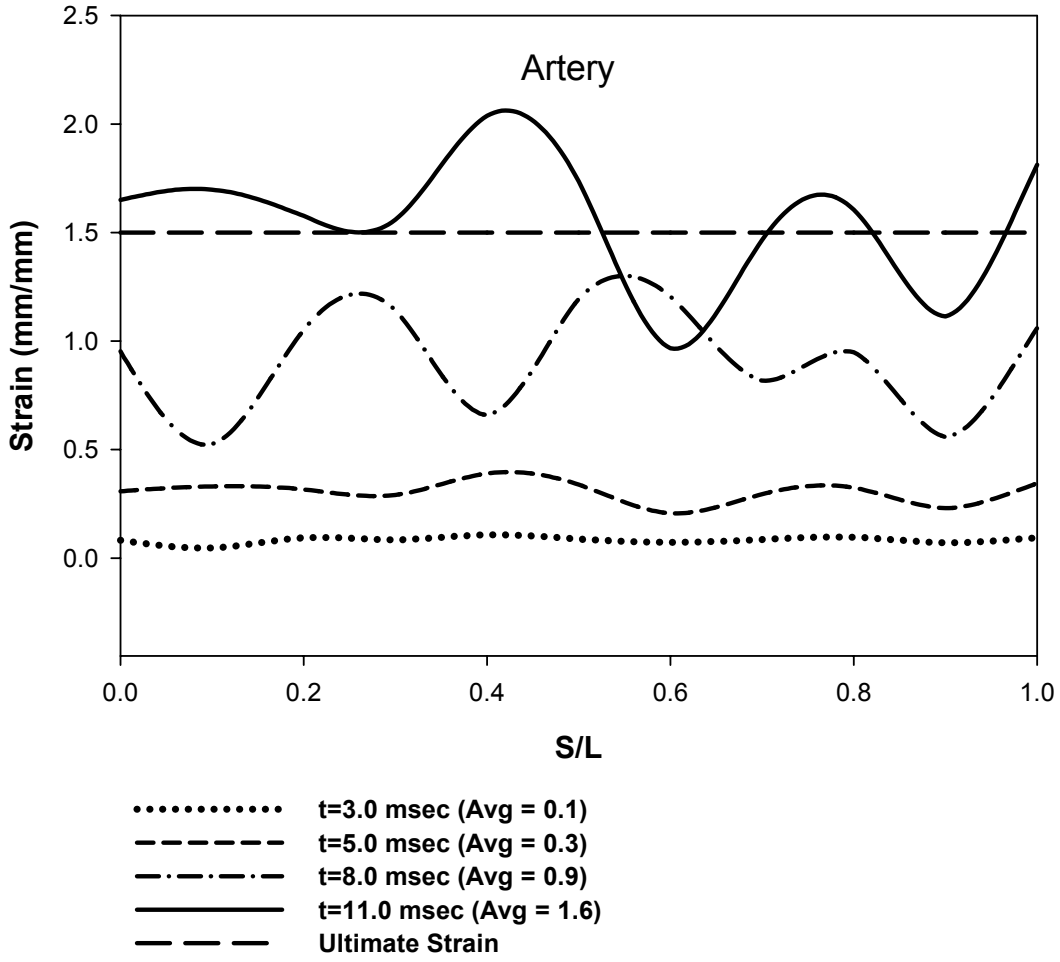

(A)

Figure 63-A. Strain versus dimensionless length of the artery. The horizontal dashed line is the ultimate strain of the blood vessels from experimental studies performed by Monson et al. (2000, 2003). The loading is taken from a model under HIC=744.

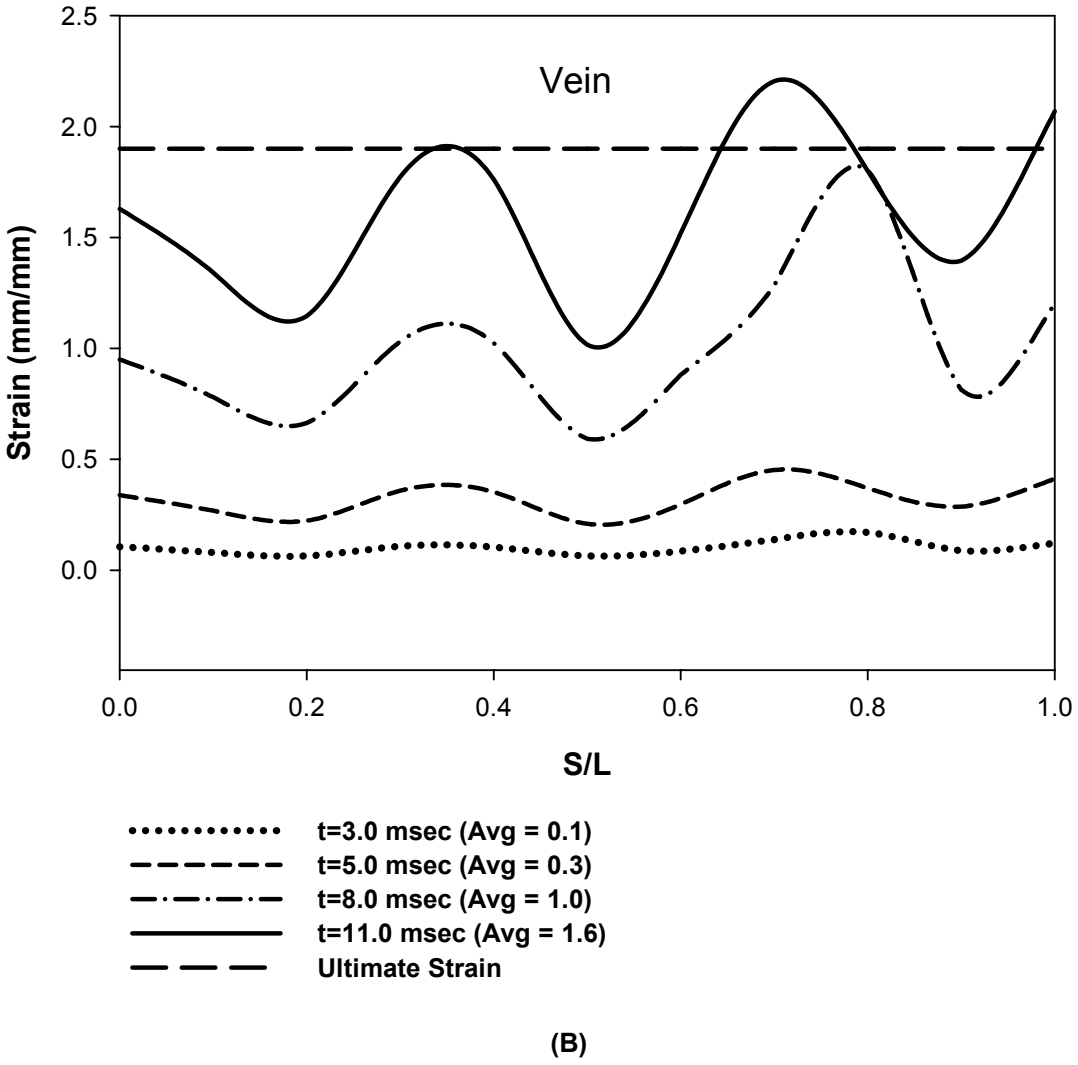

(B)

Figure 63-B. Strain versus dimensionless length of the vein. The horizontal dashed line is the ultimate strain of the blood vessels from experimental studies performed by Monson et al. (2000, 2003). The loading is taken from a model under HIC=744.

Figure 64 shows the average strain of the blood vessels in four incidences of t = 3.0 msec, t = 5.0 msec, t = 8.0 msec and t = 11.0 msec for the second loading set (HIC 1040). The average strains are drawn with respect to the normalized value of the position to length. These results are compared to the experimental results of Monson et al. (2000, 2003).

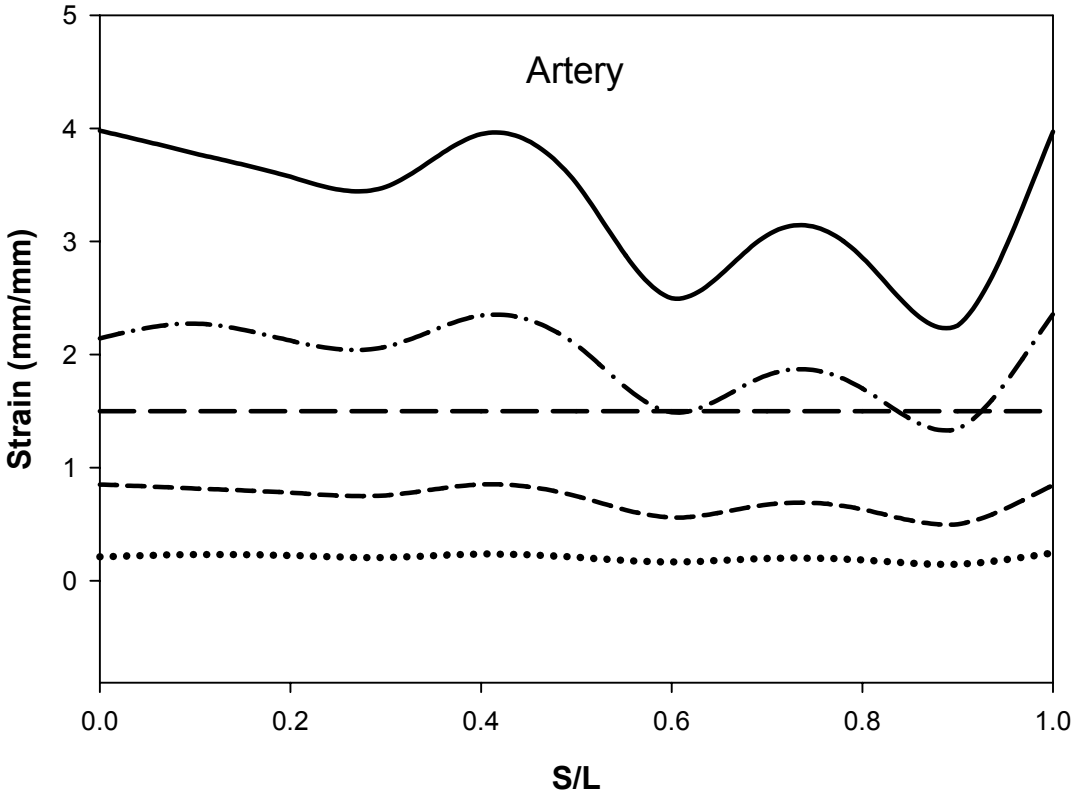

(A)

Figure 64-A. Strain versus dimensionless length of the artery. The horizontal dashed line is the ultimate strain of the blood vessels from experimental studies performed by Monson et al. (2000, 2003). The loading is taken from a model under HIC=1040.

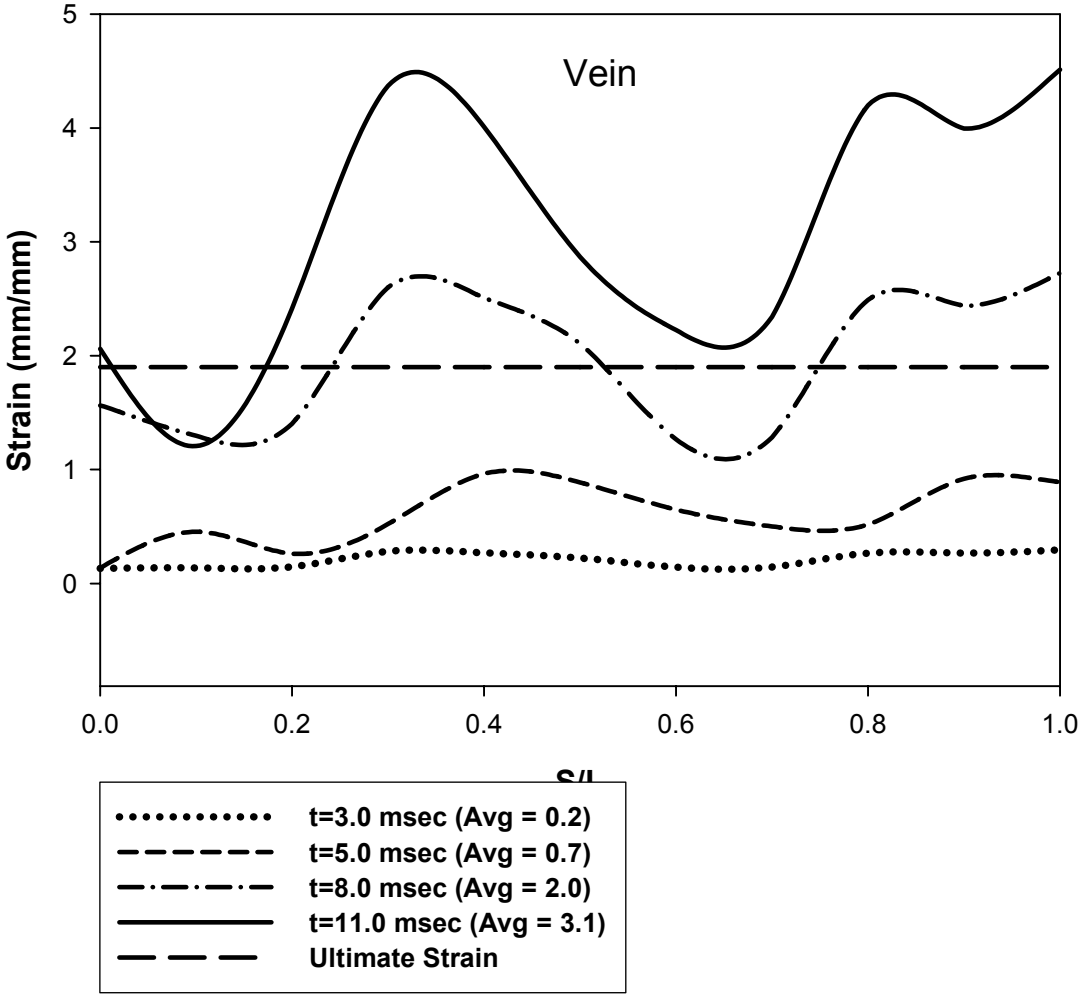

(B)

Figure 64-B. Strain versus dimensionless length of the vein. The horizontal dashed line is the ultimate strain of the blood vessels from experimental studies performed by Monson et al. (2000, 2003). The loading is taken from a model under HIC=1040.

Figure 65 shows the average strain values with respect to time for the two loading cases corresponding to HIC = 744 and HIC = 1040, respectively. The average strains along the blood vessels are calculated and are shown in Figure 65.

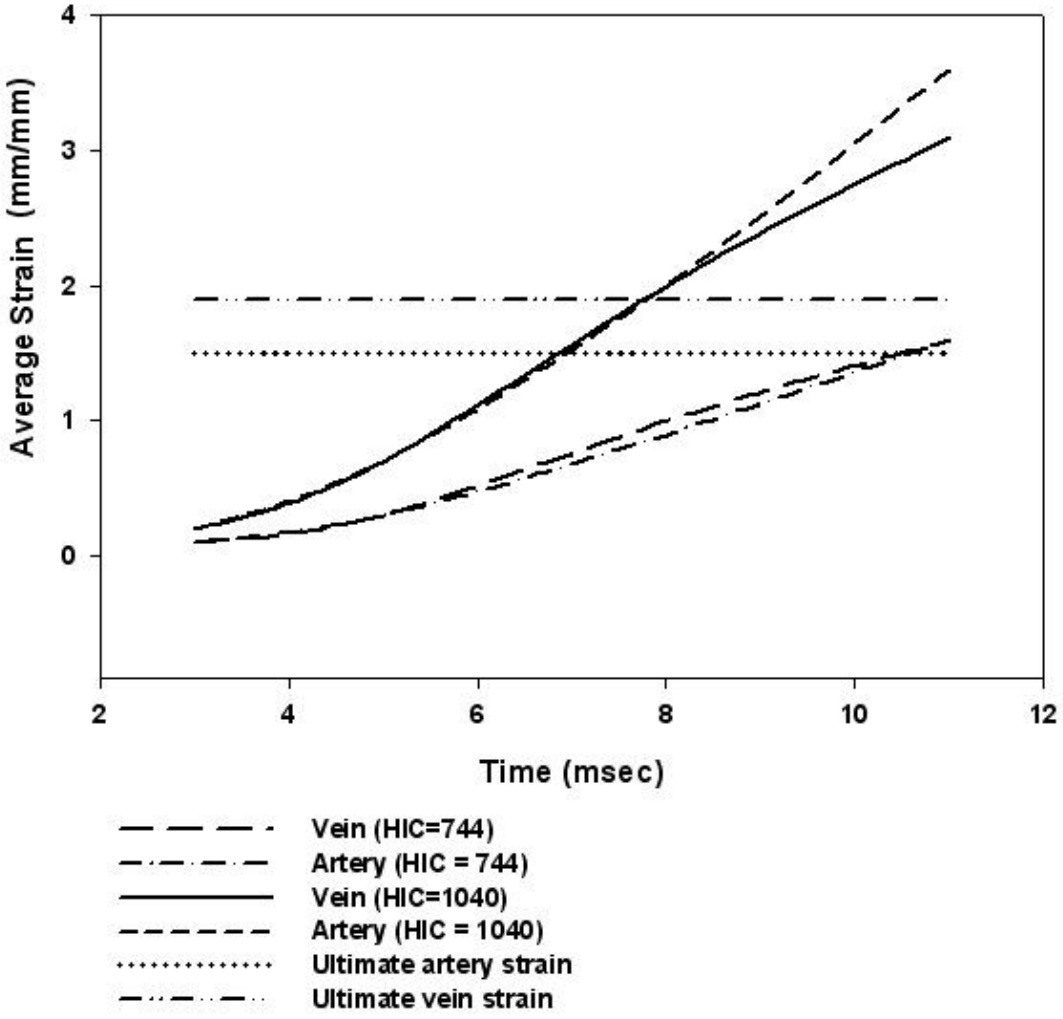

Figure 65- The average strains of the artery and vein blood vessels with respect to time for the two blunt loading cases.

9-2-2 LSM Blunt Impact Discussion

As mentioned above, the blood vessels strains were compared with the experimental data reported by Monson et al. (2001, 2003) shown in Figures 63 and 64. In their experimental study, the authors performed two sets of quasi-static and dynamic experiments. These experiments were conducted on the human cerebral vessels taken from surgeries and autopsies. They concluded

that the strain rate has no significant effect on the mechanical properties of cerebral blood vessels. This is in agreement with the conclusions of Lee and haut (1989) as well. Another conclusion that they made was the difference in the mechanical properties of arteries and veins. According to their results, cerebral arteries fail at about 54% higher stress than bridging veins. Also their results show that the cerebral arteries are less compliant (about 21%) than bridging veins. The ultimate strain values for the arteries and veins have been reported to be 1.47 and 1.88, respectively.

Figure 63 is related to a HIC value of 744, which is not known to produce severe injury (HIC < 1000), while mild traumatic brain injury is expected (Newman et al. (2000)). As Figure 63 shows, the strain values of both the arteries and veins are within the neighborhood of the tolerance level of strain. Thus, it is not expected that arteries and veins fail due to the first loading set (HIC = 744) as shown in Figures 60 and 61.

Figure 64 is related to a HIC value of 1040, which is known to produce severe injury (HIC > 1000). As Figure 64 shows, the strain value of both the arteries and veins exceed the tolerance level of strain. Thus it is expected that arteries and veins fail due to the second loading set. That is to say that, in the case of ASDH (rupture of bridging veins) and subarachnoid hemorrhage (SAH), which is the rupture of cerebral arteries, would occur. This is in agreement with the clinical observations that ASDH often accompanies SAH (Blumenfeld 2002).

The rupture of bridging veins (ASDH) normally takes place at the border of arachnoid and dura mater where the bridging veins are emptying into the

superior sagittal sinus. This would cause accumulation of blood in the subdural space. Note that the dura mater and arachnoid layer are connected tissues and there is no space between them in normal physiological situation. However in case of blood vessels rupture there would be a subdural space. The accumulation of blood in subdural space would eventually cease the blood flow to the brain due to the increase in the intracranial pressure.

The rupture of cerebral arteries in subarachnoid space (SAH) is usually accompanied by ASDH. This is a severe injury because it takes place in a region that CSF is present and the blood pressure of arteries is higher than the pressure of CSF. The average systolic and diastolic pressure is 100 mmHg (Guyton and Hall 2006) and the average pressure of CSF in normal physiological condition is 10 mmHg (Guyton and Hall 2006). This increases the intracranial pressure that would result in ceasing the blood flow.

It is worth mentioning that the average CSF pressure is 1.5 mmHg higher than the one for cerebral veins. Therefore, in SAS, the rupture of cerebral arteries is more sever than the rupture of cerebral veins. Note that the authors are not trying to compare the severity of ASDH and SAH, however the point is to explain the injury sites. That is SAH happens in SAS due to the rupture of cerebral arteries and ASDH happens in subdural space due to the rupture of bridging veins.

9-3 LSM Rotational Impact

As mentioned in section 9-2, LSM is subjected to the displacement and pressure results of GSM and GFM. For the LSM under rotational impact, both GSM and GFM were subjected into the rotational impact reported by Nahum et al. (1977). The global models (GSM and GFM) were discussed in details in sections 7-4 and 8-4, respectively.

LSM was subjected to the relative displacement between skull and brain as shown in Figures 41a,b and c. While displacement boundary condition was applied on LSM, the pressure distribution of GFM given in Figure 55 was applied to the model, as well.

9-3-1 Results of LSM Rotational Impact

Figures 66A and 66B show two incidences of the strain of the cerebral artery and bridging vein with respect to the dimensionless length and the blood vessels in the frontal region. As shown in the figures, the average strain is lower than the ultimate strain for the blood vessels.

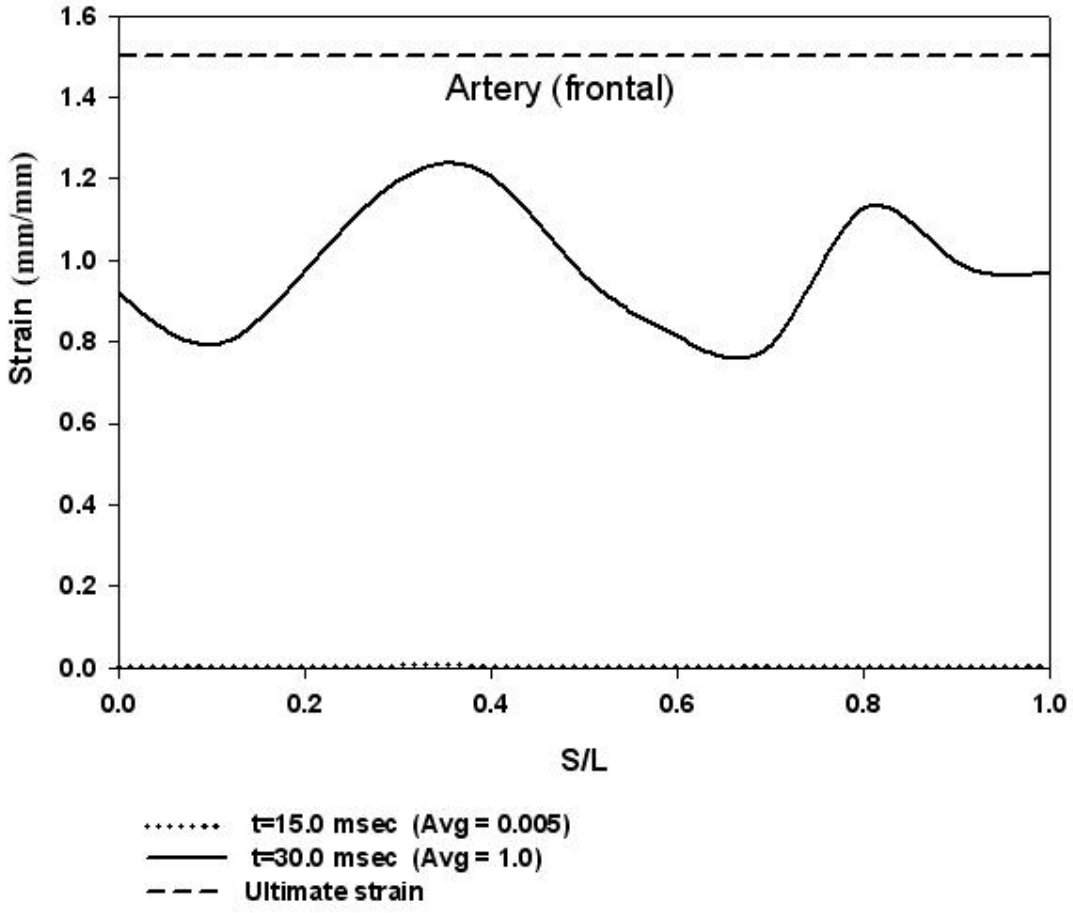

(A)

Figure 66-A. Strain versus dimensionless length of the artery in the frontal region. The dashed line is the ultimate strain of the blood vessels from experimental studies performed by Monson et al. (2000, 2003).

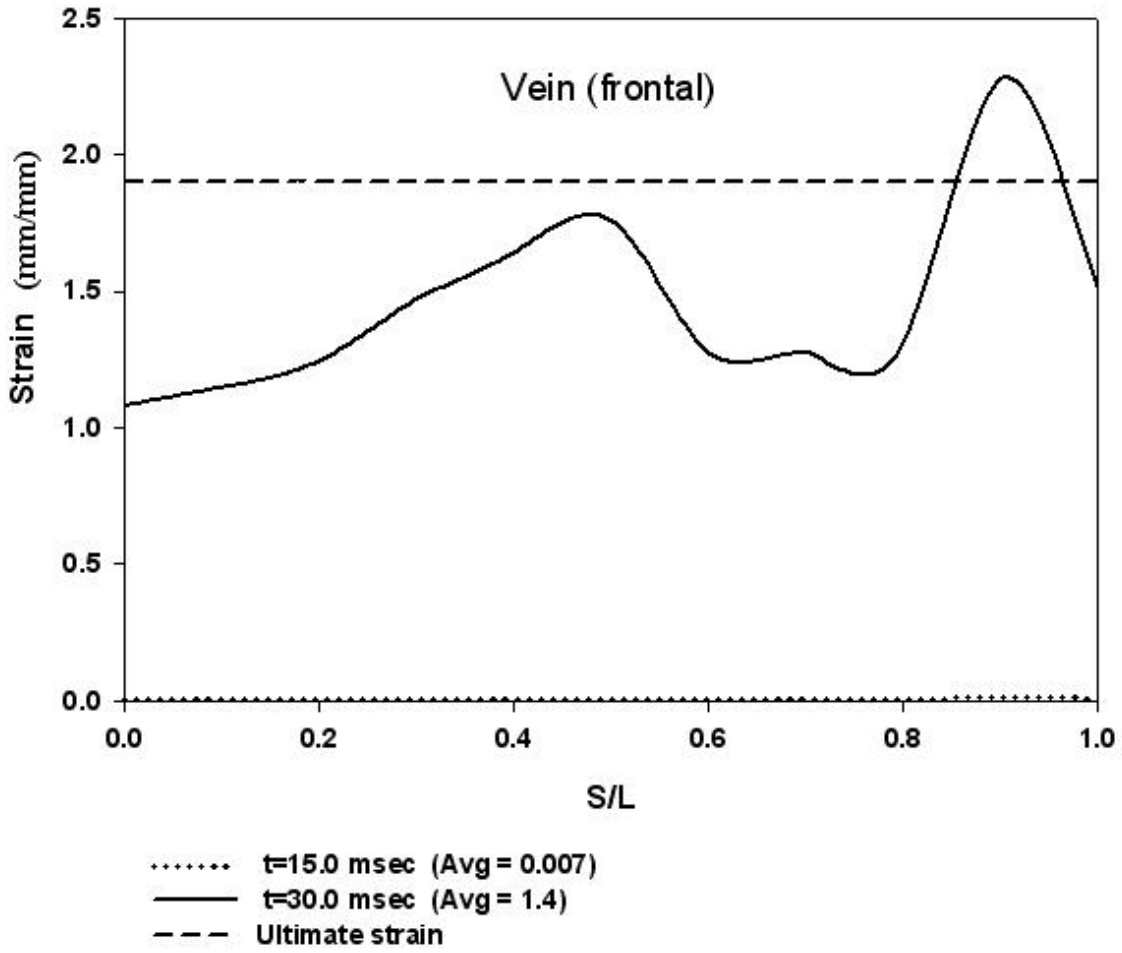

(B)

Figure 66-B. Strain versus dimensionless length of the vein in the frontal region. The dashed line is the ultimate strain of the blood vessels from experimental studies performed by Monson et al. (2000, 2003).

Figures 67A and 67B show two incidences of the strain of the cerebral artery and bridging vein with respect to the dimensionless length and the blood vessels in the occipital region. As shown in the figures, the average strain is lower than the ultimate strain for the blood vessels.

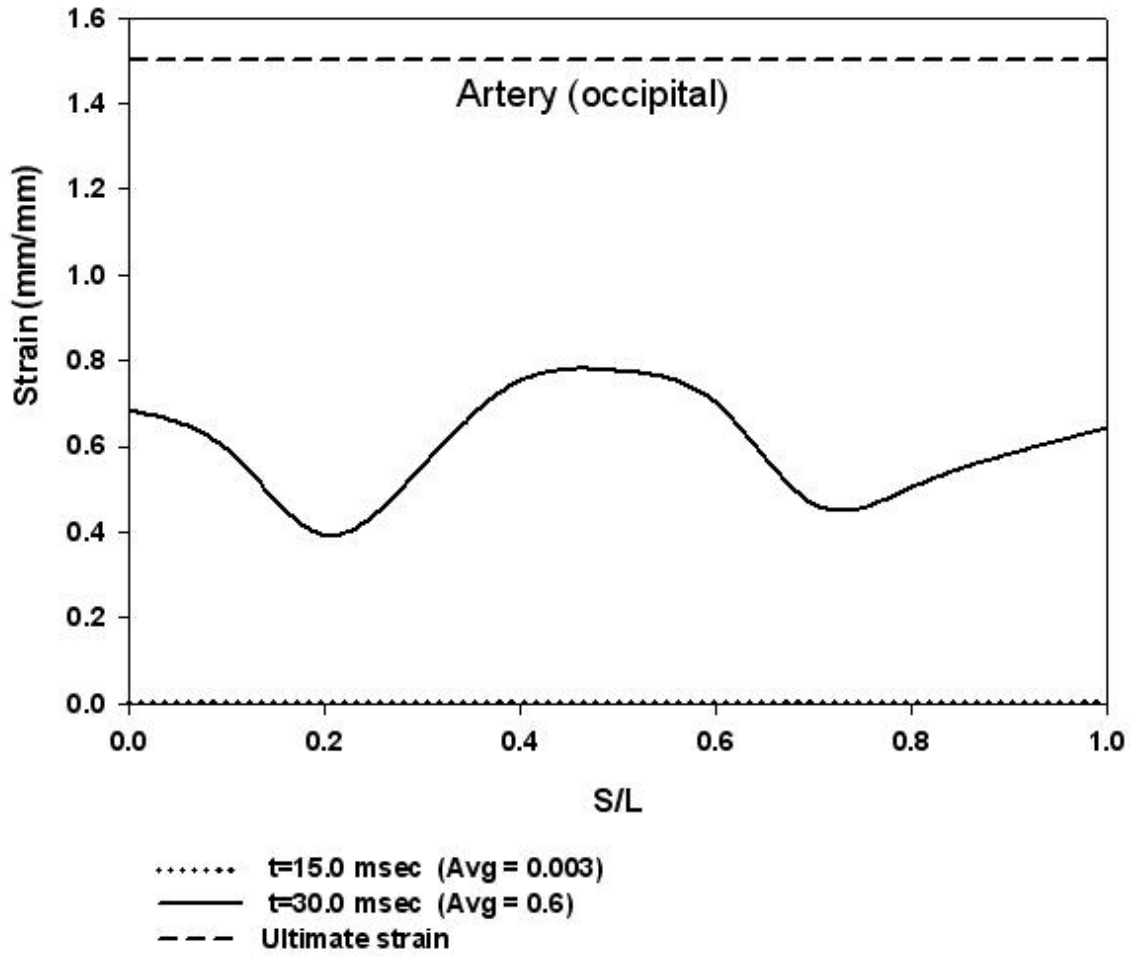

(A)

Figure 67-A. Strain versus dimensionless length of the artery in the occipital region. The dashed line is the ultimate strain of the blood vessels from experimental studies performed by Monson et al. (2000, 2003).

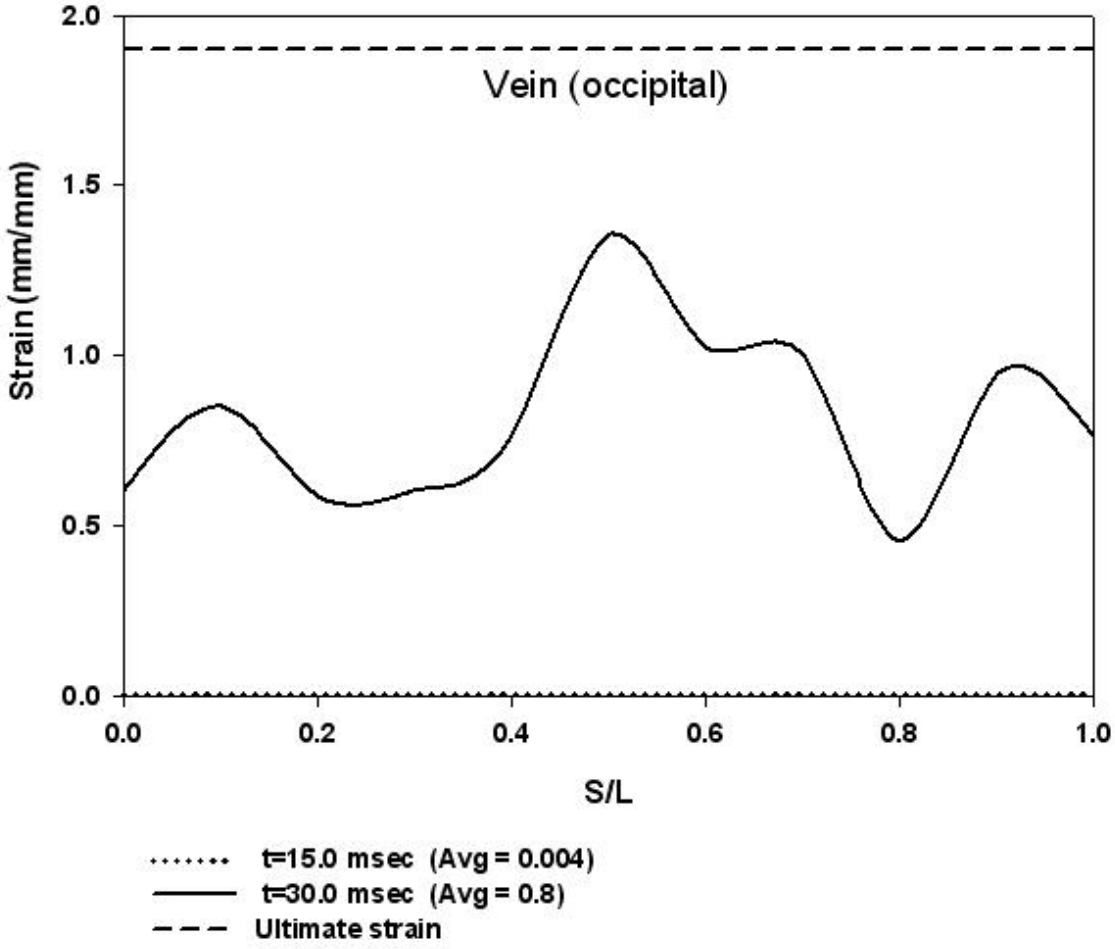

(B)

Figure 67-B. Strain versus dimensionless length of the vein in the occipital region. The dashed line is the ultimate strain of the blood vessels from experimental studies performed by Monson et al. (2000, 2003).

Figures 68A and 68B show two incidences of the strain of the cerebral artery and bridging vein with respect to the dimensionless length and the blood vessels in the superior region. As shown in the figures, at t = 15.0 msec, the average strain is lower that the ultimate strain whereas at t = 30.0 msec, the average strain is much higher that the ultimate strain. This is due to higher relative motion between the brain and skull in the superior region.

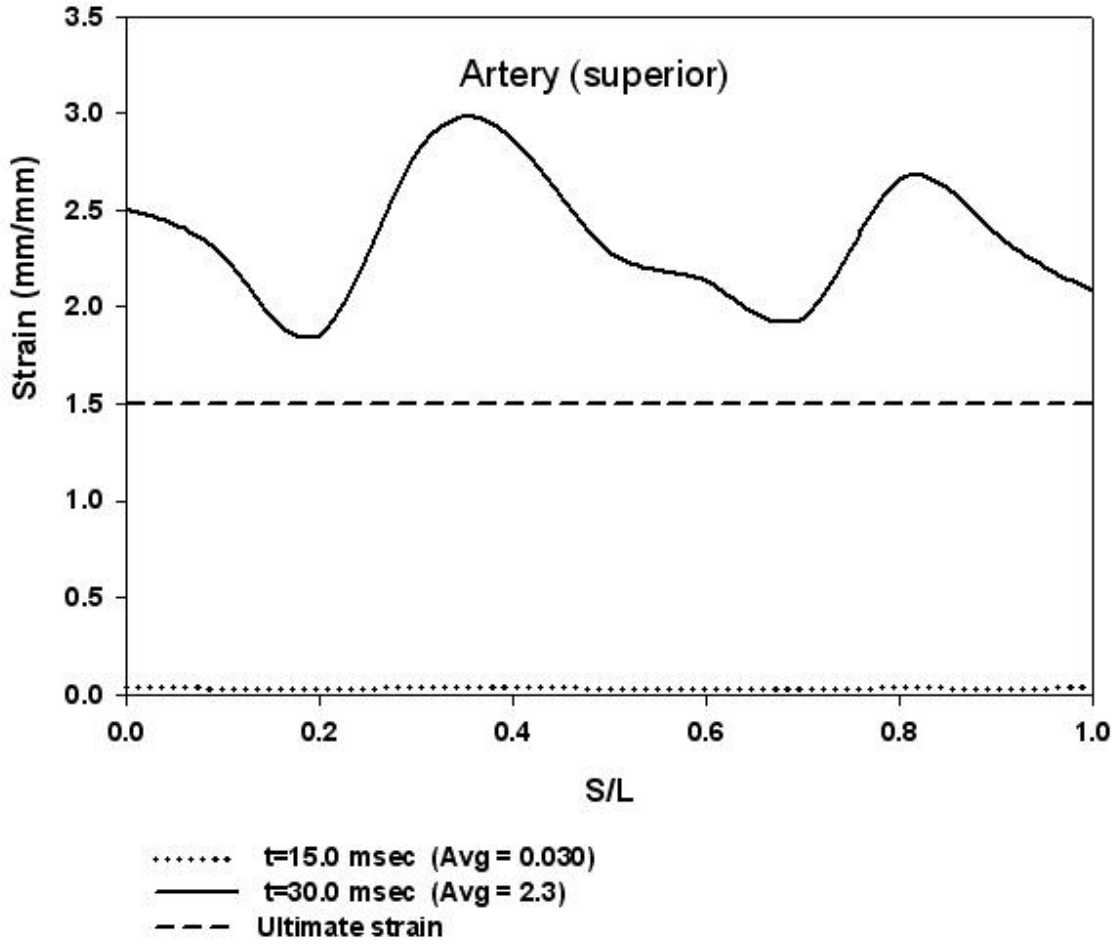

(A)

Figure 68-A. Strain versus dimensionless length of the artery in the superior region. The dashed line is the ultimate strain of the blood vessels from experimental studies performed by Monson et al. (2000, 2003).

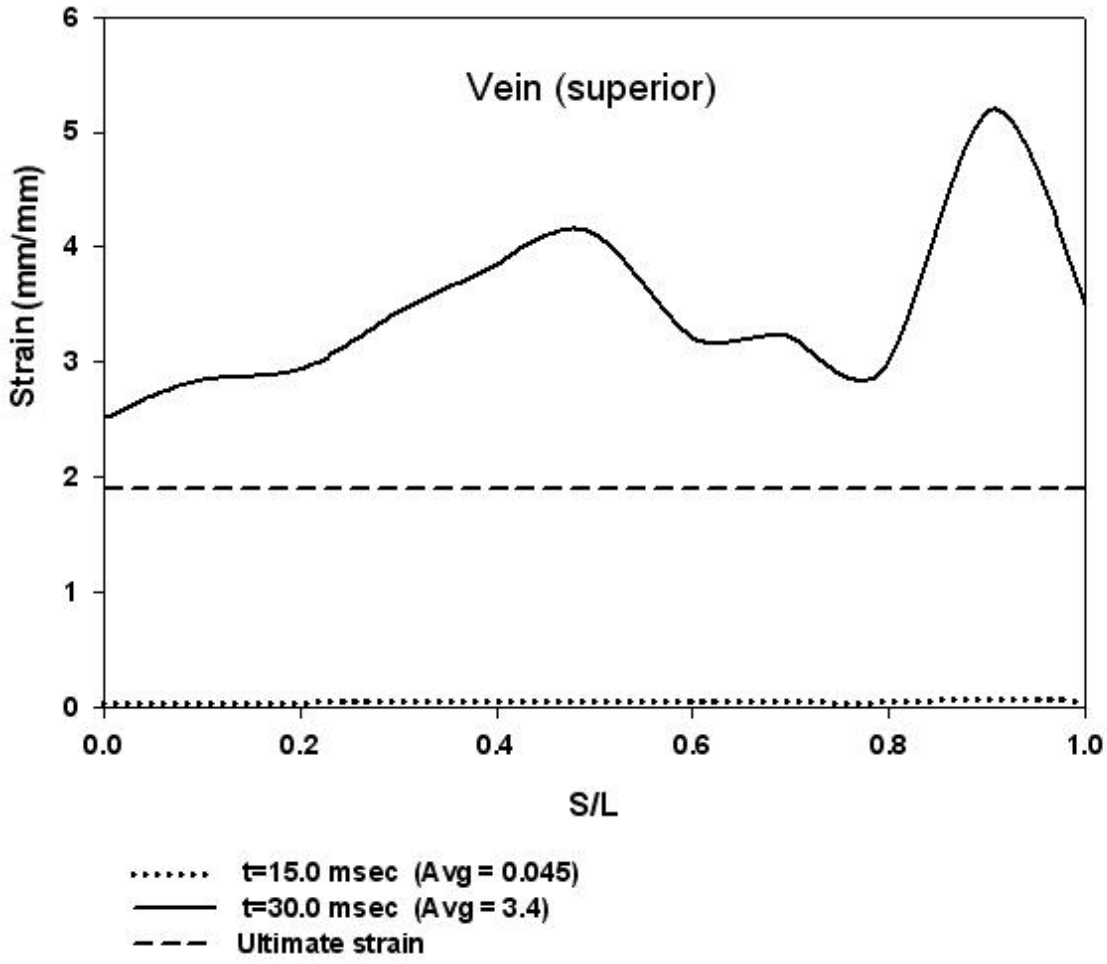

(B)

Figure 68-B. Strain versus dimensionless length of the vein in the superior region. The dashed line is the ultimate strain of the blood vessels from experimental studies performed by Monson et al. (2000, 2003).

9-3-2 LSM Rotational Impact Discussion

The rotational impacts as shown could lead to the rupture of bridging veins or cerebral arteries (ASDH and SAH). Due to the higher relative displacement between the brain and skull in the superior region, the injury is more likely to

happen in this region. This is in agreement with the results of other researchers (Gennarelli et al. (1982) and Huang et al. (1999)).

Applying different load scenarios (such as rotational impacts in different planes and different directions) into the present global/local modeling could result in analyzing the mechanisms of ASDH in more details. Improving our local model in terms of geometry and material properties could lead to a sophisticated injury criterion for different incidences. To advance the modeling of the head injuries more experimental studies on the meningeal layer or more specifically on SAS and its components are needed.

10- DISCUSSION AND CONCLUSIONS

This research focused on the biomechanics of ASDH (acute subdural hematoma), a head injury that accounts for 30% of the incidences of TBI (Kraus and Mc Arthur 1996). In this pathology bridging veins, that transverse from the deep tissue of the brain to its more superficial meningeal coverings, rupture due to the shearing and normal forces caused by the relative motion between the brain and the skull. Despite the fact that medical procedures can drain the excess blood that accumulates in ASDH, the mortality rate is 74% (Kraus and Mc Arthur 1996). Intervention strategies aimed at prevention or the minimization of these injuries is the best way to lower this mortality rate. A good understanding of the biomechanics underlying ASDH is necessary for the development of prevention strategies.

Initially a rigid body analysis was performed on a set of real life accidents involving operators of stand-up lift trucks. Specifically, a mannequin representing a 50^{th} percentile hybrid III anthropomorphic test dummy (ATD) and a lift truck models were developed. These studies determined that the average initial impact velocity for such accidents is 4.5m/s. These rigid body studies are not sufficient to understand the underlying biomechanics of head injuries. Thus initially, a set of 2D FE models was developed to analyze head injuries. The 4.5m/s impact velocity obtained from the rigid analysis was used as the boundary conditions for the FE models.

Due to the complex geometry of the head and the significant differences between the material properties of its components, it is currently not feasible to

perform a comprehensive analysis with one model. Therefore, as a pilot study, a set of three 2D FE models was constructed. The first model was a 2D global solid model, which was used to determine the relative displacement between the brain and skull. This study showed that the maximum displacement (3.2-mm) occurred in the superior region, where the bridging veins are most concentrated. The second model was a 2D global fluid model, which compared the CSF pressure in the presence and absence of subarachnoid trabeculae. It was determined that the trabeculae reduced the pressure by more than 60% indicating a significant damping effect. The third model was a 2D local model. The boundary conditions and loadings for this model were taken from the previous two global models. The local model showed that the subarachnoid trabeculae are better adapted to handling tension load compared to compression. That is, the trabeculae buckle under compression. This agrees with the idea that they contribute to the mechanical damping of the head/brain system. The general conclusion from these 2D models is that the trabeculae in SAS region reduce the CSF pressure during a head impact.

The inclusion of blood vessels in the model is important since their rupture is what leads to ASDH. However the 2D models restricted us from this inclusion. Furthermore, from the 2D analysis it was concluded that the fluid field within SAS plays a significant role in impact damping. However due to the nature of a 2D model, it is not possible to model the fluid flow around the trabeculae. These issues led us to perform a more realistic and comprehensive analysis of the

biomechanics of ASDH through three detailed FE 3D models including cerebral blood vessels.

The first 3D model was a global solid model (GSM) in which the kinematics of the impact was determined. This model did not include the CSF fluid or the cerebral blood vessels. GSM was subjected to three sets of loading, two blunt impacts and a rotational impact. The results obtained from this model were that the maximum relative displacement between the brain and skull during a blunt impact was 5.5-mm. Under a rotational impact, the maximum relative displacement took place in the superior region (10.0-mm), where the bridging veins are more concentrated.

The effect of trabeculae was implicitly included in global fluid model (GFM) where the pressure field of the CSF was determined. That is, to account for the fluid-solid interaction in subarachnoid space (SAS), CSF was replaced by an equivalent fluid with higher viscosity. The viscosity of the equivalent fluid was determined by calculating the damping characteristics of the brain/skull system through an experimental study performed by Hardy et al. (2001). To relate the damping constants of the system into the viscosity of the fluid the surface area of SAS was estimated to be 2 m^2. The viscosity was then determined to be 0.24 Pa.sec. To justify the estimation of the SAS surface area, a parametric study was performed. That is, the sensitivity of GFM to the changes in viscosity caused by the surface area variation was studied. In this parametric study it was concluded that the variation of +/- 15 % in SAS surface area changed the CSF peak pressure by less that +/- 10%, which is insignificant. GFM was then subjected to

impacts similar to GSM, namely two blunt impacts and a rotational impact. The maximum pressures of the equivalent fluid obtained from GFM under the blunt impact and rotational impact were about 140 kPa and 50 kPa, respectively.

GFM introduced a new method of accounting for the hydraulic damping characteristic of the CSF in the SAS region. Using the equivalent viscosity eliminates a tedious and time-consuming process of modeling the trabeculae, and would reduce computation time for running a head/brain model significantly. In addition, using the equivalent viscosity safeguards the accuracy of the results. Even a very elaborate and detailed model of CSF may not lead to accurate results since the material properties of the SAS trabeculae are not well established in the literature and more experimental studies are needed. That is, more experimental studies are needed to determine the geometry and mechanical properties of the meningeal layers. Although Hardy et al. (2001) performed experimental studies on human cadavers, still more experiments on human cadavers specifically for the purpose of determining the damping characteristics of the head/brain system are needed.

In light of the fact that the fluid (CSF) and solid (SAS trabeculae) interaction plays an important part of the damping head impacts and thereby protecting the brain from injuries, using this equivalent fluid method could enable the researches to create more realistic models for the study of head/brain injuries.

The cerebral blood vessels were included in the third 3D local solid model (LSM). The output of the two global models i.e., relative displacement from GSM

and CSF pressure from GFM, were employed in LSM to study the failure of the cerebral blood vessels. The results show that for a blunt impact relevant to a HIC value of 744, the average strain of the cerebral artery and vein were both measured 1.6 . Similarly, the results show that for a blunt impact relevant to a HIC value of 1040 (HIC > 1000 is known to create sever injuries), the average strains of the cerebral artery and vein were measured 3.1 and 3.6, respectively. For rotational impacts the average strain values for the artery and vein were measured 2.3 and 3.4, respectively. The strains of the cerebral artery and vein in the last two cases exceeded the failure criteria obtained from Monson et al. (2000 and 2003). The maximum failure strain for cerebral artery and vein has reported to be 1.5 and 1.9, respectively. This suggests that the threshold of the ASDH is relevant to a HIC value between 744 and 1040.

The rupture of bridging veins (ASDH) normally takes place at the border of arachnoid and dura mater where the bridging veins are emptying into the superior sagittal sinus. This would cause accumulation of blood in the subdural space. Note that the dura mater and the arachnoid layer are connected tissues and there is no space between them in normal physiological situation. However, in case of blood vessels rupture, there would be a subdural space. The accumulation of blood in the subdural space would eventually cease the blood flow to the brain due to the increase in the intracranial pressure.

The rupture of cerebral arteries in subarachnoid space (subarachnoid hemorrhage, SAH) is usually accompanied by ASDH. This is a severe injury because it takes place in a region that CSF is present and the blood pressure of

arteries is higher than the pressure of CSF. The average systolic and diastolic pressure is 100 mmHg (Guyton and Hall 2006) and the average pressure of CSF in normal physiological condition is 10 mmHg (Guyton and Hall 2006). This increases the intracranial pressure that would result in ceasing the blood flow.

It is worth mentioning that the average CSF pressure is 1.5 mmHg higher than the one for cerebral veins. Therefore, in SAS, the rupture of cerebral arteries is more severe than the rupture of cerebral veins. Note that the authors are not trying to compare the severity of ASDH and SAH, however, the point is to explain the injury sites. That is SAH happens in SAS due to the rupture of cerebral arteries and ASDH happens in subdural space due to the rupture of bridging veins.

One of the main challenges of head/brain studies is to accurately modeling the CSF and SAS trabeculae. This is due to the significance contribution of this region and its fluid-solid interaction to the damping of the head impacts and understanding of ASDH. Therefore, due to the complex geometry of SAS trabeculae and meningeal layers, the accurate modeling is an extremely difficult (if not impossible) task. In this research an equivalent fluid model representing CSF and SAS trabeculae was developed. The relationship between the applied impact and ASDH injury was quantified. It is believed that the three 3D FE models developed in this study are capable of addressing the challenges of modeling for the analysis of any given head impacts. Furthermore, the local solid model (LSM) developed in this study is capable of analyzing the failure of

the cerebral blood vessels. This research contributed to the knowledge of the head/brain biomechanics underlying the understanding of ASDH.

10-1 Future Works

In this research only two types of head impacts (namely frontal blunt impact and sagittal rotational impact) were considered. It is recommended that the three models be subjected to other types of impacts such as lateral/oblique blunt impacts and lateral/oblique rotational impacts. Then the rupture of bridging veins should be investigated for these impacts. More experimental works are also needed to support the results of this study and the future investigations. Specifically, experimental investigations are needed for measuring the structural damping of the head/brain system as well as the material properties of the meningeal layers.

11- BIBLIOGRAPHY

Abel JM, Gennaralli TA, Segawa H (1978). Incidence And Severity Of Cerebral Concussion In The Rhesus Monkey Following Sagittal Plane Angular Acceleration. *Stapp Car Crash Conference,* 22:780889.

Adams JH, Graham DI, Murray LS, Scott G (1982). Diffuse Axonal Injury Due To Nonmissile Head Injury In Humans: An Analysis Of 45 Cases. *Annals of Neurology,* 12:557-563.

Al-Bsharat AS, Hardy WN, Yang KH, Khalil TB, Tashman S, King AI (1999). Brain/Skull Relative Displacement Magnitude Due To Blunt Head Impact: New Experimental Data And Model. *Stapp Car Crash Conference,* 43:99SC22.

Al-Bsharat AS, Zhou C, Yang KH, Khalil TB, King AI (1999). Intracranial Pressure In The Human Head Due To Frontal Impact Based On A Finite Element Model. *Proc. 1999 Bioengineering Conference, BED ASME,* 42:113-114.

Alcolado JC, Moore IE, Weller RO (1986). Calcification In The Human Choroid Plexus, Meningiomas And Pineal Gland. *Neuropathology and Applied Neurobiology,* 12:235-250.

Allsop DL, Warner CY, Wille MG, Schneider DC, Nahum AM (1988). Facial Impact Response – A Comparison Of The Hybrid III Dummy And Human Cadaver. *Stapp Car Crash Conference,* 32:881719.

Anzelius A (1943). The Effect Of An Impact On A Spherical Liquid Mass. *Acta Pathol. Microbiol. Scand. (Suppl.)*, 48:153-159.

Arbogast KB and Margulies SS (1997). Regional Differences In Mechanical Properties Of The Porcine Central Nervous System. *Stapp Car Crash Conference, 41:973336.*

Bandak FA (1997). Biomechanics Of Impact Traumatic Brain Injury. *Structural impact and Occupant Protection,* 53-93.

Bandak FA, Eppinger RH (1994). A Three-Dimensional Finite Element Analysis Of The Human Brain Under Combined Rotational And Translational Acceleration. *Stapp Car Crash Conference,* 38:942215.

Bazarian JJ, Fisher SG, Flesher W, Lillis R, Knox KL, Pearson TA (2004). Lateral Automobile Impacts And The Risk Of Traumatic Brain Injury. *Annals of Emergency Medicine,* 44(2):142-152.

Bloch R and Tallala A (1976). A Mathematical Model Of Cerebrospinal Fluid Dynamics. *Journal of the Neurological Sciences,* 27:485-498.

Blumenfeld H (2002). Neuroanatomy Through Clinical Cases, Sinauer Associates Inc.

Bloomfield IG, Johnston IH, Bilston LE (1998). Effect Of Proteins, Blood Cells And Glucose On The Viscosity Of Cerebrospinal Fluid. *Pediatric Neurosurgery,* 28(5):246-251.

Bonne O, Gilboa A, Louzoun Y, Kempf-Sherf O, Katz M, Fishman Y, Ben-Nahum Z, Krausz Y, Bocher M, Lester H, Chisin R, Lerer B (2003). Cerebral Blood Flow In Chronic Symptomatic Mild Traumatic Brain Injury. *Psychiatry Research: Neuroimaging,* 124:141-152.

Bradshaw DRS, Ivarsson J, Morfey CL, Viano DC (2001). Simulation Of Acute Subdural Hematoma And Diffuse Axonal Injury In Coronal Head Impact. *Journal of Biomechanics,* 34:85-94.

Brydon HL and Hayward R (1995). Physical Properties Of Cerebrospinal Fluid Of Relevance To Shunt Function. 1: The Effect Of Protein Upon CSF Viscosity. *British Journal of Neurosurgery,* 9(5):2688697.

Cappa P, Masia L, Patane F (2005). Numerical Validation Of Linear Accelerometer Systems For The Measurement Of Head Kinematics. *Journal of Biomechanical Engineering,* 127:919-928.

Chu C, Lin M, Huang H, Lee M (1994). Finite Element Analysis Of Cerebral Contusion. *Journal of Biomechanics,* 27(2):187-194.

Cirovic S, Walsh C, Fraser WD (2000). A Mathematical Model Of Cerebral Perfusion Subjected To Gz Acceleration. *Aviation, Space, and Environmental Medicine,* 71(5):514-521.

Dai G, Gertler JP, Kamm RD (1999). The Effects Of External Compression On Venous Blood Flow And Tissue Deformation In The Lower Leg. *Journal of Biomechanical Engineering,* 121:557564.

Depreitere B, Van Lierde C, Maene S, Plets C, Vander Sloten J, Van Audekercke R, Van der Perre G, Goffin J (2004). Bicycle-Related Head Injury: A Study Of 86 Cases. *Accident Analysis and Prevention,* 36:561-567.

DiMasi FP, Eppinger RH, Bandak FA (1995). Computational Analysis Of Head Impact Responses Under Car Crash Loadings. *Stapp Car Crash Conference,* 39:952718.

Dobrin PB (1978). Mechanical Properties Of Arteries. *Physiological Reviews,* 58(2):397-460.

Dodgson MCH (1962). Colloidal Structure Of Brain. *Biorheology,* 1:21-30.

Donnelly BR and Medige J (1997). Shear Properties Of Human Brain Tissue. *Journal of Biomechanical Engineering,* 119:423-432.

Edberg S, Rieker J, Angrist A (1963). Study Of Impact Pressure And Acceleration In Plastic Skull Model. *Laboratory Investigation,* 12:1305-1311.

El-shafei I and El-Shafei H (2001). The Retrograde Ventriculosinus Shunt: Concept And Technique For Treatment Of Hydrocephalus By Shunting The Cerebrospinal Fluid To The Superior Sagittal Sinus Against The Direction Of Blood Flow. Preliminary Report. *Child's Nerv Syst,* 17:457-465.

Engin AE and Wang H (1970). A Mathematical Model To Determine Viscoelastic Behavior Of *In Vivo* Primate Brain. *Journal of Biomechanics,* 3:283-296.

Fallenstein GT and Hulce VD (1969). Dynamic Mechanical Properties Of Human Brain Tissue. *Journal of Biomechanics,* 2:217-226.

Feurer DJ and Weller RO (1991). Barrier Functions Of The Leptomeninges: A Study Of Normal Meninges And Meningiomas In Tissue Culture. *Neuropathology and Applied Neurobiology,* 17:391-405.

Flynn WJ, Pilati D, Hoover EL (1999). Effect Of Allopurinol On Venous Endothelial Dysfunction After Resuscitated Hemorrhagic Shock. *Journal of Surgical Investigation,* 1:11-18.

Fruin AH, Juhi GL, Taylon C (1984). Interhemispheric Subdural Hematoma. *Journal of Neurosurgery,* 60:1300-1302.

Galford JE and McElhaney JH (1969). A Viscoelastic Study Of Scalp, Brain, And Dura. *Journal of Biomechanics,* 3:211-221.

Gennarelli TA (1993). *Cerebral Concussion and Diffuse Brain Injuries,* Williams and Wilkins.

Gennarelli TA and Thibault LE (1982). Biomechanics Of Acute Subdural Hematoma. *Journal of Trauma,* 22(8):680-686.

Gennarelli TA, Thibault LE, Adams JH, Graham DI, Thompson CJ, Marcincin RP (1982). Diffuse Axonal Injury And Traumatic Coma In The Primate. *Annals Neurology,* 12:564-574.

Gennarelli TA, Thibault LE, Ommaya AK (1972). Pathophysiologic Responses To Rotational And Translational Accelerations Of The Head. *Stapp Car Crash Conference,* 16:720970.

Gray's Anatomy (1995). Churchill Livingstone*,* 38th Edition. *New York, NY.*

Gurdjian LS and Gurdjian ES (1978). Acute Head Injuries. *Surgery, Gyne Cology and Obstetrics,* 146:805-820.

Gurdjian ES, Lissner HR (1944). Mechanism Of Head Injury As Studied By The Cathode Ray Oscilloscope Preliminary Report. *Journal of Neurosurgery,* 1:393-399.

Gurdjian ES, Lissner HR (1961). Photoelastic Confirmation Of The Presence Of Shear Strains At The Craniospinal Junction In Closed Head Injury. *Journal of Neurosurgery,* 18:58-60.

Gurdjian ES, Lissner HR, Patrick LM (1963). Concussion - Mechanism And Pathology. *Stapp Car Crash Conference,* 7:470-482.

Gurdjian ES, Webster JE, Lissner HR (1955). Observations On The Mechanism Of Brain Concussion, Contusion, And Laceration. *Surgery, Gyne Cology and Obstetrics,* 101:680-690.

Guyton AC and Hall JE (2006). Textbook Of Medical Physiology, 10th Edition.

Hardy WN, Foster CD, King AI, Tashman S (1997). Investigation Of Brain Injury Kinematics: Introduction Of A New Technique. *Crashworthiness, Occupant Protection, BED 38 ASME,* 225:241-254.

Hardy WN, Foster CD, Mason MJ, Yang KH, King AI, Tashman S (2001). Investigation Of Head Injury Mechnisms Using Neutral Density Technology And High-Speed Biplaner X-Ray. *Stapp Car Crash Conference,* 45:2001-22-0016.

Harris C, DiRusso S, Sullivan T, Benzil DL (2003). Mortality Risk After Head Injury Increases At 30 Years. *Journal of American College of Surgeons,* 197(5):711-716.

Hodgson VR and Thomas LM (1979). Acceleration Induced Shear Strain In A Monkey Brain Hemisection. *Stapp Car Crash Conference,* 23:791023.

Hodgson VR, Thomas LM, Khalil TB (1983). The Role Of Impact Location In Reversible Cerebral Concussion. *Stapp Car Crash Conference,* 27:831618.

Holbourn AHS (1945). The Mechanics Of Brain Injury. *British Medical Bulletin,* 3:147-149.

Horgan TJ and Gilchrist MD (2003). The Creation Of Three-Dimensional Finite Element Models For Simulating Head Impact Biomechanics. *International Journal of Crashworthiness,* 8(4):353-366.

Huang HM, Lee MC, Chiu WT, Pan LC, Chen CT (1999). Three-Dimensional Finite Element Analysis Of Subdural Hematoma. *Journal of Trauma,* 47:538-544.

Hutchinson J, Kaiser MJ, Lankarani HM (1998). The Head Injury Criterion (HIC) Functional. *Applied Mathematics and Computation,* 96:1-16.

Ikeda T, Yamaguchi A, Yokose S, Nagai Y, Yamato H, Nakamura T, Tsurukami H, Tanizawa T, Yoshiki S (1996). Changes In Biological Activity Of Bone Cells In Ovariectomized Rats Revealed By In Situ Hybridization. *Journal of Bone and Mineral Research,* 11(6):780-788.

Ivarsson J, Viano DC, Lovstud P, Aldman B (2000). Strain Relief From The Cerebral Ventricles During Head Impact: Experimental Studies On Natural Protection Of The Brain. *Journal of Biomechanics,* 33(2):181-189.

Jellinek H, Krenn H, Oczenski W, Veit F, Schwarz S, Fitzgerald RD (2000). Influence On Positive Airway Pressure On The Pressure Gradient For Venous Return In Humans. *Journal of Applied Physiology,* 88:926-932.

Johnson EAC and Young PG (2005). On The Use Of A Patient-Specific Rapid-Prototyped Model To Simulate The Response Of The Human Head To Impact And Comparison With Analytical And Finite Element Models. *Journal of Biomechanics,* 38:39-45.

Kaye A, Anwar M, Banister R, Feng C, Turner K, Kadowitz P, Nossaman B (1999). Responses To Propofol In The Pulmonary Vascular Bed Of The Rat. *Acta Anaesthesiol Scand,* 43:431-437.

Kida S, Pantazis A, Weller RO (1993). CSF Drains Directly From The Subarachnoid Space Into Nasal Lymphatics In The Rat. Anatomy, Histology And Immunological Significance. *Neuropathology and Applied Neurobiology,* 19:480-488.

King AI, Chou CC (1976). Mathematical Modeling Simulation And Experimental Testing Of Biomechanical System Crash Response. *Journal of Biomechanics,* 9:301-317.

King AI, Yang KH, Hardy WN, Al-Bsharat A, Deng B, Begeman PC, Tashman

S (1999). Challenging Problems And Opportunities In Impact Biomechanics. *Proc. 1999 Summer Bioengineering Conf., ASME,* 42:269-270.

Kleilnberger M, Sun E, Eppinger R, Kuppa S, Saul R (1998). Development Of Improved Injury Criteria For The Assessment Of Advanced Automotive Restraint System. *NHTSA (www.nhtsa.dot.gov).*

Kleiven S (2003). Influence Of Impact Direction On The Human Head In Prediction Of Subdural Hematoma. *Journal of Neurotrauma,* 20(4):365-379.

Kleiven S and Hardy WN (2002). Correlation Of An FE Model Of The Human Head With Local Brain Motion - Consequences For Injury Prediction. *Stapp Car Crash Conference,* 46:2002-22-0007.

Kleiven S and Holst H (2002). Consequences Of Head Size Following Trauma To The Human Head. *Journal of Biomechanics,* 35:153-160.

Kleiven S and Holst H (2002). Consequences Of Reduced Brain Volume Following Imoact In Prediction Of Subdural Hematoma Evaluated With Numerical Techniques. *Injury Prevention,* 3:303-310.

Krabbel G and Appel H (1995). Development Of A Finite Element Model Of The Human Skull. *Journal of Neurotrauma,* 4(Dec):735-742.

Kraus JF and McArthur DL (1996). Epidemiologic Aspects Of Brain Injury. *NEUROLOGIC CLINICS,* 14(2):435-450.

Kumaresan S, Radhakrishnan S (1996). Importance Of Partitioning Membranes Of The Brain And The Influence Of The Neck In Head Injury Modeling. *In Medical & Biological Engineering & Computing,* 34:27-32.

Lee M-C, Haut RC (1989). Insensitivity Of Tensile Failure Properties Of Human Bridging Veins To Strain Rate: Implications In Biomechanics Of Subdural Hemotoma. *Journal of Biomechanics,* 22:537-542.

Lee M-C, Melvin JW, Ueno K (1987). Finite Element Analysis Of Traumatic Subdural Hematoma. *Stapp Car Crash Conference,* 31:872201.

Lee ACW, Ou Y, Fong D (2003). Depressed Skull Fractures: A Pattern Of Abusive Head Injury In Three Older Children. *Child Abuse & Neglect,* 27:1323-1329.

Lin T, Wawa C, Khalil TB (1995). Evaluation Of A Hybrid III Dummy Interactions With Air Bag In Frontal Crash By Finite Element Simulation. *Stapp Car Crash Conference*, 39:952705.

Ljung C (1975). A Model For Brain Deformation Due To Rotation Of Skull. *Journal of Biomechanics*, 8:263-274.

Lowenhielm P (1974). Strain Tolerance Of The Vv. Cerebri Sup. (Bridging Veins) Calculated From Head-On Collision Tests With Cadavers. *Z. Rechtsmedizin*, 75:131-144.

Lowenhielm P (1975). Mathematical Simulation Of Gliding Contusion. *Journal of Biomechanics*, 8:351-356.

Margulies SS, Thibault LE, Gennarelli TA (1990). Physical Model Simulation Of Brain Injury In Primates. *Journal of Biomechanics,* 23(8):823-836.

McGrath P and Mills P (1984). Atlas Of Sectional Anatomy Head, Neck And Trunk. *Basel.*

Mehlsen J (2000). Models Of The Venous System. *Stud Health Technol Inform,* 71:109-117.

Mendis KK, Stalnaker RL, Advani SH (1995). A Constitutive Relationship For Large Deformation Finite Element Modeling Of Brain Tissue. *Journal of Biomechanical Engineering*, 117:279-285.

Miga MI, Paulsen KD, Hoopes PJ, Kennedy FE, Hartov A, Roberts DW (2000). In Vivo Modeling Of Interstitial Pressure In The Brain Under Surgical Load Using Finite Elements. *Journal of Biomechanical Engineering*, 122:354-363.

Miller K (1999). Constitutive Model Of Brain Tissue Suitable For Finite Element Analysis Of Surgical Procedures. *Journal of Biomechanics*, 32:531-537.

Miller K and Chinzei K (1997). Constitutive Modeling Of Brain Tissue: Experiment And Theory. *Journal of Biomechanics*, 30(11,12):1115-1121.

Miller K and Chinzei K (2002). Mechanical Properties Of Brain Tissue In Tension. *Journal of Biomechanics*, 35:483-490.

Miller RT, Margulies SS, Leoni M, Nonaka M, Chen X, Smith DH, Meaney DF (1998). Finite Element Modeling Approaches For Predicting Injury In An Experimental Model Of Sever Diffuse Axonal Injury. *Stapp Car Crash Conference*, 43:983154.

Miller K, Chinzei K, Orssengo G, Bednarz P (2000). Mechanical Properties Of Brain Tissue In-Vivo: Experiment And Computer Simulation. *Journal of Biomechanics*, 33:1369-1376.

Miltner E, Salwender HJ (1995). Influencing Factors On The Injury Severity Of Restrained Front Seat Occupants In Car-To-Car Head-On Collisions. *Accident Analysis and Prevention*, 27(2):143-150.

Monson KL, Goldsmith W, Barbaro NM, Manley G (2000). Static And Dynamic Mechanical And Failure Properties Of Human Cerebral Vessels. *Crashworthiness, Occupant Pretection, BED 49 ASME*, 49:255-265.

Monson KL, Goldsmith W, Barbaro NM, Manley G (2003). Axial Mechanical Properties Of Fresh Human Cerebral Blood Vessels. *Journal of Biomechanical Engineering,* 125:288-294.

Monson KL, Goldsmith W, Barbaro NM, Manley G (2005). Significance Of Source And Size In The Mechanical Response Of Human Cerebral Blood Vessels. *Journal of Biomechanics,* 38-737-744.

Moore K and Dalley A (1999). Clinically Orientated Anatomy, Lippincott Williams and Wilkins, 4th edition

Nagashima T, Shirakuni T, Rapoport SI (1990). A Two-Dimensional, Finite Element Analysis Of Vasogenic Brain Edema. *Neurologia Medico Chirurfica (Tokyo)*, 30:1-9.

Nahum AM, Smith R (1976). An Experimental Model For Closed Head Impact Injury. *Stapp Car Crash Conference*, 20:760825.

Nahum AM, Smith R, Ward CC (1977). Intracranial Pressure Dynamics During Head Impact. *Stapp Car Crash Conference*, 21:770922.

National Highway Traffic Safety Administration (1981). Head And Neck Injury Criteria- A Consequence Workshop.

National Transportation Biomechanics Research Center, NHTSA (2001). Biomechanical Response Requirements If The Thor NHTSA Advanced Frontal Dummy, GESAC-01-04

Netter FH (1997). *Atlas of Human Anatomy.* NOVARTIS.

Newman JA (1980). Head Injury Criteria In Automotive Crash Testing. *Stapp Car Crash Conference,* 24:801317.

Newman JA, Shewchenko N, Welbourne E (2000). A Proposed New Biomechanical Head Injury Assessment Function - The Maximum Power Index. *Stapp Car Crash Conference*, 44:2001-01-SC16.

Nightingale RW, McElhaney JH, Richardson WJ, Myers BS (1996). Dynamic

Responses Of The Head And Cervical Spine To Axial Impact Loading. *Journal of Biomechanics*, 29(3):307-318.

Nishimoto T and Murikami S (1998). Relation Between Diffuse Axonal Injury And Internal Head Structures On Blunt Impact. *Journal of Biomechanical Engineering*, 120:140-147.

Nishimoto T and Murikami S (2000). Direct Impact Simulations Of Diffuse Axonal Injury By Axial Head Model. *JSAE Review,* 21:117-123.

Nolte J and Angevine JB, Jr (1995). The Human Brain. Mosby-Year Book, Inc., MO.

Noppens R and Brambrink AM (2004). Traumatic Brain Injury In Children - Clinical Implications. *Experimental and Toxicologic Pathology,* 56:113-125.

Oka K, Rhoton AL, Barry M, Rodriguez R (1985). Microsurgical Anatomy Of The Superficial Veins Of The Cerebrum. *Neurosugery*, 17(5):711-748.

Ommaya A (1968). Mechanical Properties Of Tissues Of The Nervous System. *Journal of Biomechanics,* 1:127-138.

Ommaya AK, Corrao P. Pathologic Biomechanics Of Central-Nervous-System Injury In Head Impact And Whiplash Trauma. *Accident Pathology Ed. K.M. Brinklous, Washington, DC*, 160-181.

Ommaya AK, Gennarelli TA (1974). Cerebral Concussion And Traumatic Unconsciousness: Correlation Of Experimental And Clinical Observations On Blunt Head Injuries. *Brain*, 97:633-654.

Ommaya AK, Grubb RL, Naumann RA (1971). Coup And Contre-Coup Injury: Observations On The Mechanics Of Visible Brain Injuries In The Rhesus Monkey. *Journal of Neurosurgery*, 35:503-516.

Ommaya AK, Yarnell P, Hirsch AE, Harris EH (1967). Scaling Of Experimental Data On Cerebral Concussion In Sub-Human Primates To Concussion Threshold For Man. *Stapp Car Crash Conference*, 11:670906.

Ono K, Kikuchi A, Nakamura M, Kobayashi H, Nakamura N (1980). Human Head Tolerance To Sagittal Impact Reliable Estimation Deduced From Experimental Head Injury Using Subhuman Primates And Human Cadaver Skulls. *Stapp Car Crash Conference*, 24:801303.

Parker JR, Parker JC, Overman JC (1990). Intracranial Diffuse Axonal Injury At Autopsy. *Annals of Clinical and Laboratory Science*, 20(3):220-224.

Parkinson J, Brass A, Canova G, Brechet Y (1997). The Mechanical Properties Of Simulated Collagen Fibrils. *Journal of Biomechanics*, 30(6):549-554.

Peters GWM, Meulman JH, Sauren AAHJ (1997). The Applicability Of The Time/Temperature Superposition Principle To Brain Tissue. *Biorheology*, 34(2):127-138.

Piechnik SK, Czosnyka M, Richards HK, Whitfield PC, Pickard JD (2001). Cerebral Venous Blood Outflow: A Theoretical Model Based On Laboratory Simulation. *Neurosurgery,* 49(5):1214-1223.

Pierpaoli C, Basser PJ (1996). Toward A Quantitative Assessment Of Diffusion Anisotropy. *Magnetic Resonance in Medicine*, 36:893-906.

Pincemaille Y, Trosseille X, Mack P, Tarriere C, Breton F, Renault B (1989). Some New Data Related To Human Tolerance Obtained From Volunteer Boxers. *Stapp Car Crash Conference*, 33:892435.

Pudenz RH, Shelden CH (1946). The Lucite Calvarium- A Method For Direct Observation Of Brain. *Journal of Neurosurgery*, 3:487-505.

Rascol MM and Izard JY (1976). The Subdural Neurothelium Of The Cranial Meninges In Man. *Anatomical Record*, 186:429-436.

Roach MR, Burton AC (1957). The Reason For The Shape Of The Distensibility Curves Of Arteries. *Canadian Journal of Biochemical Physiology*, 35:681-690.

Rohen JW, Yokochi C, Lutjen-Drecoll E (1998). Color Atlas Of Anatomy. Williams and Wilkins.

Ross DT, Meaney DF, Sabol MK, Smith DH, Gennarelli TA (1994). Distribution Of Forebrain Diffuse Axonal Injury Following Inertial Closed Head Injury In Miniature Swine. *Experimental Neurology*, 126:291-299.

Ruan JS, Prasad P (1995). Coupling Of A Finite Element Human Head Model With A Lumped Parameter Hybrid III Dummy Model: Preliminary Results. *Journal of Neurotrauma*, 12:725-734.

Ruan JS, Khalil T, King AI (1994). Dynamic Response Of The Human Head To Impact By Three-Dimensional Finite Element Analysis. *Journal of Biomechanical Engineering*, 116:44-50.

Ruan JS, Khalil TB, King AI (1993). Finite Element Modeling Of Direct Head Impact. *Stapp Car Crash Conference*, 37:933114.

Sahay KB, Mehrotra R, Sachdeva U, Banerji AK (1992). Elastomechanical Characterization Of Brain Tissues. *Journal of Biomechanics*, 25(3):319-326.

Sarkar S, Majumder S, Roychowdhury A (2004). Response Of Human Head Under Static & Dynamic Load Using Finite Element Method. *Trends in Biomaterials & Artificial Organs,* 17(2):130-134.

Sarre H, Sieberth H, Noltenius H (1964). Goodpasture's Syndrome. *Germ. Med. Mth.,* 280-284.

Sauren AAHJ, Claessens MHA (1993). Finite Element Modeling Of Head Impact: The Second Decade. *Proc. 1993 Int. IRCOBI Conf. On the Biomechanics of Impact*, 241-254.

Sawicki B and Starzynski J (2000). Human Head Model In Constructive Solid Geometry (CSG), www.iem.pw.edu.pl/~sawickib/artykul1/artykul.html.

Schachenmayr W and Friede RL (1978). The Origin Of Subdural Neomembranes. I. Fine Structure Of The Dura-Arachnoid Interface In Man. *American Journal of Pathology*, 92:53-68.

Shah CS, Yang KH, Hardy W, Wang HK, King AI (2001). Development Of A Computer Model To Predict Aortic Rupture Due To Impact Loading. *Stapp Car Crash Conference*, 45:2001-22-0007.

Shykoff BE, Hawari FI, Izzo JL (2001). Diameter, Pressure And Compliance Relationships In Dorsal Hand Veins. *Vascular Medicine,* 6:97-102.

Steffan H, Moser A, Geigl BC, Motomiya Y (2000). Validation Of The Coupled PC-CRASH-MADYMO Occupant Simulation Model. *Stapp Car Crash Conference*, 44:2000-01-0471.

Stern SA, Zink BJ, Mertz M, Wang X, Dronen SC (2000). Effect Of Initially Limited Resuscitation In A Combined Model Of Fluid-Percussion Brain Injury And Severe Uncontrolled Hemorrhage Shock. *Journal of Neurosurgery,* 93:305-314.

Thurman D and Guerrero J (1999). Trends In Hospitalization Associated With Traumatic Brain Injury. *Journal of the American Medical Association*, 282(10):954-957.

Trosseille X, Tarriere C, Lavaste F, Guillon F, Domont A (1992). Development Of A F.E.M. Of The Human Head According To A Specific Test Protocol. *Stapp Car Crash Conference*, 36:922527.

Truong T-K, Clymer BD, Chakeres DW, Schmalbrock P (2002). Three-

Dimensional Numerical Simulations Of Susceptibility-Induced Magnetic Field Inhomogeneties In The Human Head. *Magnetic Resonance Imaging,* 20:759-770.

Turquire F, Kang HS, Trosseille X, Willinger R, Lavaste F, Tarriere C, Domont A (1996). Validation Study Of A 3D Finite Element Head Model Against Experimental Data. *Stapp Car Crash Conference*, 40:962431.

Ueno K, Melvin JW (1996). Tissue Level Injury Criteria Using Brain Finite Element Analysis, Bilateral Impact Model. *AGARD/AMP Specialists' Meeting on "Impact Head Injury"*, 9(1):9-15.

Ueno K, Melvin JW, Li L, Lighthall JW (1995). Development Of Tissue Level Brain Injury Criteria By Finite Element Analysis. *Journal of Neurotrauma*, 12(4): 695-706.

Ugural AC and Fenster SK (1995). Advanced Strength And Applied Elasticity. *Prentice-Hall, Inc., NJ.*

Unterharscheidt F, Higgins LS (1969). Traumatic Lesions Of Brain And Spinal Cord Due To Nondeforming Angular Acceleration Of The Head. *Texas Reports on Biology and Medicine*, 27:127-166.

Viano DC (1983). Biomechanics Of Nonpenetrating Aortic Trauma: A Review. *Stapp Car Crash Conference*, 27:831608.

Viano DC and Lovsund P (1998). Biomechanics Of Brain And Spinal-Cord Injury: Analysis Of Neuropathologic And Neurophysiologic Experiments. *Journal of Crash Prevention and Injury Control*, 1(Jan):35-43.

Viano D, Aldman B, Pape K, van Hoof J, von Holst J (1997). Brain Kinematics In Physical Model Test With Translational And Rotational Acceleration. *International Journal of Crashworthiness,* 2(2):191-206.

Wang H, Wineman AS (1972). A Mathematical Model For The Determination Of Viscoelastic Behavior Of Brain In Vivo-I Oscillatory Response. *Journal of Biomechanics*, 5:431-446.

Ward CC, Thompson RB (1975). The Development Of The Detailed Finite Element Brain Model. *Stapp Car Crash Conference*, 19:751163.

Ward C, Chan M, Nahum A (1980). Intracranial Pressure - A Brain Injury Criterion. *Stapp Car Crash Conference*, 24:801304.

Ward CC, Nikravesh PE, Thompson RB (1978). Biodynamic Finite Element Models Used In Brain Injury Research. *Aviation, Space, and Environmental*

Medicine, 136-142.

Willinger R, Taleb L, Kopp C-M (1995). Modal And Temporal Analysis Of Head Mathematical Models. *Journal of Neurotrauma,* 12 :743-754.

Willinger R, Kang H, Diaw B (1999). Three-Dimensional Human Head Finite-Element Model Validation Against Two Experimental Impacts. *Annals of Biomedical Engineering*, 27:403-410.

Young PG (2003). An Analytical Model To Predict The Response Of Fluid-Filled Shells To Impact - A Model For Blunt Head Impacts. *Journal of Sound and Vibration,* 267:1107-1126.

Zhang ET, Inman CBE, Weller RO (1990). Interrelationship Of The Pia Mater And The Privascular (Virchow-Robin) Spaces In The Human Cerebrum. *Journal of Anatomy*,170: 111-123.

Zhang ET, Richards HK, Kida S, Weller RO (1992). Directional And Compartmentalized Drainage If Interstitial Fluid And Cerebrospinal Fluid From The Rat Brain. *Acta:Neuropathology,* 83: 233-239.

Zhang L, Bae J, Hardy WN, Monson KL, Manley GT, Goldsmith W, Yang KH, King AI (2002). Computational Study Of The Contribution Of The Vasculature On The Dynamic Response Of The Brain. *Stapp Car Crash Conference,* 46: 2002-22-0008.

Zhang L, Yang KH, Dwarampudi R, Omori K, Li T, Chang K, Hardy WN, Khalil TB, King AI (2001a). Recent Advances In Brain Injury Research: A New Human Head Model Development And Validation. *Stapp Car Crash Conference,* 45: 2001-22-0017.

Zhang L, Yang KH, King AI (2001b). Biomechanics Of Neurotrauma. *Neurological Research,* 23: 144-156.

Zhang L, Yang KH, King AI (2001c). Comparison Of Brain Responses Between Frontal And Lateral Impacts By Finite Element Modeling. *Journal of Neurotrauma,* 18: 21-30.

Zhang L, Yang KH, King AI, Viani D (2003). A New Biomechanical Predictor For Mild Traumatic Brain Injury - A Preliminary Finding. *Summer Bioengineering Conference June 25-29,* 137-138.

Zhang QH, Teo, EC, Ng HW (2005). Development And Validation Of A C0-C7 FE Complex For Biomechanical Study. *Journal of Biomechanical Engineering,* 127:729-735.

Zhou C, Khalil TB, King AI (1995). A New Model Comparing Impact Responses Of The Homogeneous And Inhomogeneous Human Brain. *Stapp Car Crash Conference,* 39: 952741.

Zink BJ, Schultz CH, Stern SA, Mertz M, Wang X, Johnston P, Keep RF (2001). Effect Of Ethanol And Naltrexone In A Model Of Traumatic Brain Injury With Hemorrhagic Shock. *ALCOHOLISM:CLINICAL AND EXPERIMENTAL RESEARCH,* 25(6):913-923.

Zoghi-Moghadam M, Watkins CB, Sadegh A, Dunlap D (2002a). Simulation Of Stand-Up Lift Truck Accidents To Evaluate Their Design And Operator Training Implications. *Safety Engineering and Risk Analysis Division, Proceedings of the International Mech. Engr. Congress and Exposition, BED/ASME, (IMECE) New Orleans, November, 2002.*

Zoghi-Moghadam M, Sadegh A, Watkins CB, and Dunlap D (2002b). Biodynamics Of Stand-Up Rider Lift Truck Accidents. *Bioengineering Division, Proceedings of the International Mech. Engr. Congress and Exposition, BED/ASME, (IMECE) New Orleans, November, 2002.*

Zoghi-Moghadam M, Sadegh A, Watkins CB (2003). Arachnoid Trabeculae And CSF Roles In Blunt Head Impacts. *Paper Number 42965, Proceedings of the International Mech. Engr. Congress and Exposition, (IMECE), BED/ASME, Washington DC, November 2003.*

Zoghi-Moghadam M and Sadegh A (2004). Biomechanics Of Head/Brain Due To Angular Head Acceleration. *Proc. 2004 IMECE2004,* 60935.

Zoghi-Moghadam M and Sadegh A (2005). Damping Characteristics Of Subarachnoid Trabeculae In Rotational Head Impact. *Proc. of the 2005 Summer Bioengineering Conference, Vail, CO, June 2005, 187601.*

Zoghi-Moghadam M, Watkins CB, Sadegh A, Dunlap D (2006 - In Press). Biodynamics Of Operators Injury In Stand-Up Rider Lift Trucks. *Submitted to Computer Methods in Biomechanics and Biomedical Engineering.*

Zoghi-Moghadam M and Sadegh A (2006 - In Press). Equivalent Fluid Model For CSF And SAS Trabeculae Using Head/Brain Damping. *Submitted to Journal of Biomechanics.*

Zoghi-Moghadam M and Sadegh A (In preparation). Three Dimensional Global/Local Head Models To Quantify ASDH. *To be submitted to the Journal of Biomechanical Engineering.*

Zoghi-Moghadam M and Sadegh A (2006) A New Fluid Model Representing Damping Characteristics Of CSF And SAS Trabeculae In Head Impacts. *Submitted to Summer Biomechanics Conference of ASME.*